

HEAT AND FRESHWATER CONTROLLING PROCESSES ON THE NORTHERN
GULF OF ALASKA SHELF

A
THESIS

Presented to the Faculty
of the University of Alaska Fairbanks

in Partial Fulfillment of the Requirements
for the Degree of

DOCTOR OF PHILOSOPHY

By

Markus A. Janout

Fairbanks, Alaska

December 2009

UMI Number: 3401162

All rights reserved

INFORMATION TO ALL USERS

The quality of this reproduction is dependent upon the quality of the copy submitted.

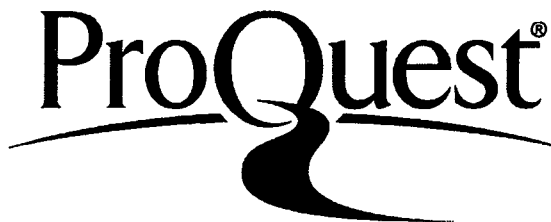
In the unlikely event that the author did not send a complete manuscript and there are missing pages, these will be noted. Also, if material had to be removed, a note will indicate the deletion.



UMI 3401162

Copyright 2010 by ProQuest LLC.

All rights reserved. This edition of the work is protected against unauthorized copying under Title 17, United States Code.



ProQuest LLC
789 East Eisenhower Parkway
P.O. Box 1346
Ann Arbor, MI 48106-1346

HEAT AND FRESHWATER CONTROLLING PROCESSES ON THE NORTHERN

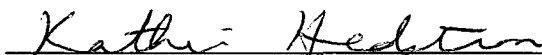
GULF OF ALASKA SHELF

By

Markus A. Janout


RECOMMENDED:

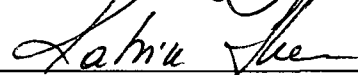

Dr. Kenneth Coyle


Dr. Katherine Hedstroem

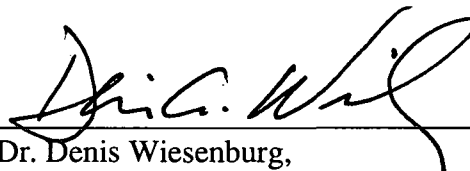

Dr. Mark Johnson

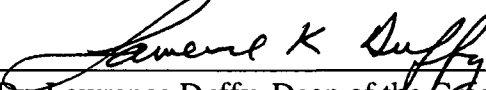

Dr. Stephen Okkonen


Dr. Thomas Weingartner, Advisory Committee Chair


Dr. Katrin Iken,
Head, Program in Marine Science and Limnology

APPROVED:


Dr. Denis Wiesenburg,
Dean, School of Fisheries and Ocean Sciences


Dr. Lawrence Duffy, Dean of the Graduate School

Dec 2, 2009

Date

Abstract

We examined conditions and processes that control the distribution of heat and freshwater on the northern Gulf of Alaska (GOA) shelf. Cross-shelf heat gradients are weak throughout the year, while salinity gradients are substantial due to the impact of coastal freshwater runoff. Outer shelf water properties are influenced by large anticyclonic eddies, while the inner and middle shelves may be regulated by wind and freshwater runoff dynamics around the Alaska Coastal Current (ACC).

On the outer shelf, anticyclonic eddies propagate from the eastern GOA southwestward along the continental slope, where they favor on-shelf (off-shelf) transport of saline and nutrient-rich (fresh and iron-rich) waters. Certain along-shelf locations are identified where low-salinity coastal waters are found near the shelfbreak within reach of eddies and may be regions of enhanced cross-shelf freshwater transport. The eddies have lifetimes of ~5 years and increase in size and sea level anomaly west of the Seward Line, which implies more vigorous eddy cross-shelf exchange in the northwestern GOA.

By comparison, on the inner shelf the heat and freshwater distribution is dominated by large coastal river runoff, which forces the ACC and controls the vertical distribution of temperatures through stratification. In May 2007, the coastal GOA revealed some of the lowest ocean temperatures since the early 1970s, initiated by strong atmospheric cooling and reduced coastal runoff in November 2006. Stepwise regression shows that 81% of the variability of deep temperatures is

explained by salinity stratification and air-sea heat fluxes. Weak baroclinic flow in May 2007 likely aided the cooling through reduced along-shore heat transport.

A more detailed examination of heat transport indicated that along-shore heat flux convergence in the ACC may re-supply 10-35% of the heat removed by air-sea fluxes throughout the coastal GOA cooling season, while the annual mean cross-shore heat flux convergence is insignificant. Spatial gradients show increasing heat fluxes from off- to on-shore and from east to west. The cross-shore gradients result from wind speed gradients due to ageostrophic near-shore wind jets near coastal mountains, while the along-shore gradients result from larger-scale pressure systems. While the ACC advects coastal freshwater around the GOA shelf its waters are subjected to disproportional heat loss west of the Seward Line.

Table of Contents

	Page
Signature Page	i
Title Page	ii
Abstract	iii
Table of Contents	v
List of Figures	viii
List of Tables	xi
Acknowledgements	xii
Introduction	1
References	5
Chapter 1 Some characteristics of Yakutat Eddies propagating along the continental slope of the northern Gulf of Alaska	9
Abstract.....	9
1.1 Introduction	10
1.2 Methods and Data Description	14
1.2.1 Vessel-mounted ADCP and towed CTD Mesoscale cruises.....	14
1.2.2 Thermosalinograph (TSG)	15
1.2.3 Array for Real-time Geostrophic Oceanography (ARGO)	16
1.2.4 Satellite Sea Surface Height Anomalies (SSHA).....	16
1.3 Results	17
1.3.1 Lifecycles of E01 and E03	17

1.3.2 ARGO float 49070 and E01	19
1.3.3 TSG (E03)	21
1.3.4 SeaSoar Hydrography (E03)	23
1.3.5 ADCP (E03)	27
1.4 Summary and Discussion	31
1.5 Acknowledgments	35
1.6 References	36
1.7 Tables	44
1.8 Figures	45
Chapter 2 On the nature of winter cooling and the recent temperature shift on the northern Gulf of Alaska shelf.....	61
Abstract.....	61
2.1 Introduction	62
2.2 Data and methods	64
2.3 Results and analysis.....	66
2.3.1 Hydrographic observations at GAK1 in spring 2007 and 2008	66
2.3.2 The onset of the cooling in November 2006	68
2.3.3 The evolution of the 2006/07 cooling compared to other years.....	71
2.3.4 Atmospheric forcing parameters and their interannual variability at GAK1	74
2.3.5 On the timing of cooling events	77
2.3.6 The effect of downwelling	78

2.4 Summary and Conclusion.....	81
2.5 Acknowledgments	86
2.6 References	87
2.7 Figures	92
Chapter 3 Air-sea and oceanic heat flux contributions to the heat budget of the northern Gulf of Alaska shelf.....	106
Abstract.....	106
3.1 Introduction	107
3.2 Datasets.....	109
3.3 Results	110
3.3.1 Annual cycles of salinity and temperature along the Seward Line	110
3.3.2 Air-sea fluxes and oceanic heat content	113
3.3.3 Cross-shore heat transport	115
3.3.4 Along-shore heat transport	117
3.3.5 Cross- and along-shelf air-sea heat flux variability.....	120
3.3.6 The role of northern GOA low sea level pressure events.....	123
3.4 Summary and conclusion	126
3.5 Acknowledgments	130
3.6 References	131
3.7 Figures	136
Summary and Conclusion.....	151

List of Figures

	Page
Figure 0.1: Map of the Gulf of Alaska.	5
Figure 1.1: Trajectory of the 2001-eddy.....	45
Figure 1.2: Trajectory of the 2003-eddy.....	46
Figure 1.3: Salinity, temperature and dynamic height of ARGO float 49070.	47
Figure 1.4: Tanker cruise tracks and surface salinity.	48
Figure 1.5: Eddy survey cruise tracks in May and August 2003.....	51
Figure 1.6: SeaSoar eddy survey May transect 1.	52
Figure 1.7: SeaSoar eddy survey May transect 2.	53
Figure 1.8: SeaSoar eddy survey August transect 1.....	54
Figure 1.9: SeaSoar eddy survey August transect 2.	55
Figure 1.10: Azimuthal eddy velocities.....	56
Figure 1.11: May eddy velocities.	57
Figure 1.12: August eddy velocities.	58
Figure 1.13: Linear regressions of sigma-theta.	59
Figure 1.14: Drifter trajectory and eddy.....	60
Figure 2.1: Map of the northern Gulf of Alaska.....	92
Figure 2.2: Annual number of GAK1 CTD profiles.	93
Figure 2.3: May 2007 and 2008 temperature and salinity profiles.....	94
Figure 2.4: GAK1 temperature anomalies time series.	95
Figure 2.5: Seward Line 1998-2008 temperature anomalies.....	96

Figure 2.6: Seward Line 1998-2008 salinity anomalies.....	97
Figure 2.7: Seasonal cycle of GAK1 temperatures.	98
Figure 2.8: Seasonal cycle of GAK1 density stratification.	99
Figure 2.9: Temperature, salinity and winds in November 2006.....	100
Figure 2.10: High resolution GAK1 temperature and salinity records.....	101
Figure 2.11: Wind, runoff and heat flux anomalies.....	103
Figure 2.12: Winter anomalies of atmospheric variables 1970-2008.....	104
Figure 2.13: Sea level pressure patterns.	105
Figure 3.1: Map of the northern Gulf of Alaska.....	136
Figure 3.2: Seasonal mean Seward Line salinity.....	137
Figure 3.3: Seasonal mean Seward Line temperature.	138
Figure 3.4: Climatology of wind and coastal runoff.	139
Figure 3.5: Northern Gulf of Alaska heat flux climatology.	140
Figure 3.6: Seward Line oceanic heat content.....	141
Figure 3.7: Coastal Gulf of Alaska heat deficit.	142
Figure 3.8: Seward Line heat gradients and Ekman heat flux convergence.....	143
Figure 3.9: Seward Line geostrophic velocities.	144
Figure 3.10: Gulf of Alaska turbulent heat fluxes.....	145
Figure 3.11: Cross-shelf wind speed gradients.....	146
Figure 3.12: Winter coast to off-shore wind ratio.	147
Figure 3.13: 1948-2009 frequency of Gulf of Alaska lows.....	148
Figure 3.14: Gulf of Alaska low and air temperature anomalies.....	149

Figure 3.15: Winter heat fluxes and anomalies. 150

List of Tables

	Page
Table 1.1: Eddy transport estimates.	44

Acknowledgements

My sincere gratitude goes to my major advisor Dr. Tom Weingartner, who provided guidance and support, ideas, discussions and outstanding expertise on the oceanography of Alaskan waters throughout my years at UAF. I sincerely thank Dr. Kate Hedstroem from the Arctic Region Super Computer and Dr. Stephen Okkonen, Dr. Mark Johnson, Dr. Ken Coyle, and Dr. Dave Musgrave from UAF's Institute of Marine Science for serving on my graduate committee and offering advice and reviews for my dissertation.

Data and/or advice leading to chapter 1 were kindly provided by Dr. Stephen Okkonen, Dr. Terry Whitledge, and Dr. Dave Musgrave from UAF. Advice and expertise leading to chapter 2 were provided by Dr. Tom Royer from Old Dominion University and Seth Danielson from UAF. All three chapters benefited significantly from the editing and writing expertise of Dr. Tom Weingartner.

Additional thanks goes to Dr. Jackie Grebmeier and Dr. Lee Cooper from the University of Maryland, and to Dr. Eddy Carmack from IOS, Canada who allowed me to expand my horizon during several research cruises in the Bering and Chukchi Seas, and to Professor Sei-Ichi Saitoh from the University of Hokkaido for being my host during my exchange visit in Japan.

I am grateful for the friendship and the collegiality of many of the SFOS faculty, staff and fellow graduate students, office mates and Liquid30 fellows who all helped me along in one way or another and made work and beyond more than enjoyable. I am grateful for the love and support of my family and apologize for

roaming the opposite side of this planet, and last but not least I am indebted to my wife, Lisa, whose moral support and formatting skills saved my day on more than one occasion.

Introduction

The northern Gulf of Alaska (GOA) (Figure 0.1) shelf is deep (150-270 m) and wide (50-150 km) and supports one of the world's richest ecosystems, which is of high cultural and economical importance. The GOA's climate is largely governed by the strength and position of the Aleutian Low, which causes predominantly along-shore (downwelling-favorable) winds from fall through spring (Wilson and Overland, 1986). Downwelling regions are not typically characterized by high biological productivity, and therefore relevant research questions on the northern GOA shelf often evolve around the understanding of physical, biological, and chemical processes that support this rich ecosystem.

The circulation on this shelf is governed by the swift and variable (0.2-1.8 m s⁻¹ Johnson et al., 1988) Alaska Coastal Current (ACC, Royer, 1981; Schumacher et al., 1989; Stabeno et al., 1995; Weingartner et al., 2005). The ACC is a buoyant current, driven by along-shore winds and large freshwater runoff supplied from the numerous small streams fed by glacial and snow melt and from runoff from some of the world's largest precipitation rates (Wilson and Overland, 1986). As the dominant near-shore circulation feature, the ACC is an important advective pathway for organisms and water properties that extends ~2000 km from the British-Columbian to the western GOA shelf, where it advects GOA waters into the Bering Sea through passes in the Aleutian Islands. The mid-shelf circulation is less pronounced and characterized by strong variability due to eddies and meanders. The circulation on the

eastern shelf is governed by the broad and shallow Alaska Current (AC). In the northern GOA, the AC transforms into the deeper, narrower and swifter Alaskan Stream, and these currents form the eastern and western boundary currents around the cyclonic Alaska Gyre.

Large (~200 km) anticyclonic eddies form along distinct locations off Sitka and Yakutat in the eastern GOA (Figure 0.1) and subsequently propagate along the shelfbreak and are assumed to play an important role in the region's biological productivity by promoting exchange between nutrient-rich (but iron-depleted) offshore waters and the low nutrient (but iron-rich) waters on the shelf. Other cross-shelf mechanisms include current-topography interactions due to the GOA's irregular coastline, marked by numerous capes, islands, canyons and seamounts (Stabeno et al., 2004). In addition, the nutrient reservoir in the deep shelf waters is replenished during the recession of downwelling winds (or the occurrence of weak upwelling winds) in summer (Childers et al., 2005) and are then vertically mixed by Ekman pumping due to wind stress curl (Schroeder, 2007; Fiechter and Moore, 2009) or tide-induced mixing over shoals and canyons (Stabeno et al., 2004).

Temperature and salinity each have a significant impact on the northern GOA ecosystem. While the GOA fisheries in the early 1970s were dominated by shellfish (shrimp and crab), they then rapidly changed to a fisheries dominated by pelagic fish species (salmon, Pollock, cod, etc.; Anderson and Piatt, 1999) shortly after the 1977 regime shift to a warmer ocean climate in the GOA (Mantua et al., 1997). Ocean temperatures profoundly influence many aspects of marine ecosystems. The metabolic

rates of most ectotherms (e.g., zooplankton, fish) increase with increasing temperature, so water temperatures affect growth, behavior, feeding, predation, and spawning activity of these organisms throughout their life history (Rombough, 1997). The ecosystem's food availability (i.e. primary production) is largely governed by nutrient availability, light and stratification. While temperature effects are relatively greater on stratification over the outer shelf than inner shelf during summer, shelf stratification is dominated by salinity due to the large influence of coastal freshwater runoff. Coastal runoff varies seasonally and interannually, and generally shows a maximum in spring and fall (Royer, 1982). Once snow melt begins in spring, freshwater runoff increases and, in combination with solar radiation, provides the stability needed in the upper water column to initiate the spring bloom (Henson, 2007). The timing and magnitude of the runoff are therefore crucial parameters in the seasonal cycle of biological productivity. A deviation from the "optimal" magnitude of runoff may have negative effects on the ecosystem. For example, too little runoff may not provide enough stratification to suspend biological matter in the euphotic layer, while a too strongly stratified water column due to too much runoff may prevent vertical entrainment of nutrients. Overall, the understanding of the ecosystem requires detailed understanding of both ocean temperature and salinity, and processes and conditions that govern their seasonal, interannual, and spatial variability on the northern GOA shelf.

The major part of the hydrographic data used for the studies presented below was acquired from the recent Northeast Pacific Global Ocean Ecosystem Dynamics (GLOBEC) program (Weingartner et al., 2002), which included seven annual surveys

of the Seward Line (Figure 0.1) and additional shelf stations from 1998-2004, and was supported by the National Science Foundation in order to improve the understanding of the physical environment and the impact of a changing climate on the GOA's ecosystem. Annual monitoring of Seward Line conditions is presently continued with two (May and September) surveys, sponsored by the North Pacific Research Board. The longest hydrographic time series on the northern GOA shelf (~1970-present) is at GAK1, the in-shore station of the Seward Line, and consists of ~450 CTD profiles, with 2-10 profiles acquired per year before 1985, and quasi-monthly profiles acquired thereafter. In addition, moored temperature and salinity records are available since 1997. Earlier comprehensive research programs in the northern GOA include the Outer Continental Shelf Environmental Assessment Program (OCSEAP) from 1975-1985 funded by the National Oceanic and Atmospheric Administration (NOAA) to provide baseline data in anticipation of oil development on Alaska's continental shelves, and the NOAA-funded Fishery-Oceanography Coordinated Investigations (FOCI) began in 1985 and focused on the relationship between the physical environment and commercial fish in Shelikof Strait.

This dissertation is aimed at improving the understanding of physical conditions and processes that determine the heat and freshwater distribution and variability on the northern GOA shelf. Chapter 1 examines the characteristics of mesoscale eddies that propagate along the northern GOA shelf break and their role on cross-shelf exchange. Chapter 2 presents the analysis of hydrographic and atmospheric time series on the northern GOA shelf, with the focus on winter-time conditions and

processes that determine stratification and ocean temperatures in spring. Chapter 3 focuses on the quantitative understanding of the northern GOA heat budget. In particular, we investigate air-sea heat fluxes and their spatial gradients and estimate the contribution of ocean heat flux convergences in the ACC and in cross-shore Ekman transport to the near-shore oceanic heat budget.

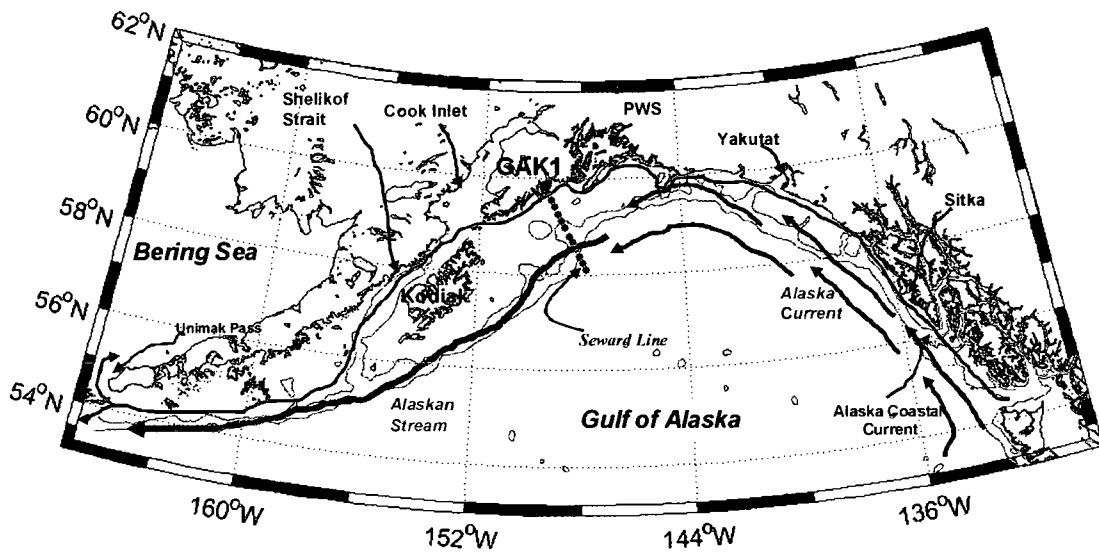


Figure 0.1: Map of the Gulf of Alaska. Map of the Gulf of Alaska including location names and a sketch of major currents.

References

Anderson, P.J. and J.F. Piatt (1999), Community reorganization in the Gulf of Alaska following ocean climate regime shift, *Mar. Ecol. Prog. Ser.*, 189, 117-123.

Childers, A.R., T.E. Whitley, and D.A. Stockwell (2005), Seasonal and interannual variability in the distribution of nutrients and chlorophyll-a across the Gulf of Alaska shelf: 1998–2000, *Deep-Sea Res. II*, 52, 193–216.

Fiechter, J., and A. M. Moore (2009), Interannual spring bloom variability and Ekman pumping in the coastal Gulf of Alaska, *J. Geophys. Res.*, 114, C06004, doi:10.1029/2008JC005140.

Henson, S.A. (2007), Water column stability and spring bloom dynamics in the Gulf of Alaska, *J. Mar. Res.*, 65, 715–736.

Johnson, W.R., T.C. Royer, and J.L. Luick (1988), On the seasonal variability of the Alaska Coastal Current, *J. Geophys. Res.*, 93(C10), 12423-12437.

Mantua, N.J., S.R. Hare, Y. Zhang, J.M. Wallace, and R.C. Francis, (1997), A Pacific interdecadal climate oscillation with impacts on salmon production. *Bull. Am. Meteorol. So.* 78 (6), 1069–1080.

Rombough, P.J. (1997), The effects of temperature on embryonic and larval development, in *Global warming: Implications for freshwater and marine fish*, edited by C.M. Wood and D.G. McDonald. Society for Experimental Biology Seminar Series 61, Cambridge University Press.

Royer, T.C. (1981), Baroclinic transport in the Gulf of Alaska, Part II: Freshwater driven coastal current, *J. Mar. Res.*, 39, 251-266.

Royer, T.C. (1982), Coastal freshwater discharge in the Northeast Pacific, *J. Geophys. Res.*, 87(C3), 2017-2021.

Schroeder, I. (2007), Annual and interannual variability in the wind field and the hydrography along the Seward Line in the northern Gulf of Alaska, PhD dissertation, 80 pp., Old Dominion University, Norfolk, VA.

Schumacher, J.D., P.J. Stabeno, and A.T. Roach (1989), Volume transport in the Alaska Coastal Current, *Cont. Shelf Res.*, *9*, 1071-1083.

Stabeno, P.J., R.K. Reed and J.D. Schumacher (1995), The Alaska Coastal Current: continuity of transport and forcing, *J. Geophys. Res.*, *100(C2)*, 2477-2485.

Stabeno, P.J., N.A. Bond, A.J. Hermann, N.B. Kachel, C.W. Mordy, and J.E. Overland (2004), Meteorology and oceanography of the northern Gulf of Alaska, *Cont. Shelf Res.*, *24*, 859-897.

Weingartner, T.J., K. Coyle, B. Finney, R. Hopcroft, T. Whitley, R. Brodeur, M. Dagg, E. Farley, D. Haidvogel, L. Halderson, A. Hermann, S. Hinckley, J. Napp, P. Stabeno, T. Kline, C. Lee, E. Lessard, T. Royer, and S. Strom (2002), The Northeast Pacific GLOBEC Program: Coastal Gulf of Alaska, *Oceanography*, *15*, 48 – 63.

Weingartner, T.J., S.L. Danielson, and T.C. Royer (2005), Freshwater variability and predictability in the Alaska Coastal Current, *Deep-Sea Res. II*, *52*, 169-191.

Wilson, J.G. and J.E. Overland (1986), Meteorology, in *The Gulf of Alaska, Physical Environment and Biological Resources*, edited by D.W. Hood and S.T. Zimmerman, pp. 31–53, Alaska Office, Ocean Assessments Division, National Oceanic and Atmospheric Administration, US Department of Commerce.

Chapter 1 Some characteristics of Yakutat Eddies propagating along the continental slope of the northern Gulf of Alaska¹

Abstract

Data from ARGO profiling floats, oil tanker thermosalinographs, shipboard ADCP and towed-CTD surveys, and satellite altimetry were used to examine properties of two ~200 km diameter, anticyclonic Yakutat Eddies that propagated westward at ~1.5 km day⁻¹ along the continental slope of the northern Gulf of Alaska (GOA) in 2001 and 2003. The eddies had lifetimes of up to 5 years, remained close to the shelfbreak, and had relatively constant size and strength until they encountered the Alaskan Stream where they appeared to spawn smaller, shorter-lived anticyclones. The azimuthal velocity field was vigorous (25-40 cm s⁻¹) and in gradient wind balance with Rossby numbers of ~0.05. Conservation of salt and azimuthal mass transports (between 20 m and the depth of the 32.2 isohaline) from shipboard surveys in May and August 2003 suggest little mass exchange occurred between the surface layers of the eddy and ambient waters. Chlorophyll concentrations were greater in the eddy than in ambient waters in both May and August. In May, the chlorophyll was patchily distributed, while in August dense chlorophyll concentrations occurred in and beneath

¹ Janout, M.A., T.J. Weingartner, S.R. Okkonen, T.E. Whitledge, and D.L. Musgrave (2009), Some characteristics of Yakutat Eddies propagating along the continental slope of the northern Gulf of Alaska, *Deep-Sea Research II*, 56, 2444-2459.

the seasonal thermocline within 50 km of the eddy center. The high August chlorophyll concentrations might have been fostered by a broad and shallow (<~150 m) upwelling of the eddy center between May and August.

It appears likely that as Yakutat Eddies approach the shelfbreak non-linear processes will modify the slope flow field (and the stability and structure of the shelfbreak front), leading to cross-slope flows and flow reversals. This interaction may induce ~30 km-wide streamers of shelf water to flow around the trailing edge of the anticyclone. The role of streamers in the freshwater and nutrient budgets of the GOA shelf and basin is unknown, but their contribution to these budgets will depend on the trajectory of a Yakutat Eddy, especially its proximity to the shelfbreak as the eddy propagates along the GOA continental slope.

1.1 Introduction

The dominant circulation features of the northern Gulf of Alaska (GOA) are the wind- and buoyancy-forced Alaska Coastal Current (ACC) (Schumacher and Reed, 1980; Royer, 1981; Johnson et al., 1988; Schumacher et al., 1989; Stabeno et al., 1995; Stabeno et al., 2004; Weingartner et al., 2005) and the slope boundary currents. The latter include the broad, relatively sluggish Alaska Current in the northeastern Gulf and the western-intensified Alaskan Stream in the western Gulf. The shelf and slope currents transport waters from the southern Gulf into the Bering Sea and the western Pacific Ocean, with the ACC being an important freshwater source for the Bering Sea and Bering Strait (Aagaard et al., 2006). Transport variations in the

Alaska Current/Alaskan Stream appear small (Royer, 1982), with perhaps the largest source of variability induced by large (~ 150 km), slowly-propagating (~ 2 km day⁻¹) anticyclonic eddies.

Maps of GOA sea surface height anomalies (SSHA) from satellite altimetry suggest the frequent occurrence of these eddies, which develop in the Alaska Current. There are three distinct eddy formation regions along the eastern GOA boundary and the eddies generated here are named based on their geographical origin: the Haida Eddy offshore northern British Columbia, the Sitka Eddy in the eastern Gulf, and the Yakutat Eddy in the northeastern Gulf. All have similar properties, but differ in trajectories. All Haida and most Sitka Eddies propagate from the eastern GOA into the deep basin, releasing shelf water (Whitney and Robert, 2002) and coastal species (Mackas and Galbraith, 2002) upon decay. Some Sitka Eddies, however, propagate north along the shelf and then follow the typical trajectory of the northernmost eddies (Crawford et al., 2000). In this paper, northward moving Sitka Eddies will be included in the family of Yakutat Eddies, which propagate westward and thence southwestward, often in close contact with the continental slope. Of the three, the Haida Eddies are best understood in terms of physical characteristics (Crawford, 2002), heat and freshwater content (Crawford, 2005), currents (Yelland and Crawford, 2005), and biology (Crawford et al., 2005). Some sampling has been conducted within the less accessible Sitka (Tabata, 1982) and Yakutat eddies (Ladd et al., 2005a; Ladd et al., 2009). Satellite observations have yielded considerable information on the

eddies as well (Meyers and Basu, 1999; Crawford et al., 2000; Okkonen et al., 2001; Okkonen et al., 2003).

Large eddy generation has been ascribed to a variety of processes. Swaters and Mysak (1985) argue that topographic irregularities are the cause, while Thomson and Gower (1998) and Melsom et al. (1999) suggest the eddies originate by Alaska Current baroclinic instabilities triggered by variability in the wind field. GOA eddies are often associated with increased primary production (Childers et al., 2005) and likely deliver iron-rich (Johnson et al., 2005, Ladd et al., 2009) coastal waters into the high-nutrient-low-chlorophyll (HNLC) GOA (Martin et al., 1989).

Of the three eddy types, Yakutat Eddies have the greatest potential for effecting shelf-basin exchanges since these tend to propagate along a considerable portion of the GOA continental slope. In this regard they are analogous to Gulf Stream rings (Joyce, 1984; Joyce and Kennelly, 1985; Olson et al., 1985; Olson, 1991; Hooker and Brown, 1994), which impact shelf-slope circulation processes (Garvine et al., 1988; Garvine et al., 1989; Yankovsky and Chapman, 1997; Gawarkiewicz et al., 2001), and influence water properties of the outer shelf and continental slope (Evans et al., 1985; Churchill et al., 1986; Garfield and Evans, 1987).

The interaction of eddies with the background flow field can promote upwelling and downwelling, which appears to enhance biological production in Gulf Stream rings and adjacent waters (Gawarkiewicz et al., 2001). Similarly, Musgrave et al. (1992) and Okkonen et al. (2003) suggest that the Yakutat Eddies might stimulate biological production through eddy-enhanced vertical motions and influence shelf-

slope exchange. With respect to the last issue, Okkonen et al. (2003) suggested that Yakutat Eddies may substantially influence the freshwater budget of the GOA shelf and basin and, consequently, the freshwater budget of the eastern Bering Sea shelf. The cross-shelf flux of shelf water may also be an important pathway by which iron reaches the basin (Ladd et al., 2009).

This study focuses on several characteristics and processes associated with the propagation of Yakutat Eddies along the northern GOA slope. We use a variety of datasets to ask: 1) Is there evidence of cross-slope transport due to eddy-topography interaction and, if so, what are the spatial and temporal scales of this transport? 2) Do Yakutat Eddies affect the freshwater exchange between the GOA shelf and basin and how is this exchange mediated? 3) Is there evidence of increased biological productivity in the eddy, and what are the mechanisms responsible for this enhancement? In addressing these questions we examined three data sets obtained from two eddy surveys using a vessel-mounted ADCP and a towed-CTD, profiling floats, and thermosalinographs (TSGs) mounted on oil tankers transiting between Alaska and the US west coast. However, we provide only partial answers since none of these data were obtained from dedicated “eddy missions”. Indeed, the data obtained by the profilers and TSGs were fortuitous, e.g., the instruments happened to chance across an eddy. The ADCP and towed CTD transects were collected opportunistically when a dedicated shelf cruise was re-directed to briefly sample a nearby eddy. While our observations are limited, they nonetheless allow new insights on several aspects of Yakutat Eddies and their interaction with the slope. The outline of the paper is as

follows: Section 1.2 explains the various datasets used to describe the eddies, Section 1.3 presents the results, and Section 1.4 concludes with a discussion and summary of the key points.

1.2 Methods and Data Description

1.2.1 Vessel-mounted ADCP and towed CTD Mesoscale cruises

Two small-scale surveys were carried out aboard the *R/V Wecoma* between 1-21 May 2003 and 21 July-12 August 2003 as part of the Northeast Pacific Global Ocean Ecosystem Dynamics (NEP-GLOBEC; Weingartner et al., 2002) Program mesoscale project. The surveys addressed small-scale (~internal Rossby radius) processes on the GOA shelf involving the ACC and the shelf break frontal region. The surveys were extended by conducting two transects across a Yakutat Eddy as it passed along the continental slope near $\sim 146^\circ\text{W}$ in May and $\sim 147^\circ\text{W}$ in August. Hydrographic data were recorded with a SeaSoar undulating towed vehicle, which provided high-resolution measurements of temperature, salinity, fluorescence and nitrate in the upper 100 m of the water column. The nitrate measurements were obtained from a Satlantic *In-situ* Ultraviolet Sensor (ISUS) mounted on the SeaSoar. The towing speed was ~ 7 knots, yielding a horizontal resolution of ~ 500 m. Water samples were taken at selected stations with 10 liter Niskin bottles and analyzed for chlorophyll-a and nitrate. *In-situ* water samples compared with ISUS data indicate that the accuracy and precision of the nitrate sensor was $0.5 \mu\text{M l}^{-1}$. Regressions between

the SeaSoar fluorometer and *in-situ* chlorophyll samples were used to convert the SeaSoar fluorescence signals into chlorophyll-a concentrations. Water column profiles of horizontal current velocities were simultaneously obtained from the *R/V Wecoma's* 150-kHz ADCP. These data were blended with p-code global positioning data and a 3D Ashtech heading system and processed using the University of Hawaii's Common Ocean Data Access System (CODAS) software. After quality controlling the data and applying corrections for transducer misalignment we estimate the precision of the ADCP data to be $\pm 3 \text{ cm s}^{-1}$. Measured current speeds were typically (20-50 cm s^{-1}) and much larger than the uncertainty of the tidal currents. The latter are $\sim 5 \text{ cm s}^{-1}$ (Foreman et al., 2000) over the slope, even smaller over the basin, and are neglected herein.

1.2.2 Thermosalinograph (TSG)

Along-track temperature and salinity were recorded with a Seabird SBE-45 thermosalinograph (TSG) mounted on the *T/V Polar Alaska* in 2002. Okkonen et al. (2005) describe the TSG data and processing procedures. We used a subset of these data obtained from repeated crossings near and within a Yakutat Eddy in March and April of 2003. The TSG sampled at a depth of 13 m on southbound transects when the tankers were laden with oil, while northbound cruises sampled at a depth of 8 m. The late winter mixed layer is much deeper, so that temperature and salinity differences between these depths are negligible. The horizontal resolution of the processed TSG data is 2 km.

1.2.3 Array for Real-time Geostrophic Oceanography (ARGO)

We also analyzed data from Project ARGO float 49070 as it drifted around the GOA, repeatedly entering and leaving the same eddy. (ARGO is an integrated part of a global observing system monitoring water properties throughout the global ocean through the use of profiling floats. For technical descriptions and data quality discussions, see the ARGO website: www.argo.ucsd.edu.) We combined the float trajectory and satellite altimetry data to ascertain the position of the profiler with respect to the eddy, which permitted us to examine hydrographic properties within and outside of the same eddy over a 24-month period. We obtained 24 eddy profiles during three separate eddy-profiler encounters: 10/15/2001 and 01/29/2002, 07/27/2002 and 08/28/2002, and 06/08/2003 and 09/22/2003. These 24 encounters were a subset of the 171 profiles that we examined and that had data to at least 900 dbars (22 of these 171 profiles had data to 2000 dbars).

1.2.4 Satellite Sea Surface Height Anomalies (SSHA)

Weekly sea surface height anomaly (SSHA) data were downloaded from the webpage (www.aviso.oceanobs.com) of the AVISO-group (Archiving, Validation and Interpretation of Satellite Oceanographic data). Ladd et al. (2007) provided a detailed discussion on the SSHA data and our utilization of these data followed their approach. Where appropriate, we have overlain the oceanographic data onto nearly coincidental SSHA maps.

1.3 Results

Our results include data collected from two different Yakutat Eddies. The first eddy was identified in altimeter data acquired in winter 2001 near 57°N, 137°W (Ladd et al., 2007) and was later sampled by the ARGO profiler. This eddy, referred to as E01 (eddy 2001), remained in the GOA until it decayed in April 2006. The second eddy formed in winter 2002/2003 offshore of Yakutat and we call it E03 (eddy 2003). Altimeters have now tracked this eddy for nearly five years. *In-situ* data from E03 were acquired by both the TSG and SeaSoar during 2003. We begin with a description of the E01 and E03 eddy lifecycles, then present the ARGO results for E01, and finally discuss the data from E03 collected by the tanker-TSG and the SeaSoar and ADCP surveys. Ladd et al. (2005a) and Ladd et al. (2007) provide additional information on the interior water properties of both eddies.

1.3.1 Lifecycles of E01 and E03

The lifecycles of E01 and E03 are discussed with reference to Figures 1.1 and 1.2, which show their trajectories and sizes as a function of time and location in the GOA. Figure 1.1 also identifies the geographical place names used in the text. The lower panels of both figures depict the eddies' maximum SSHAs and their distances from the shelfbreak as a function of longitude.

E01 first appeared in the altimetry in January 2001 at 57°N, 137°W (Figure 1.1), in the Sitka formation region discussed by Tabata (1982). After formation, the eddy moved offshore of the shelf and then northwestward and parallel to the

continental slope at an average translation speed of 1.5 km day^{-1} . In 2002, the translation speed increased to $\sim 2 \text{ km day}^{-1}$ and the eddy moved southwestward along the continental slope east of Kodiak Island. Maximum SSHA ranged between 20 and 30 cm in 2002. However, in early 2003, the eddy substantially increased its diameter from 180 to 270 km and attained a maximum SSHA of $\sim 60 \text{ cm}$ after it passed the mouth of Shelikof Sea Valley (Figure 1.1). In April, E01 spawned a smaller anticyclone, which was accompanied by a reduction in the maximum SSHA of E01 to 40 cm. The spawned eddy propagated downstream faster than E01 and decayed over the next 4 months. In 2004, the E01 translation speed decreased to $\sim 1.4 \text{ km day}^{-1}$ and the maximum SSHA increased again to $\sim 60 \text{ cm}$, where it remained for the next 6 months after passing to the west of Unimak Pass. In February 2005, E01 split into two eddies; one propagated westward and decayed within ~ 6 months, while the maximum SSHA of the parent eddy (E01) decreased to $\sim 20 \text{ cm}$. SSHA decreased gradually thereafter as E01 moved seaward of the continental slope. The eddy was last detected in April 2006 at 48.5°N , 174.3°W . It thus had a lifetime of ~ 5.5 years and propagated some 2800 km along the GOA slope.

E03 was first observed over the slope near Yakutat in November 2002 (Figure 1.2; Ladd et al., 2005a). Yearly averaged translation speeds between 2003 and 2006 ranged between 1.2 and 1.7 km day^{-1} , and $<0.7 \text{ km day}^{-1}$ during 2007. Shortly before reaching the mouth of Shelikof Sea Valley in November 2004, E03 spawned a smaller anticyclone, which continued downstream with the Alaskan Stream, but decayed shortly thereafter. In May 2005, E03 was southwest of Shelikof Sea Valley and split

into two eddies of similar size. One eddy moved south, away from the slope, and decayed after five months, while the other (E03) continued southwestward along the slope. West of 160°W the characteristics of E03 were similar to E01 in terms of SSHA and distance from the shelfbreak. The maximum SSHA of both E01 and E03 increased to ~60 cm near Unimak Pass before decreasing with further propagation. In March/April 2007, E03 started to move offshore (at the general location where E01 departed from the shelf). As of 16 October 2007 (after almost 5 years), E03 had an SSHA of ~47 cm near 50°N, 171.5°W, and was about 2200 km downstream from its generation site.

1.3.2 ARGO float 49070 and E01

The trajectory of ARGO profiler 49070 followed the northern and western boundaries of the cyclonic Alaska Gyre (Figure 1.1). Spacing between successive surfacings of the profiler provides qualitative estimates of the deep current velocities, with closely-spaced surfacings in the Alaska Current and central gyre and widely-spaced surfacings in the swift Alaskan Stream. Looped profiler trajectories reflect eddy encounters. The profiler data began in May 2001 and ended in April 2006 after operating for ~1800 days and collecting 171 profiles.

Contour plots of profiler potential temperature and salinity overlaid by several representative σ_θ isopleths (Figure 1.3) show distinct variations in water properties. Seasonal variations are apparent in the upper 150 m of the water column. Surface waters within E01 were substantially fresher (by up to 2 Practical Salinity Units over

the upper 50 m of the water column, as observed in the August 2003 profiles) compared to those outside the eddy. Subsurface isotherms and isohalines were also considerably deeper inside the eddy than outside. For example, below 200 m (the approximate depth of the permanent pycnocline of the GOA) isohalines and isotherms were ~250 m deeper within E01 compared to ambient waters and are still depressed at 2000 m, the deepest available ARGO depth in 22 profiles (not shown).

The dynamic signature of the eddy is evident in the 0/900 dbar dynamic heights computed from the ARGO profiles shown in the upper panel of Figure 1.3 along with coincident SSHA. The agreement is remarkably good, especially during the three eddy-profiler encounters. Indeed, the SSHA maximum at the profiler's location during the third eddy encounter (~39 cm) is very close to the highest SSHA (~40 cm) estimated on 13 August 2003, suggesting that the profiler was probably close to the eddy center at this time. During the first and second eddy encounters, the float was likely on the outer edge of the eddy, so that the dynamic heights were somewhat lower than the maximum SSHA of 15 cm and 29 cm, respectively. The dynamic height relative to 900 dbars in the profile closest to the eddy center (22 cm) increased steadily by 1 cm per 200 dbars to 28 cm relative to 2000 dbars. This value is comparable to dynamic heights of 26 cm (0/1500 dbars) and 30 cm (0/2400 dbars) for E03 given by Ladd et al. (2005a).

The profiler entered E01 on the three occasions shown in Figure 1.1 and collected a total of 24 profiles. The freshest surface water was observed in the profiler's final encounter with E01, when it entered the eddy downstream of the mouth

of Shelikof Sea Valley. Schumacher et al. (1989) show that low-salinity ACC waters cross the shelf and enter the Alaskan Stream at the mouth of this valley. The apparent freshening of E01 surface waters in this region might be related to this efflux. We will return to this issue later but caution that temporal and spatial aliasing of the profiler data do not permit us to conclude firmly that the low-salinity waters observed at the surface of E01 on this occasion were a result of recently injected ACC waters.

1.3.3 TSG (E03)

We next describe six TSG transects collected between 23 February and 19 April 2003, which provide additional information on surface salinities inside, outside, and along the boundaries of E03. The salinity and concurrent SSHA data are shown in Figures 1.4a-f. (Surface temperatures showed little spatial variability and are not shown). At this time, E03 was seaward of the shelfbreak between Kayak Island and Prince William Sound (Figure 1.2) and translated ~90 km westward from ~143.5°W to ~145.5°W. The edge of the eddy (defined in Figure 1.2 as the 10 cm SSHA contour) stayed ~30 km offshore of the 200 m isobath, with the eddy center some ~75-100 km south of this isobath. E03 remained stationary through February (Figures 1.4a and b), but then interacted with a small cyclone and a larger anticyclone to the south through March and April (Figures 1.4c-f). The southern anticyclone is in fact a Sitka Eddy that formed in the winter of 2002 and propagated westward where it encountered E03 in March 2003.

The southbound transect of February 26 (Figure 1.4b), well to the west of E03, shows that ambient surface salinities over the slope and basin were ~ 32.4 and relatively constant. In contrast, four other transects (Figures 1.4a, c, d, and f) captured portions of E03 where surface salinities were ~ 32 or ~ 0.5 fresher than the slope and basin salinities. The salinity anomalies within E03 also coincided with positive SSH anomalies of 10-15 cm in all but one case. The exception occurred along the transect that cut slightly outside of and along the northeast edge of E03 on April 14 (Figure 1.4e). Here, the TSG detected a ~ 30 -km wide band of dilute (30.5-31.5) water that was coincident with a slightly lower (~ 5 cm) SSH anomaly than the ambient higher salinity water. This water likely originated in the ACC, since ACC salinities in the upper 50 m were < 31 in March and April 2003 (<http://www.ims.uaf.edu/GLOBEC/results/index.html>). The low salinity filament was probably quite shallow since it did not register as a positive SSH anomaly. The filament might have formed during separation of the ACC as the current rounds Kayak Island (Ahlén et al., 1987). Satellite imagery suggests that ACC separation into filaments and/or small eddies occurs episodically at the island's tip, with the separated water remaining trapped to the shelf. ACC separation is probably governed by shelf processes (Klinger, 1994; Chapman, 2003) and not affected by the eddy, but the transport of ACC filaments across the shelfbreak and into the basin is likely achieved by the eddy, as we argue later.

1.3.4 SeaSoar Hydrography (E03)

SeaSoar sampling of the shelf and E03 occurred in both May and August 2003. On each cruise E03 was sampled by two transects (M1 and M2 in May and A1 and A2 in August). To illustrate concurrent conditions on the shelf we also present data from representative shelf transects from both months (Ms in May and As in August). The locations of these transects, along with the SSHA, are shown in Figure 1.5. Figure 1.6 shows the SeaSoar data from transects Ms and M1; the latter extended southeastward from the shelfbreak across the eddy center. Data from transect M2 are shown in Figure 1.7. M2 ran east - west nearly through the center of E03 and also along the southern boundary of a second, but weaker, anticyclone to the east of E03.

Transect Ms (Figure 1.6; left panel) captured the low-salinity (31.3-31.7) ACC, which was within ~25 km from the coast. A modest salinity front, indicated by the steeply inclined isohalines, separated the ACC from the mid-shelf region and the shelfbreak, which was ~100 km seaward of the ACC front. The mid-shelf was saltier than the ACC and the large vertical excursions of the 32.2 isohaline suggest a variable mid-shelf flow field associated with small (~20 km) shelf eddies or meanders. Data from Ms and M1 (Figure 1.6; right panel) show that relatively high salinity (>32.2) water separated the mid-shelf from the fresher (<32.2) surface and interior waters of E03. Within E03, isohalines were asymmetrically distributed about the eddy center; isohalines sloped gently upward toward the southwest boundary, but were more steeply sloped toward the shelfbreak. This asymmetry was also apparent in the May

SSHA contours (Figure 1.5) and the 20-m depth velocity vectors (Figure 1.6; uppermost panel). Consistent with anticyclonic rotation, current speeds were $\sim 20\text{-}40$ cm s^{-1} to the southwest on the outer segment of M1 and to the northeast along the northwest boundary of the eddy. Between here and the shelfbreak, the currents at 20 m veered from northeast to southwest and intensified. The strong southwestward flow at the shelfbreak is consistent with this being the region where the Alaska Current is transforming into the western-intensified Alaskan Stream.

There was little horizontal variation in temperatures, which were $\sim 8^{\circ}\text{C}$ on the shelf and slightly greater within the eddy. Below 40 m depth, temperatures were $< 6^{\circ}\text{C}$, and coldest at the eddy edges, where temperatures were $\sim 5^{\circ}\text{C}$ at 100 m depth. Thermal stratification was weak, varying by $\sim 2^{\circ}\text{C}$ over the upper 40 m because solar heating had only recently begun to warm the sea surface. Temperatures and salinities on M2 within E03 (Figure 1.7) and in the weaker anticyclone to the east of E03 were similar to those along M1. However, higher salinities (> 32.3) occurred between the two eddies.

Nitrate and chlorophyll concentrations in May (Figure 1.6; bottom panel) suggest that the entire shelf was blooming as chlorophyll-a concentrations were ~ 10 $\mu\text{g l}^{-1}$ and nitrate concentrations were ≥ 10 $\mu\text{M l}^{-1}$. In contrast, chlorophyll-a within E03 was patchy, although surface nitrate concentrations were high. Large chlorophyll-a concentrations ($10\text{-}15$ $\mu\text{g l}^{-1}$) occurred along the eddy boundaries (including at 143.5°W on the boundary of the smaller anticyclone to the east of E03; Figure 1.7), and slightly lower concentrations occurred in 5-10 km-wide bands within

the eddy interior. The boundary patches may be associated with frontal processes at the edge of the eddy, while the interior patches are reminiscent of the chlorophyll-a distributions discussed by Martin and Richards (2001) and McGillicuddy et al. (1995) in North Atlantic eddies. Martin and Richards (2001) found that ageostrophic motions due to mesoscale perturbations of the azimuthal circulation about the eddy establish upwelling and downwelling cells of similar horizontal scale. The absence of substantial chlorophyll along M1 and M2 may reflect a lack of available iron and the HNLC conditions typical of the surface waters of the Northeast Pacific (Martin et al., 1989). If, in fact, iron-limitation prevailed in the surface mixed layer and upwelling cells were present in E03, the vertical motion might have provided the iron required to stimulate production. Note that the chlorophyll-a patches within E03 were not consistently related to doming of subsurface isohalines. However, a 20 May 2003 SeaWiFS image (not shown) shows chlorophyll-a spirals about the eddy center. Conceivably, the patches were formed in upwelling cells located elsewhere in E03 and subsequently advected around the eddy center by the anticyclonic circulation. Chlorophyll-a was conspicuously absent at the surface along M2 in the region between E03 and the small anticyclone to the east, even though nitrate was abundant and the surface stratification was similar to eddy waters. Instead, this area contained relatively modest chlorophyll-a concentrations of $\leq 5 \mu\text{g l}^{-1}$, which were largely confined within and below the seasonal thermocline at 25 m depth.

The August transects included the shelf (As) and eddy transect A1 and A2 (Figure 1.5). Transect As and A1, which ran southeastward across the eddy center

from the shelfbreak, are shown in Figure 1.8. Transect A2 (Figure 1.9) was more nearly meridionally-oriented. The ACC (Figure 1.8) in August was significantly fresher (~ 29) than in May, and relatively dilute ($S \leq 31$) water had spread nearly 100 km offshore at the surface. These changes reflect the seasonal adjustment of the ACC to a reduction in downwelling-favorable winds and increased coastal runoff (Weingartner et al., 2005; Williams et al., 2007). Mid-shelf isopycnal slopes were again variable, although the variability was less than that observed in May. Isohalines gently sloped upwards towards the shelf break, and the 32.2 isohaline intersected the sea surface at the northwest edge of E03. Upwelling had occurred across the interior of E03, as evidenced by the doming isopycnals and the shallower depth of the 32.2 isohaline in August compared to May. Ladd et al. (2005a) showed that the upwelling in the interior of E03 was limited to the upper ~ 150 m of the water column.

Summer warming resulted in a shallow mixed layer and strong near-surface stratification in August; vertically, the temperature decreased by 8°C over the upper 30 m. Below 40 m, the isopycnals (e. g., $\sigma_\theta = 25.4 \text{ kg m}^{-3}$) paralleled the isohalines. In contrast, the near-surface 25.2 σ_θ isopycnal tracked the isotherms, implying that temperature controlled the mixed layer depth in August.

Chlorophyll-a and nitrate concentrations were negligible in the shelf surface mixed layer. However, chlorophyll-a concentrations were $\sim 5 \mu\text{g l}^{-1}$ and relatively constant across the shelf at ~ 25 m depth. The phytoplankton were presumably utilizing the high nitrate concentrations below the mixed layer, although growth may have been impeded by light-limitation at these depths (Strom, pers. comm.). Similarly,

chlorophyll-a and nitrate concentrations were negligible within the mixed layer along A1 and A2, but chlorophyll-a concentrations were enhanced along the eddy boundary where the surface waters had relatively high nitrate concentrations. Very high chlorophyll-a concentrations of 12-20 $\mu\text{g l}^{-1}$ (with some patches being 40 $\mu\text{g l}^{-1}$) were present in the seasonal thermocline in a 100 km-wide band across the eddy center, where nitrate concentrations were 5-20 $\mu\text{M l}^{-1}$. A SeaWiFS image obtained on August 6, 2003 registered only the shallower, 30-km wide, portion of this band at the center of E03. Hence, ocean color sensors may substantially underestimate chlorophyll biomass within these eddies.

We estimated the de-correlation length scales along the four eddy transects using the density at 25 m and 75 m depth and the azimuthal velocity components (orthogonal to the transect) at 20 m and 200 m depth. These were identical in both surveys and were ~ 25 km for density and ~ 30 km for the azimuthal velocity.

1.3.5 ADCP (E03)

A first order description of the velocity structure is obtained from the contour plots of the azimuthal velocities between the surface and 240 m (Figure 1.10). In constructing Figure 1.10, we linearly extrapolated velocities at 20 m depth to the surface and applied a 3-point horizontal running mean (~ 5 km) to the data before contouring. The white vertical bars in each plot mark where the 32.2 isohaline intersects the sea surface and defines the horizontal boundaries of E03 used in subsequent transport estimates. Maximum azimuthal velocities were ~ 30 -40 cm s^{-1}

within 30-60 km of the eddy center and decreased to zero at the eddy center. Ladd et al. (2005a) estimated velocities to be 20-25 cm s⁻¹ based on drifters drogued at 40 m depth within 20 km of the eddy center, and these agree with the ADCP velocities near the center of E03. Vertical shears were small within the eddy, but larger at the eddy boundaries, especially over the continental slope. Indeed, the largest shear was over the continental slope along A1, where the velocity reversed from being northeastward above 50 m to southwestward below this depth.

The eddy relative vorticity (ζ), estimated from the slope of least squares fits of the azimuthal velocities against the eddy radial coordinate along each transect, was between -0.5 and $-0.9 \times 10^{-5} \text{ s}^{-1}$ and similar to ζ of Haida Eddies (Yelland and Crawford, 2005). Hence, E03 completes one rotation in ~ 1.3 -2.3 days. Within the eddy, the Rossby number (ζ/f , with $f = 1.23 \times 10^{-4} \text{ s}^{-1}$ being the Coriolis parameter at 57.5°N) was 0.04-0.07.

Although the azimuthal velocity field reflects the anticyclonic sense of eddy rotation, there were several departures from this flow structure. These include radial velocity perturbations at both 20 and 240 m depth within the eddy in both May (Figures 1.11a and b) and August (Figures 1.12a and b) that are reminiscent of the flow perturbations examined by Martin and Richards (2001). The eddy may also perturb the slope current as seen in the vectors at 20 and 240 m in both May and August. In May, there was a strong ($\sim 50 \text{ cm s}^{-1}$) and horizontally-sheared cross-slope flow over the upper 240 m (at least). The shear is such that slope waters were

deflected offshore and, nearer to the eddy, reversed to flow along the eddy boundary. The latter feature was also noted by Ladd et al. (2005b). Such eddy-slope interactions may account for the frequently observed patterns in satellite images of enhanced chlorophyll concentrations that appear to peel off the shelfbreak and stream around the upstream boundary of Yakutat Eddies (e.g., Okkonen et al., 2003). It is also consistent with the fresh water intrusion observed in the TSG track of 14 April 2003 (Figure 1.4e and the discussion in section 3.3). In August, it appears that the eddy induced a reversal in the along-slope flow at 20 m depth (which extended to about 50 m; Figure 1.10c), while the current at 240 m depth continued to the southwest. Li and Pohlmann (2002) described similar eddy-slope flow interactions in the South China Sea. Alterations in the slope flow field might have implications for the shelfbreak front. For example, changes in the shelfbreak flow will modify the bottom boundary layer and affect the structure of shelfbreak front (Gawarkiewicz and Chapman, 1992), while changes in the vertical shear of the along-slope flow will alter the stability properties of the shelfbreak front (Lozier et al., 2002).

We also examined the gradient wind balance, e.g., $\rho \partial v / \partial z (f + 2v/r) = g \partial \rho / \partial r$, where v is the azimuthal velocity, ρ the density, and r the radial coordinate. We used the ADCP estimates for v and integrated with respect to r outward from the center of the eddy. The integrations were performed at 7 depths (30-90 m) at 10 m depth intervals. We then regressed the predicted density against the observed density (expressed in σ_θ units in Figure 1.13). The predictions are quite

good, except for points along transect M1 between the shelfbreak and the eddy periphery (these points are circled in the upper left hand plot of Figure 1.13). Here the relationship falters, suggesting that other dynamics are operant. Indeed, over the slope on transect M1, the local Rossby number increased to ~ 0.3 , indicating that non-linear dynamics were important here. Within the eddy, on the other hand, the ratio of the centripetal term to the Coriolis parameter was < 0.1 and so consistent with small Rossby numbers.

Mass transports within E03 were estimated along each transect segment, with a segment being between the juncture of the two transects and the edge of the eddy (yielding four segments per survey). Transports were computed between 20 m and the depth of the 32.2 isohaline, with the calculation confined to the region of E03 between the surface outcroppings of the 32.2 isohaline. The results are given in Table 1.1, along with the transport difference between each segment. Transports varied between segments, implying vertical motions in or out of the upper 20 m of the water column of $1\text{-}3 \text{ m day}^{-1}$. These speeds are averaged over the eddy sectors defined by adjacent segments and the eddy perimeter. However, the net transport difference around the eddy was zero, indicating that mass was conserved over each survey. Moreover, there was little difference in the mean and standard deviations in the segment transports between May and August. These were $0.9 \pm 0.3 \text{ Sv}$ for both May and August. The results are consistent with the fact that the mean salinity for E03 waters with salinities ≤ 32.2 differed by only 0.03 between May and August (August fresher). In aggregate, the results suggest that there was little exchange across the lateral boundaries of the

eddy between the two surveys. We also estimated the azimuthal transport in E03 between 0 and 240 m depth assuming a cylindrical eddy confined between the surface outcrops of the 32.2 isohaline (indicated by the white vertical bars in Figure 1.10). The average of the eight May and August segment transports is ~ 5 Sv, which is $\sim 1/4$ the 0/1500 dbar mass transport of the Alaskan Stream (Musgrave et al., 1992).

1.4 Summary and Discussion

We used data from ARGO profiling floats, ship-of-opportunity thermosalinographs, vessel-mounted ADCP and SeaSoar (towed-CTD) surveys, and satellite altimetry to examine properties of two large (150-200 km diameter) “Yakutat” Eddies. Yakutat Eddies (including some eddies that form off Sitka and propagate north) differ from their GOA cousins, the Sitka and Haida eddies, in that Yakutat Eddies typically propagate westward along the continental slope of the northern GOA, whereas Sitka and Haida eddies propagate westward across the basin. Haida and Sitka eddies will therefore only affect the shelf and slope upon formation and when (and if) they collide with the western boundary. Hence, Yakutat Eddies can potentially foster substantial shelf-basin exchanges throughout their lifetime. Our observations, as well as those of Tabata (1982), Crawford (2002), Okkonen et al. (2003), Yelland and Crawford (2005), Ladd et al. (2005a) and Ladd et al. (2009), suggest that all these anticyclones share several features in common. Each forms roughly once per year (in late fall/early winter) in specific locales along the eastern GOA. Yakutat Eddies are the most northerly of the three and form in the northeast Gulf (south of Yakutat). The

eddies propagate westward at $\sim 1\text{-}2 \text{ km day}^{-1}$ and have lifetimes of up to 5 years. The surface waters of each are relatively fresh and imply that upper layer waters are drawn from the continental shelf at the time of formation. However, the dynamic and hydrographic expressions of the eddies extend to at least 2000 m depth. We find that eddy sea surface height anomalies (SSHA) may vary through time, particularly after they encounter the Alaskan Stream east of Kodiak Island. Here, the eddies may increase both their diameter and SSHA before spawning smaller eddies that propagate into the basin, where they apparently decay in less than a year.

The eddies have small Rossby numbers, but support a vigorous ($25\text{-}40 \text{ cm s}^{-1}$) anticyclonic circulation that to first order is in gradient wind balance. Our salinity and mass transport estimates for eddy waters with salinities ≤ 32.2 indicate that mass balance was achieved between May and August 2003 and that little exchange occurred between the eddy and ambient waters during this time. The net transport difference during both shipboard surveys was zero, even though convergence or divergence in portions of the eddy was implied. This result was consistent with the finding that the mean salinity changed negligibly between the May and August surveys. Although the scales of divergence and convergence could not be resolved by the ship surveys, upwelling within the eddy occurred down to at least 150 m (Ladd et al., 2005a). Upwelling from depths below the mixed layer can replenish the euphotic zone with nitrate- (and possibly iron-) enriched waters and therefore sustain biological production.

Spring and summer chlorophyll concentrations within E03 were greater than ambient basin waters. The highest chlorophyll concentrations were within the front bounding the eddy perimeter, while chlorophyll distributions in the eddy interior were patchy and perhaps associated with upwelling cells described by Martin and Richards (2001). In August, high chlorophyll concentrations were observed in the summer thermocline at or below ~25 m depth and within 50 km of the eddy center. Most of the chlorophyll was at depths deeper than space-based color sensors measure (Pegau and Potter, 2004; Stramska and Stramski, 2005 and references therein), which suggests caution must be exercised when inferring eddy biological production from surface ocean color signals alone.

As Yakutat Eddies approach the shelfbreak, the gradient wind balance is disrupted and nonlinear processes become important. The eddy's influence may substantially alter the circulation in the slope boundary flow and affect the structure and stability of the shelfbreak front. Eddy-slope current interactions may reverse the shelfbreak flow and advect slope and shelf waters around the upstream portion of the eddy's perimeter. Indeed, on one occasion we detected a 30 km-wide filament of Alaska Coastal Current water along the trailing and inshore edge of the eddy. Another example of how Yakutat Eddies may introduce shelf waters into the basin interior is illustrated by the trajectory of a satellite-tracked drifter (drogued at 9 m) superimposed on SSHA contours (Figure 1.14). The drifter exited the shelf through the mouth of Shelikof Sea Valley and into the Alaskan Stream, where it drifted southwestward along the ~1500 m-isobath. Upon encountering the eddy, the drifter was deflected

southward around the eddy perimeter at an average speed of $\sim 20 \text{ cm s}^{-1}$, but remained in contact with the edge of the eddy for only 8 days before entering the basin. The drifter trajectory and the TSG data suggest that the eddy carries shelf waters into the basin in the form of “streamers” similar to those associated with Gulf Stream rings that brush against the shelf (Evans et al., 1985; Joyce et al., 1992; Gawarkiewicz et al., 2001; Olson, 2001). While we find no evidence of eddy-ambient water exchange in the near-surface waters of Yakutat Eddies, it is clear that exchanges do occur since the ARGO profiler entered and exited from E01 on several occasions. Presumably, these were accomplished by along-isopycnal flows at depths below the permanent pycnocline.

Ladd et al. (2009) show elevated levels of iron in newly formed Yakutat, Sitka, and Haida eddies, which entrain substantial quantities of dilute shelf water upon formation. Eddy generation thus affects the shelf freshwater budget and may be an important means by which iron-enriched shelf waters are carried into the HNLC interior. However, we lack a quantitative assessment of the importance of streamers in the freshwater and nutrient budgets of the shelf and basin. If streamers contribute substantially to these budgets, then Yakutat Eddies may be a source of interannual variability for both the basin and shelf. One source of this variability is the quantity of shelf waters entrained into the eddy at formation. The other is the frequency of streamer formation and the volume of shelf water incorporated into the streamer as the eddy approaches the shelfbreak. This source of variability implies that eddy-induced

shelf-basin exchange depends crucially on the details of the eddy's trajectory and, in particular, its proximity to the shelfbreak as it propagates around the GOA.

1.5 Acknowledgments

We thank Scott Pegau for processing the fluorometer and chlorophyll data, Rachel Potter for processing the SeaSoar and ADCP data. Howard Freeland provided helpful discussions on the ARGO data set. The ARGO-data were collected and made freely available by the International ARGO Project and the national programmes that contribute to it (<http://www.argo.ucsd.edu>, <http://argo.jcommops.org>). ARGO is a pilot programme of the Global Ocean Observing System. We thank Polar Tankers and the officers and crew of the T/V Polar Alaska for installation and maintenance of the thermosalinograph (TSG) and the officers and crew of the R/V Wecoma for their assistance with SeaSoar/ADCP data collection. The latter were collected as part of the NSF-NOAA US Northeast Pacific Program (NEP) GLOBEC under grant OCE0242102 to Musgrave. Whitley and Weingartner were supported under NEP-GLOBEC grant OCE 1019078. Okkonen's support for the acquisition and analyses of the TSG data was provided by the Exxon Valdez Oil Spill Trustee Council under project 040614. Mark Johnson provided the drifter data used to construct Figure 1.14. The altimeter products were produced by Ssalto/Duacs and distributed by Aviso, with support from Cnes. We thank Nick Bond and three anonymous reviewers for helpful comments on this manuscript.

1.6 References

Aagaard, K., T.J. Weingartner, S.L. Danielson, R.A. Woodgate, G.C. Johnson, and T.E. Whitledge, 2006. Some controls on flow and salinity in Bering Strait, *Geophysical Research Letters*, 33, L19602, doi:10.1029/2006GL026612.

Ahlnäs, K., T.C. Royer, and T.H. George, 1987. Multiple dipole eddies in the Alaska Coastal Current detected with Landsat thematic mapper data. *Journal of Geophysical Research*, 92, 13041-13047.

Chapman, D.C., 2003. Separation of an advectively trapped buoyancy current at a bathymetric bend. *Journal of Physical Oceanography*, 33, 1108 – 1121.

Childers, A.R., T.E Whitledge, and D.A. Stockwell, 2005. Seasonal and interannual variability in the distribution of nutrients and chlorophyll-a across the Gulf of Alaska shelf: 1998–2000. *Deep-Sea Research II*, 52, 193–216.

Churchill, J.H., P.C. Cornillon, and G.W. Milkowski, 1986. A cyclonic eddy and shelf-slope water exchange associated with a Gulf Stream warm-core ring. *Journal of Geophysical Research*, 91(C8), 9615-9623.

Crawford, W.R., 2002. Physical characteristics of Haida Eddies. *Journal of Oceanography*, 58 (5), 703–713.

Crawford, W.R., 2005. Heat and fresh water transport by eddies in the Gulf of Alaska. *Deep-Sea Research II*, 52, 893-908.

Crawford, W.R., J.Y. Cherniawsky, and M.G.G. Foreman, 2000. Multi-year meanders and eddies in the Alaskan Stream as observed by TOPEX/Poseidon altimeter. *Geophysical Research Letters*, 27(7), 1025-1028.

Crawford, W.R., P.J. Brickley, T.D. Peterson, and A.C. Thomas, 2005. Impact of Haida Eddies on chlorophyll distribution in the eastern Gulf of Alaska. *Deep-Sea Research II*, 52, 975-989.

Evans, R.H., K.S. Baker, O.B. Brown, and R.C. Smith, 1985. Chronology of Warm-Core Ring 82B. *Journal of Geophysical Research*, 90, 8803-8811.

Foreman, M.G.G., W.R. Crawford, J.Y. Cherniawsky, R.F. Henry and M.R. Tarbotton, 2000. A high-resolution assimilating tidal model for the northeast Pacific Ocean. *Journal of Geophysical Research*, 105, 28,629-28,652.

Garvine, R.W., Wong, K.C., Gawarkiewicz, G.G., McCarthy, R.K., Houghton, R.W., Aikman III, F., 1988. The morphology of shelfbreak eddies. *Journal of Geophysical Research* 93 (C12), 15593–15607.

Garvine, R.W., K. Wong, and G.G. Gawarkiewicz, 1989. Quantitative properties of shelfbreak eddies. *Journal of Geophysical Research*, 94(C10), 14475-14483.

Garfield, N. and D.L. Evans, 1987. Shelf water entrainment of Gulf Stream warm core rings. *Journal of Geophysical Research*, 92, 13003-13012.

Gawarkiewicz, G.G., and D.C. Chapman, 1992. The role of stratification in the formation and maintenance of shelf-break fronts. *Journal of Physical Oceanography*, 22(7), 753-772.

Gawarkiewicz, G.G., F. Bahr, R.C. Beardsley, and K.H. Brink, 2001. Interaction of a slope eddy with the shelfbreak front in the middle Atlantic Bight. *Journal of Physical Oceanography*, 31, 2783–2796.

Hooker, S.B. and J.W. Brown, 1994. Warm core ring dynamics derived from satellite imagery. *Journal of Geophysical Research*, 99(C12), 25181-25194.

Johnson, W.R., T.C. Royer, and J.L. Luick, 1988. On the seasonal variability of the Alaska Coastal Current. *Journal of Geophysical Research*, 93(C10), 12423-12437.

Johnson, K., L.A. Miller, N.E. Sutherland and C.S. Wong, 2005. Iron transport by mesoscale Haida eddies in the Gulf of Alaska. *Deep-Sea Research II*, 52(7-8), 933-954.

Joyce, T.M., 1984. Velocity and hydrographic structure of a Gulf Stream Warm-Core Ring. *Journal of Physical Oceanography*, 14, 936-947.

Joyce, T.M. and M.A. Kennelly, 1985. Upper-Ocean Velocity structure of Gulf Stream Warm-Core Ring 82B. *Journal of Geophysical Research*, 90(C5), 8839-8844.

Joyce, T.M., J.K. Bishop, and O.B. Brown, 1992. Observations of offshore shelf water transport induced by a warm core ring. *Deep-Sea Research*, 39(1), S97-S113.

Klinger, B.A., 1994. Inviscid current separation from rounded capes. *Journal of Physical Oceanography*, 24, 1805 – 1811.

Ladd, C., N.B. Kachel, C.W. Mordy, and P.J. Stabeno, 2005a. Observations from a Yakutat Eddy in the Northern Gulf of Alaska. *Journal of Geophysical Research*, 110, C03003, doi: 10.1029/2004JC002710.

Ladd, C., P.J. Stabeno, and E.D. Cokelet, 2005b. A note on cross-shelf exchange in the northern Gulf of Alaska. *Deep-Sea Research II*, 52, 667-679.

Ladd, C., C.W. Mordy, N.B. Kachel, and P.J. Stabeno, 2007. Northern Gulf of Alaska Eddies and Associated Anomalies. *Deep-Sea Research I*, 54, 487-509.

Ladd, C., W.R. Crawford, C.E. Harpold, W.K. Johnson, N.B. Kachel, P.J. Stabeno, F. Whitney, 2009. A synoptic survey of young mesoscale eddies in the Eastern Gulf of Alaska, *Deep Sea Research. II*, 56 (24), 2460-2473.

Li, L. and T. Pohlmann, 2002. The South China Sea Warm-Core Ring 94S and its influence on the distribution of chemical tracers. *Ocean Dynamics*, 52, 116-122.

Lozier, M.S., M.S.C. Reed, and G.G. Gawarkiewicz, 2002. Instability of a shelfbreak front. *Journal of Physical Oceanography*, 32, 924 - 944.

Mackas, D.L. and M.D. Galbraith, 2002. Zooplankton distribution and dynamics in a North Pacific eddy of coastal origin: 1. Transport and loss of continental margin species. *Journal of Oceanography*, 58 (5), 725–738.

Martin, J., R. Gordon, S. Fitzwater, and W. Broenkow, 1989. VERTEX: phytoplankton/iron studies in the Gulf of Alaska. *Deep-Sea Research*, 36 (5A), 649–680.

Martin, A.P. and K.J. Richards, 2001. Mechanisms for vertical nutrient transport within a North Atlantic mesoscale eddy. *Deep-Sea Research II*, 48, 757-773.

McGillicuddy, D.J., A.R. Robinson, and J.J. McCarthy, 1995. Coupled physical and biological modeling of the spring bloom in the North Atlantic (I): three dimensional bloom and post-bloom processes. *Deep-Sea Research I*, 42, 1359 – 1398.

Melsom, A., S.D. Meyers, H.E. Hurlburt, J.E. Metzger, and J.J. O'Brien, 1999. ENSO effects on Gulf of Alaska eddies. *Earth Interactions*, 3, 1-30.

Meyers, S.D. and S. Basu, 1999. Eddies in the eastern Gulf of Alaska from TOPEX/POSEIDON altimetry. *Journal of Geophysical Research*, 104(C6), 13,333–13,343.

Musgrave, D.L., T.J. Weingartner, and T.C. Royer. 1992. Circulation and hydrography in the northwestern Gulf of Alaska. *Deep-Sea Research*, 39, 1499-1519.

Okkonen, S.R., G.A. Jacobs, E.J. Metzger, H.E. Hurlburt, and J.F. Shriver, 2001. Mesoscale variability in the boundary currents of the Alaska Gyre. *Continental Shelf Research*, 21, 1219-1236.

Okkonen, S.R., T.J. Weingartner, S.L. Danielson, D.L. Musgrave, and M. Schmidt, 2003. Satellite and hydrographic observations of eddy-induced shelf-slope exchange in the northwestern Gulf of Alaska. *Journal of Geophysical Research*, 108(C2), 3033, doi:10.1029/2002JC001342.

Okkonen, S.R., D.L. Cutchin, and T.C. Royer, 2005. Seasonal variability of near-surface hydrography and frontal features in the northern Gulf of Alaska and Prince William Sound. *Geophysical Research Letters*, 32, L11611.

Olson, D.B., 1991. Rings in the Ocean. *Annual Review of Earth and Planetary Sciences*, 19, 283-311.

Olson, D.B., 2001. Biophysical dynamics of western transition zones: a preliminary synthesis. *Fisheries Oceanography* 10 (2), 133-150.

Olson, D.B., R.W. Schmitt, M. Kennelly, and T.M. Joyce, 1985. A two-layer diagnostic model of the long term physical evolution of Warm-Core Ring 82B. *Journal of Geophysical Research*, 90(C5), 8813-8822.

Pegau, S. and R. Potter, 2004. Visible remote sensing of the Gulf of Alaska. Gulf Ecosystem Monitoring project G030685 final report, 51 pp.

Royer, T.C., 1981. Baroclinic transport in the Gulf of Alaska, Part II: Freshwater driven coastal current. *Journal of Marine Research*, 39, 251-266.

Royer, T.C., 1982. Coastal freshwater discharge in the Northeast Pacific. *Journal of Geophysical Research*, 87, 2017-2021.

Schumacher, J.D., and R.K. Reed, 1980. Coastal flow in the northwest Gulf of Alaska: the Kenai Current. *Journal of Geophysical Research*, 85, 5580-6688.

Schumacher, J.D., P.J. Stabeno, and A.T. Roach, 1989. Volume transport in the Alaska Coastal Current. *Continental Shelf Research*, 9, 1071-1083.

Stabeno, P.J., R.K. Reed and J.D. Schumacher, 1995. The Alaska Coastal Current: continuity of transport and forcing. *Journal of Geophysical Research*, 100, 2477-2485.

Stabeno, P.J., N.A. Bond, A.J. Hermann, N.B. Kachel, C.W. Mordy, J.E. Overland, 2004. Meteorology and oceanography of the northern Gulf of Alaska. *Continental Shelf Research*, 24, 859-897.

Stramska, M. and D. Stramski, 2005. Effects of a nonuniform vertical profile of chlorophyll concentration on remote-sensing reflectance of the ocean. *Applied Optics*, 44, 1735-1747.

Swaters, G.E., and L.A. Mysak, 1985. Topographically-induced baroclinic eddies near a coastline, with application to the Northeast Pacific. *Journal of Physical Oceanography*, 15, 1470-1485.

Tabata, S., 1982. The anticyclonic, baroclinic eddy off Sitka, Alaska, in the northeast Pacific Ocean. *Journal of Physical Oceanography*, 12(11), 1260-1282.

Thomson, R.E. and J.F.R. Gower, 1998. A basin-scale oceanic instability event in the Gulf of Alaska. *Journal of Geophysical Research*, 103 (C2), 3033–3040.

Weingartner, T.J., K. Coyle, B. Finney, R. Hopcroft, T. Whitledge, R. Brodeur, M. Dagg, E. Farley, D. Haidvogel, L. Haldorson, A. Hermann, S. Hinckley, J. Napp, P. Staben, T. Kline, C. Lee, E. Lessard, T. Royer, and S. Strom, 2002. The Northeast Pacific GLOBEC Program: Coastal Gulf of Alaska. *Oceanography*, 15, 48 – 63.

Weingartner, T.J., S.L. Danielson, and T.C. Royer, 2005. Freshwater Variability and Predictability in the Alaska Coastal Current. *Deep-Sea Research II*, 52, 169-191.

Whitney, F. and M. Robert, 2002. Structure of Haida eddies and their transport of nutrient from coastal margins into the NE Pacific Ocean. *Journal of Oceanography*, 58 (5), 715–723.

Williams, W.J., T. J. Weingartner, and A. Hermann, 2007. Idealized three-dimensional modeling of seasonal variation in the Alaska Coastal Current. *Journal of Geophysical Research*, 112, C07001; doi:10.1029/2005JC003285.

Yankovsky, A.E., and D.C. Chapman, 1997. Anticyclonic eddies trapped on the continental shelf by topographic irregularities. *Journal of Geophysical Research*, 102(C3), 5625-5640.

Yelland, D., and W.R. Crawford, 2005. Currents in Haida Eddies. *Deep-Sea Research II*, 52, 875-892.

1.7 Tables

Table 1.1: Eddy transport estimates. Transport and transport difference estimates between 20 m and the depth of the 32.2 isohaline for the May and August E03 surveys. Transport (in Sv) estimates between the intersection of the transects and the edge of the eddy are denoted by regular font. Transport differences between segments (in Sv) are italicized. Positive (negative) transport differences imply divergence (convergence). Arrows indicate the circulation pathway between SeaSoar segments. The net transport difference within the eddy is indicated in bold (Net D/C) listed in the central box for each survey.

MAY SURVEY			AUGUST SURVEY		
M1 (inshore) 0.6	→ <i>Divergent</i> +0.2	M2 (offshore) 0.8	A2 (inshore) 1.2	→ <i>Convergent</i> -0.2	A1 (offshore) 1.0
↑ <i>Convergent</i> -0.2	Net D/C 0	<i>Divergent</i> +0.5 ↓	↑ <i>Divergent</i> +0.5	Net D/C 0	<i>Convergent</i> -0.3 ↓
M2 (inshore) 0.8	← <i>Convergent</i> -0.5	M1 (offshore) 1.3	A1 (inshore) 0.7	← <i>Divergent</i> +0.0	A2 (offshore) 0.7

1.8 Figures

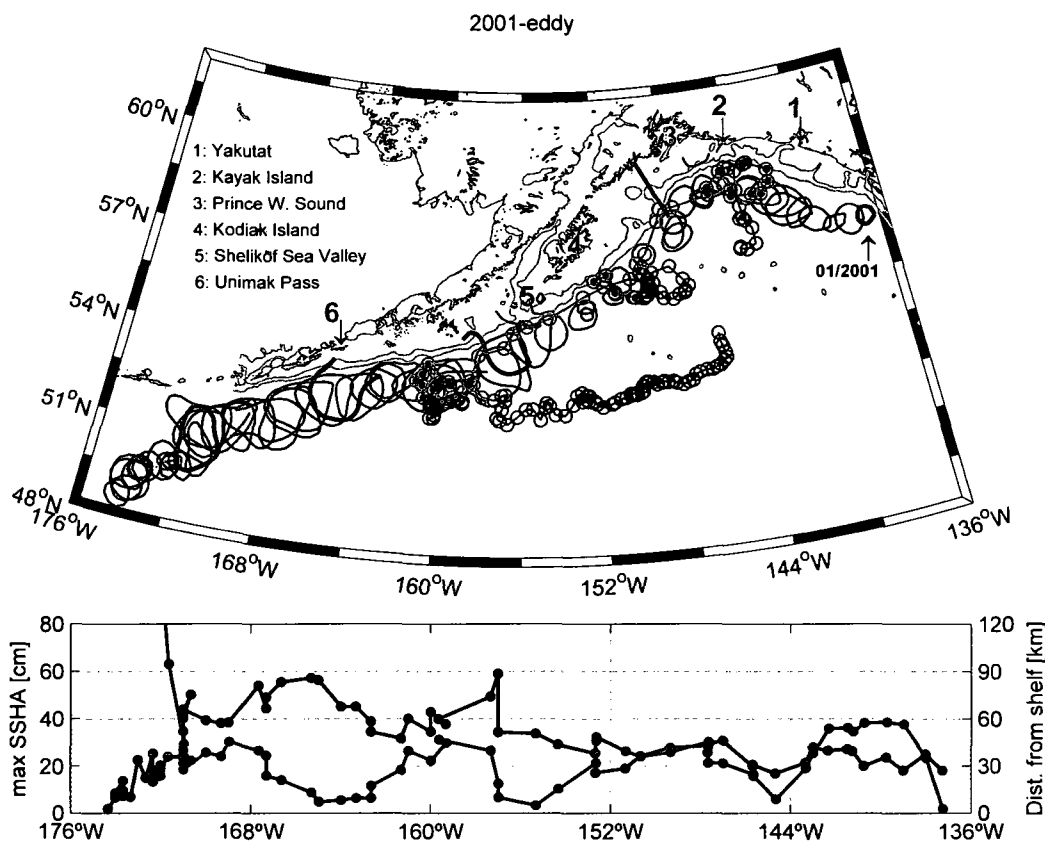


Figure 1.1: Trajectory of the 2001-eddy. The upper panel shows profile locations of ARGO float 49070 (red) relative to the altimetry of E01. Green filled stations indicate eddy profiles used herein. The black and blue lines are the 15 cm SSHA contour of E01 at monthly intervals beginning with its formation in January 2001 near southeast Alaska to its decay at $\sim 176^\circ\text{W}$ in April 2006. The blue contours indicate the January position of E01 at the beginning of each year. Grey contours depict the 200 m and 1500 m isobaths. Numbered locations are geographical features mentioned in the text and the legend included in the figure. The lower panel is the monthly maximum SSHA of E01 (black) and the minimum distance between the 10 cm SSHA isopleth and the 200 m isobath (blue) as a function of longitude.

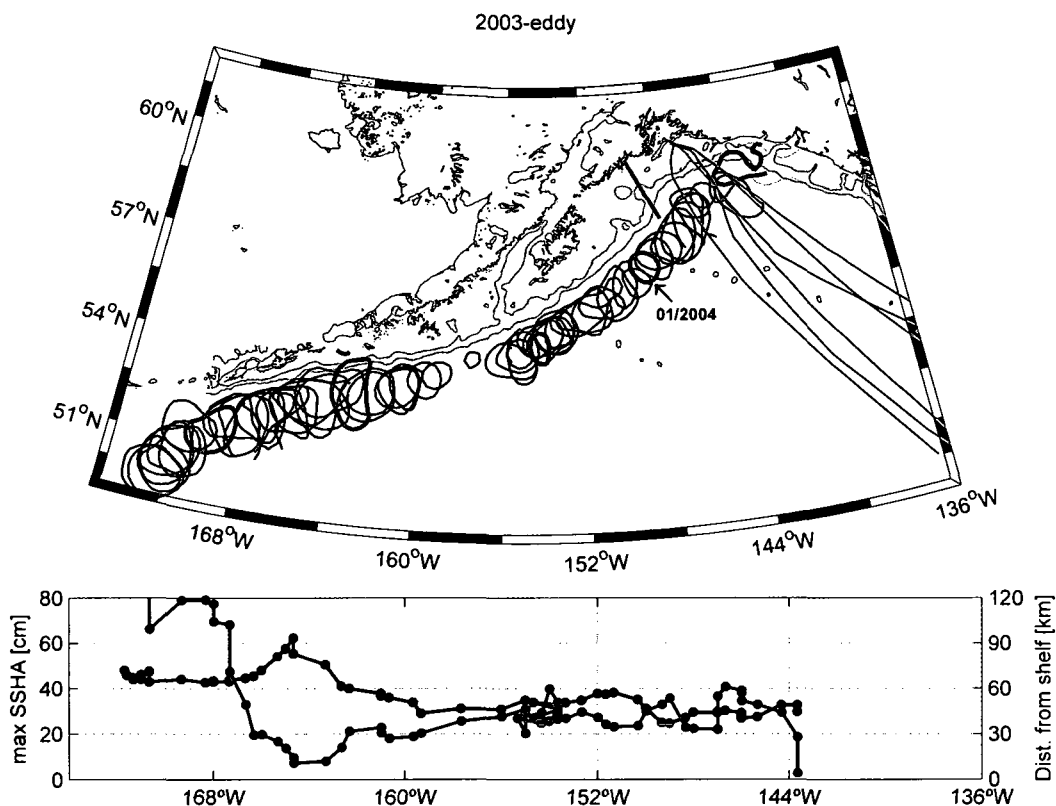


Figure 1.2: Trajectory of the 2003-eddy. The upper panel shows the trajectory of E03 based on the 15 cm SSHA contour along the continental slope of the northern GOA from its formation in January 2003 to its location at $\sim 171.7^\circ\text{W}$ on 13 October 2007. Blue contours are the position of E03 in January of each year. The six tanker transects (red lines) were made between February and April 2003. Grey contours depict the 200 m and 1500 m isobaths. The lower panel is the monthly maximum SSHA of E01 (black) and the minimum distance between the 10 cm SSHA isopleth and the 200 m isobath (blue) as a function of longitude.

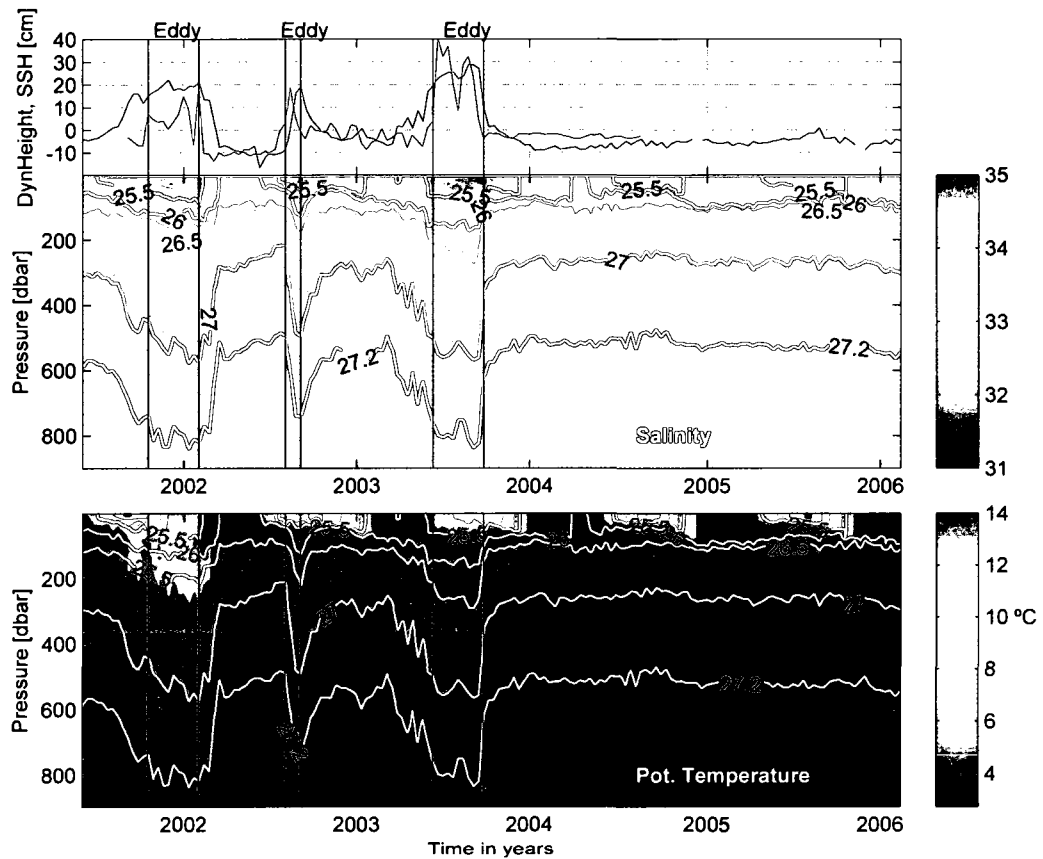


Figure 1.3: Salinity, temperature and dynamic height of ARGO float 49070. The upper panel compares the 0/900 dbar dynamic height (blue) calculated from ARGO float 49070 with the SSHA (red) obtained from AVISO and interpolated onto the profiler's position. The middle and lower panels show salinity and temperature as a function of pressure and time from the profiler. Representative σ_θ isopleths (white) are superimposed on the salinity and temperature panels. The black vertical lines bound the time periods of encounters between the profiler and E01.

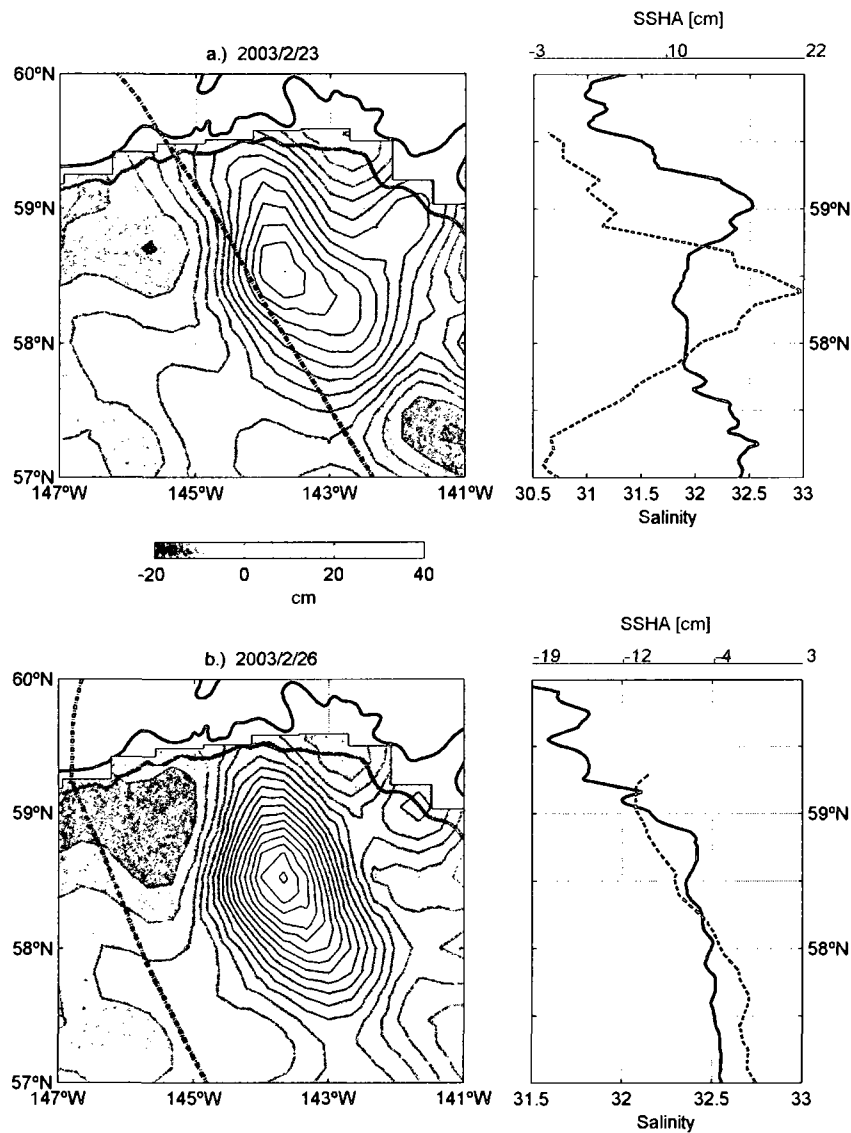


Figure 1.4: Tanker cruise tracks and surface salinity. The left panels are SSHA contour maps associated with E03 relative to the tanker cruise tracks (black dotted line) on a) 02/23/2003, b) 02/26/2003, c) 03/13/2003, d) 03/19/2003, e) 04/14/2003, f) 04/19/2003. Bold black contours show the 200 m and 1500 m isobaths. The right panels are surface salinity (black) and SSHA (grey) plotted against latitude along the tanker cruise tracks. SSHA contours are not shown on the shelf.

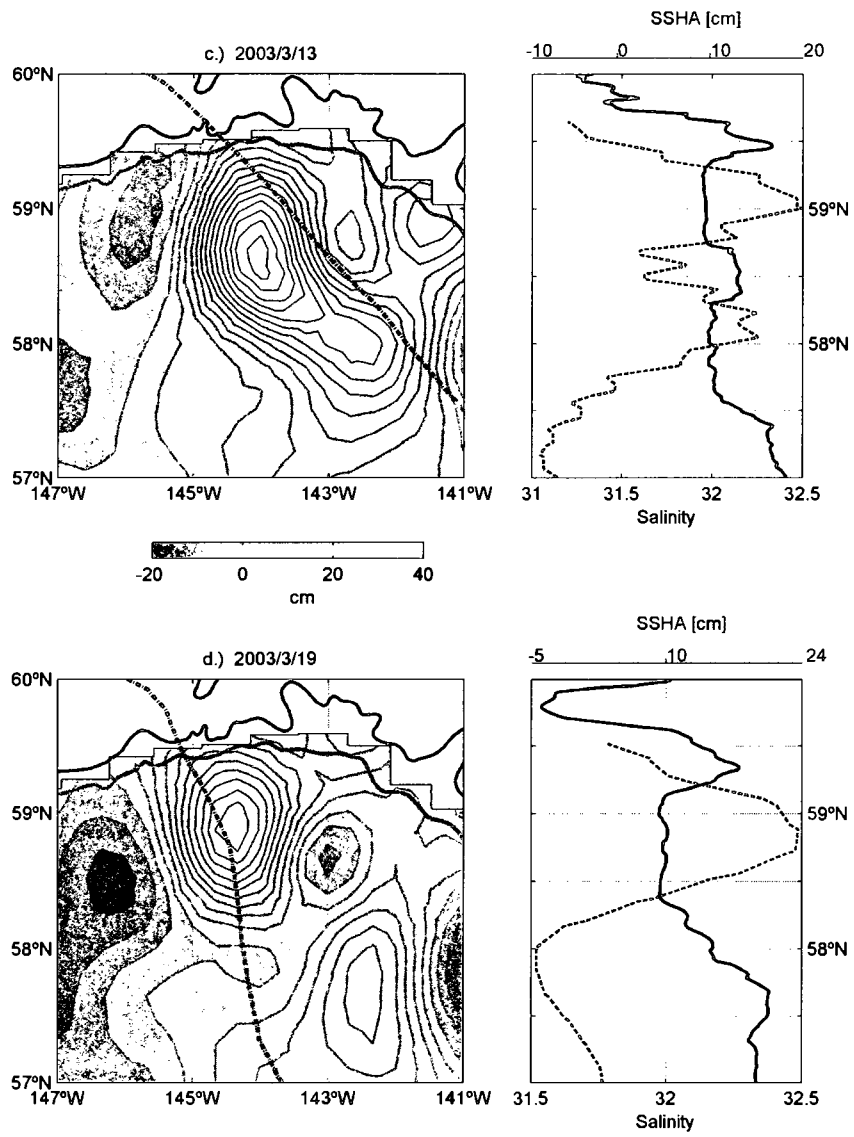


Figure 1.4. continued

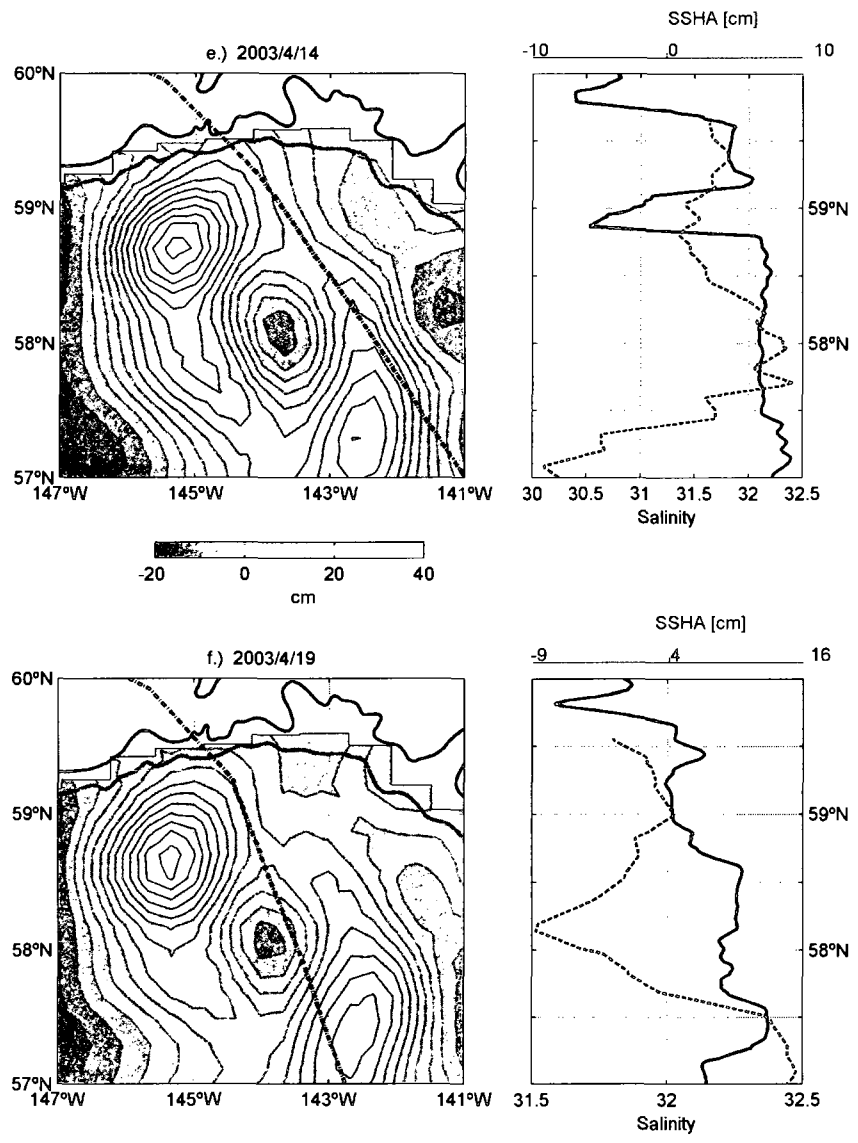


Figure 1.4. continued

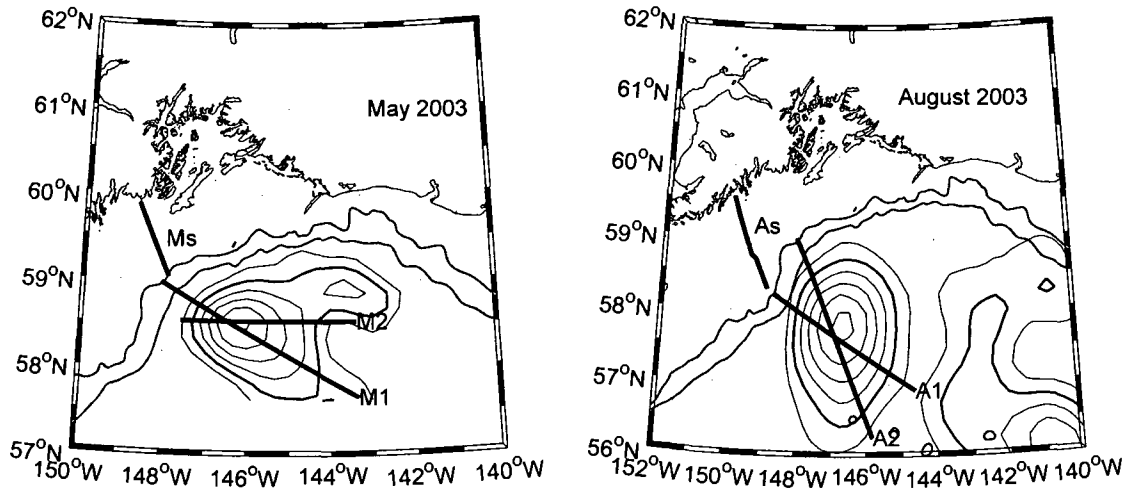


Figure 1.5: Eddy survey cruise tracks in May and August 2003. Maps of the northern GOA with SSHA contours showing the location of E03 on 17 May 2003 (left) and 6 August 2003 (right) at the time of the May and August SeaSoar surveys. SSHA contour intervals are 5 cm and the bold line is the 5 cm SSHA contour. The continental slope is marked by the 200 m and 1500 m isobaths (grey). The transects across E03 in May (M1 and M2) and August (A1 and A2) are shown along with the May (Ms) and August (As) shelf transects.

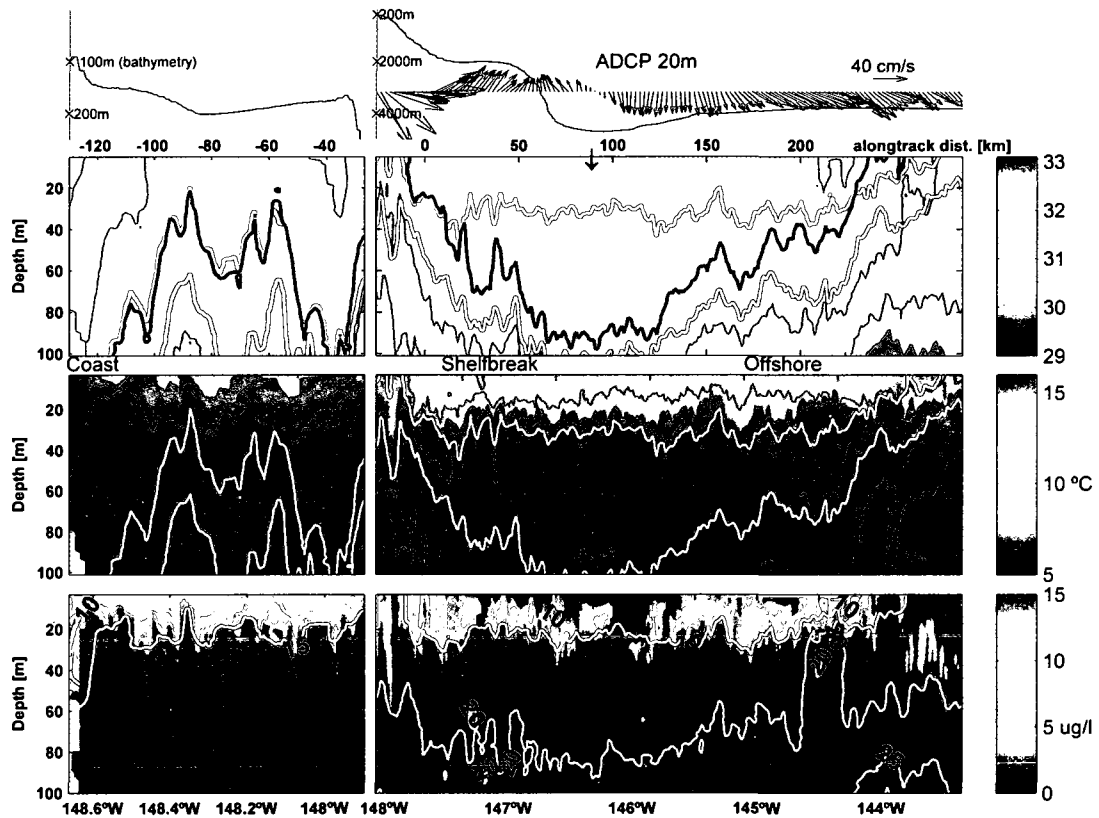


Figure 1.6: SeaSoar eddy survey May transect 1. The topmost panel shows ADCP velocities at 20 m and bottom depths along the Ms and M1 transects. (Note the change in depth scale between the shelf and eddy transects.) The remaining panels are salinity (top), temperature (middle) and chlorophyll-a concentration ($\mu\text{g l}^{-1}$; bottom) contoured against distance (and longitude) from the beginning of transect M1. The 32.2 isohaline is delineated by the bold black line. The 25.3 and 25.4 σ_{θ} isopycnals (white) are superimposed on the salinity and temperature plots. Nitrate isopleths (white, in $5 \mu\text{M l}^{-1}$ increments) are superimposed on the chlorophyll plot. Figure 1.5 shows locations of these transects in plan view. The small arrow in the salinity panel points to the location of the estimated eddy center.

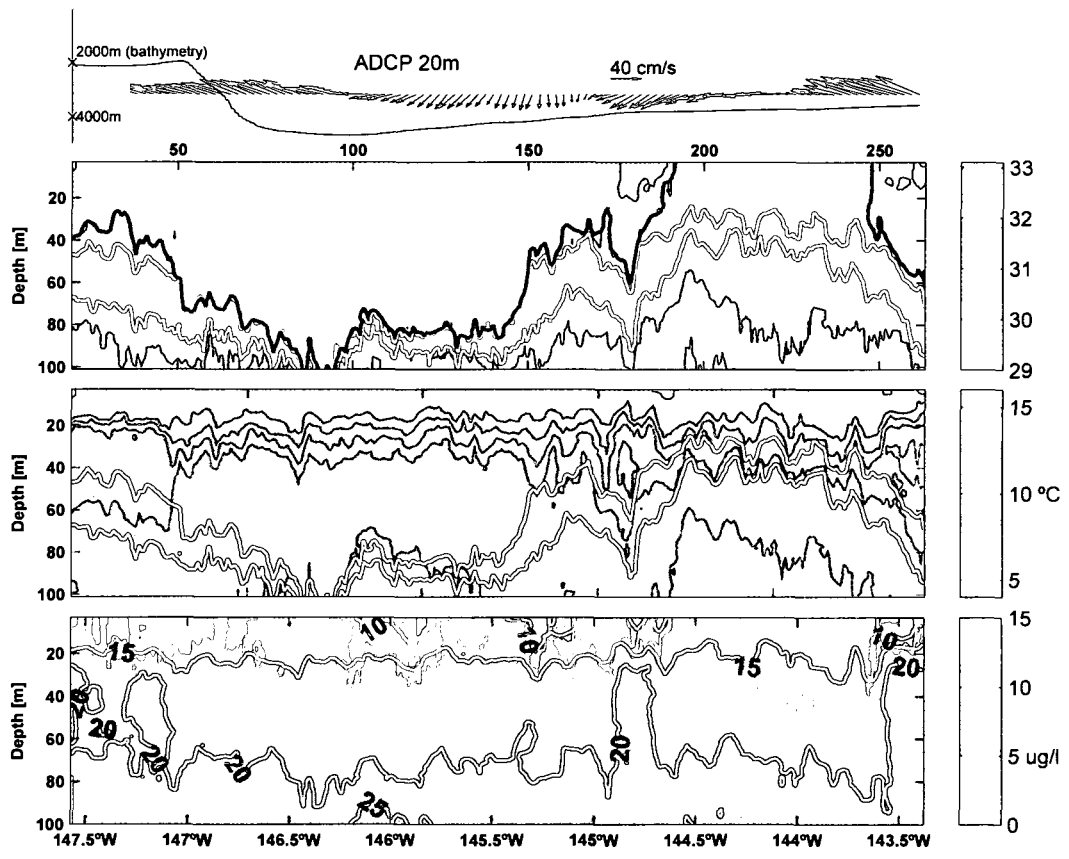


Figure 1.7: SeaSoar eddy survey May transect 2. Same as Figure 1.6 but for transect M2.

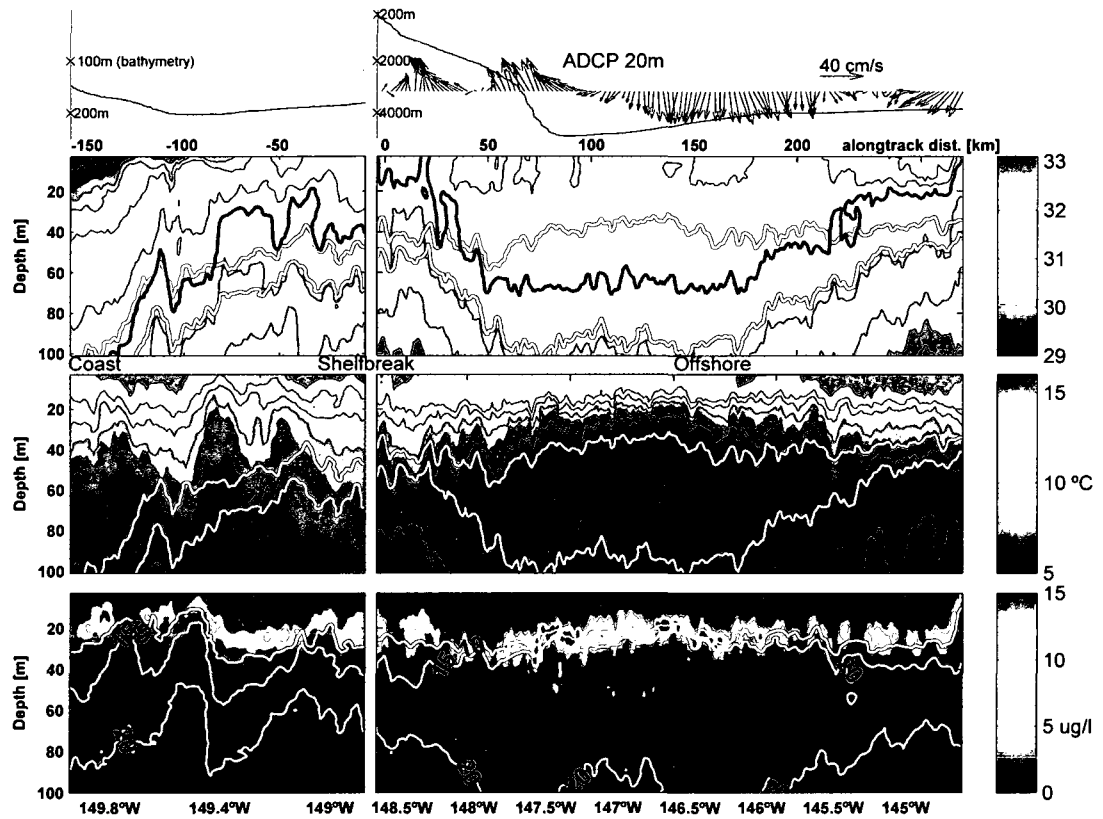


Figure 1.8: SeaSoar eddy survey August transect 1. Same as Figure 1.6 but for transects As and A1. White contours in the salinity and temperature panels denote the 25.2 and 25.4 σ_θ isopycnals.

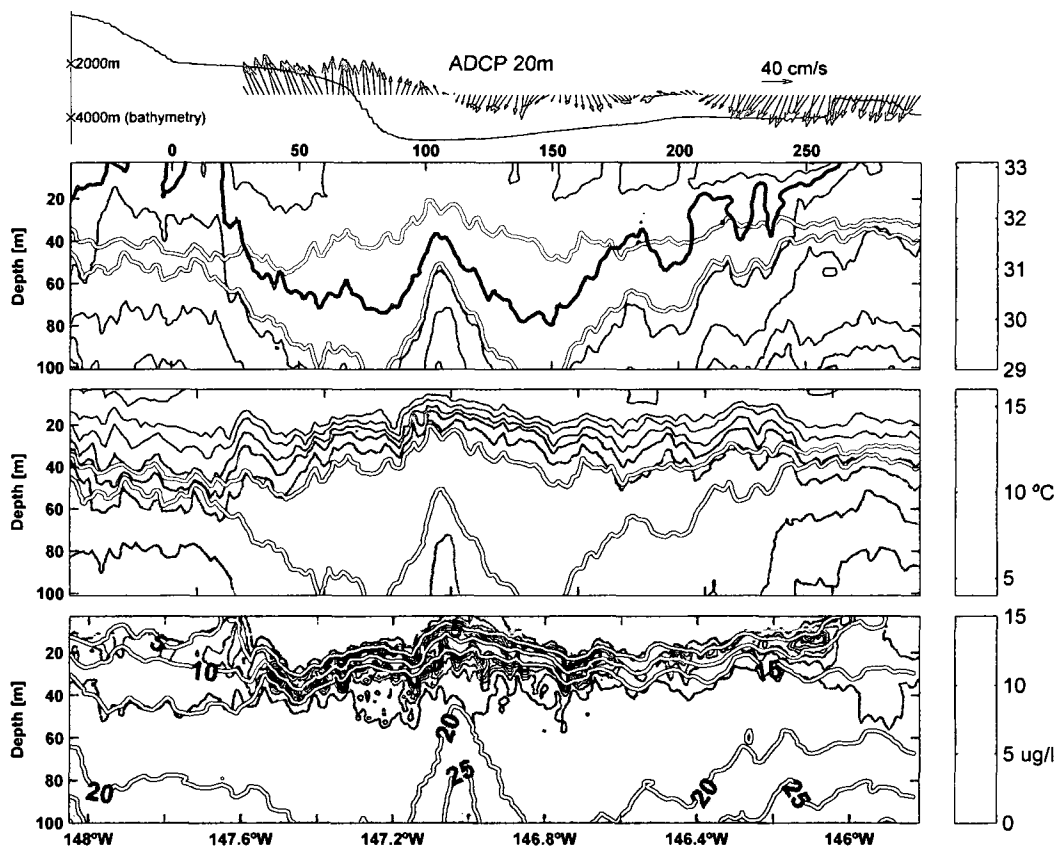


Figure 1.9: SeaSoar eddy survey August transect 2. Same as Figure 1.8 but for transect A2.

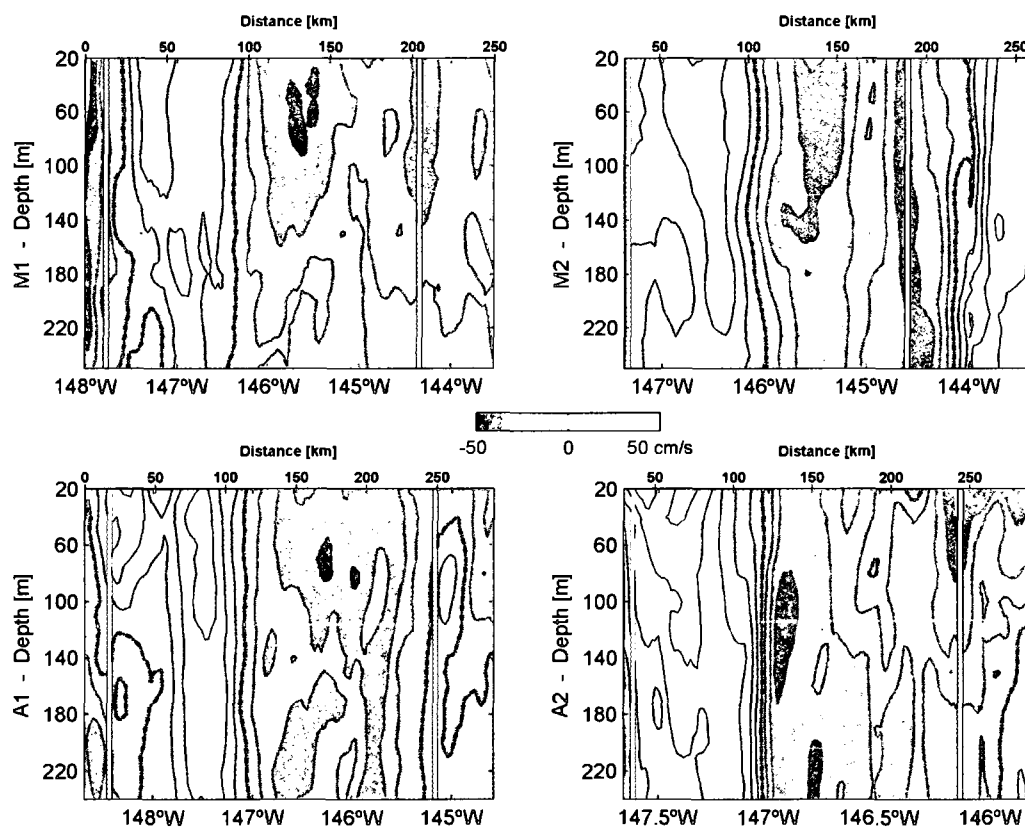


Figure 1.10: Azimuthal eddy velocities. The panels show the azimuthal velocities (cm s^{-1}) along the transects in May (M1 in upper left, M2 in upper right) and in August (A1 in lower left, A2 in lower right). Distances are from the beginning of each transect, similar to the along-track distance used in Figures 1.6-9. The white vertical lines are the eddy's boundary, estimated from the outcropping of the 32.2 isohaline.

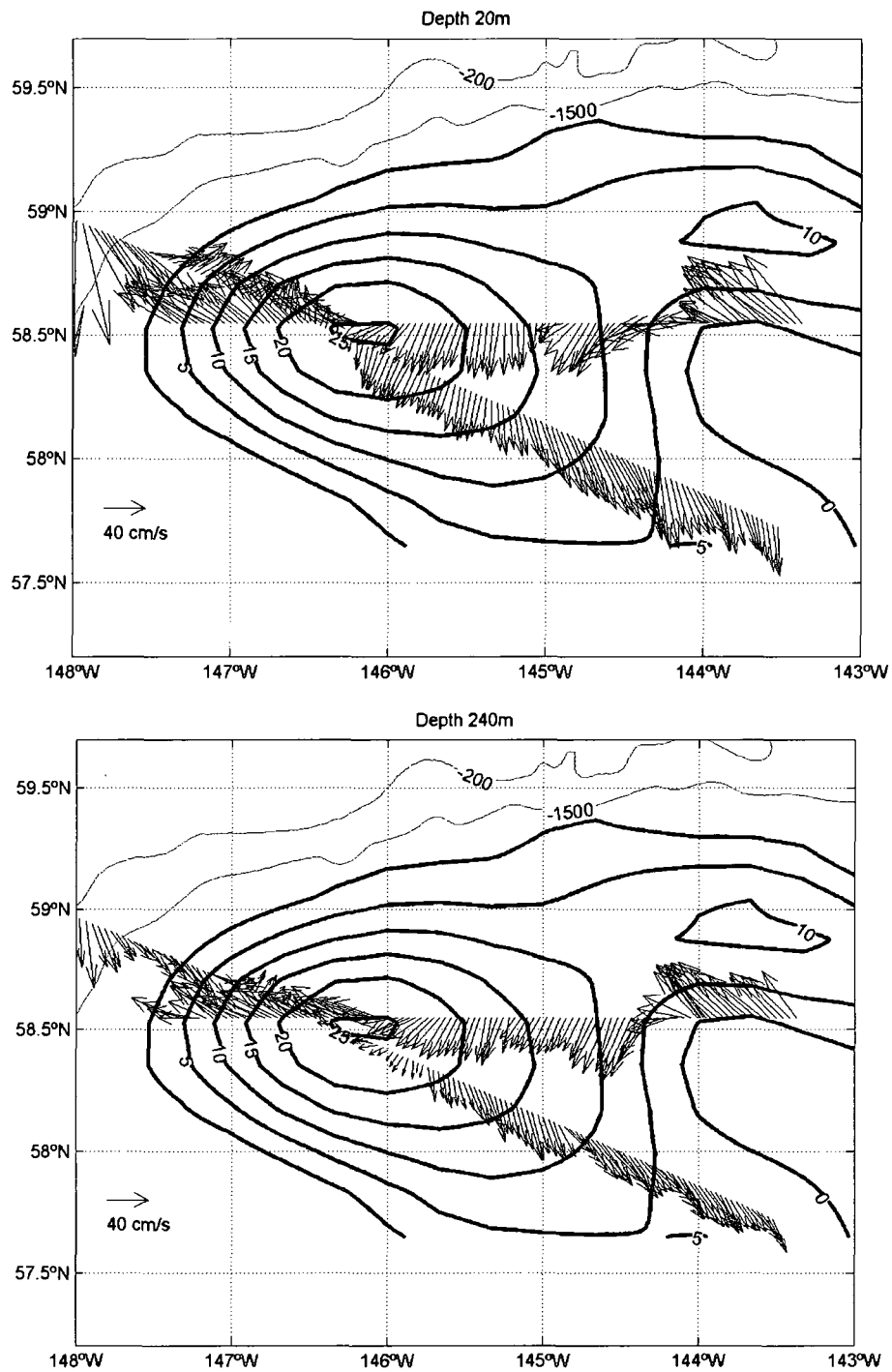


Figure 1.11: May eddy velocities. Contours of SSHA and ADCP vectors at a) 20 m and b) 240 m from May overlaid on the 200 m and 1500 m isobaths. The 40 cm s^{-1} scale arrow is in the lower left of each figure. The portion of transect M1 where the gradient wind balance fails is denoted by the circle.

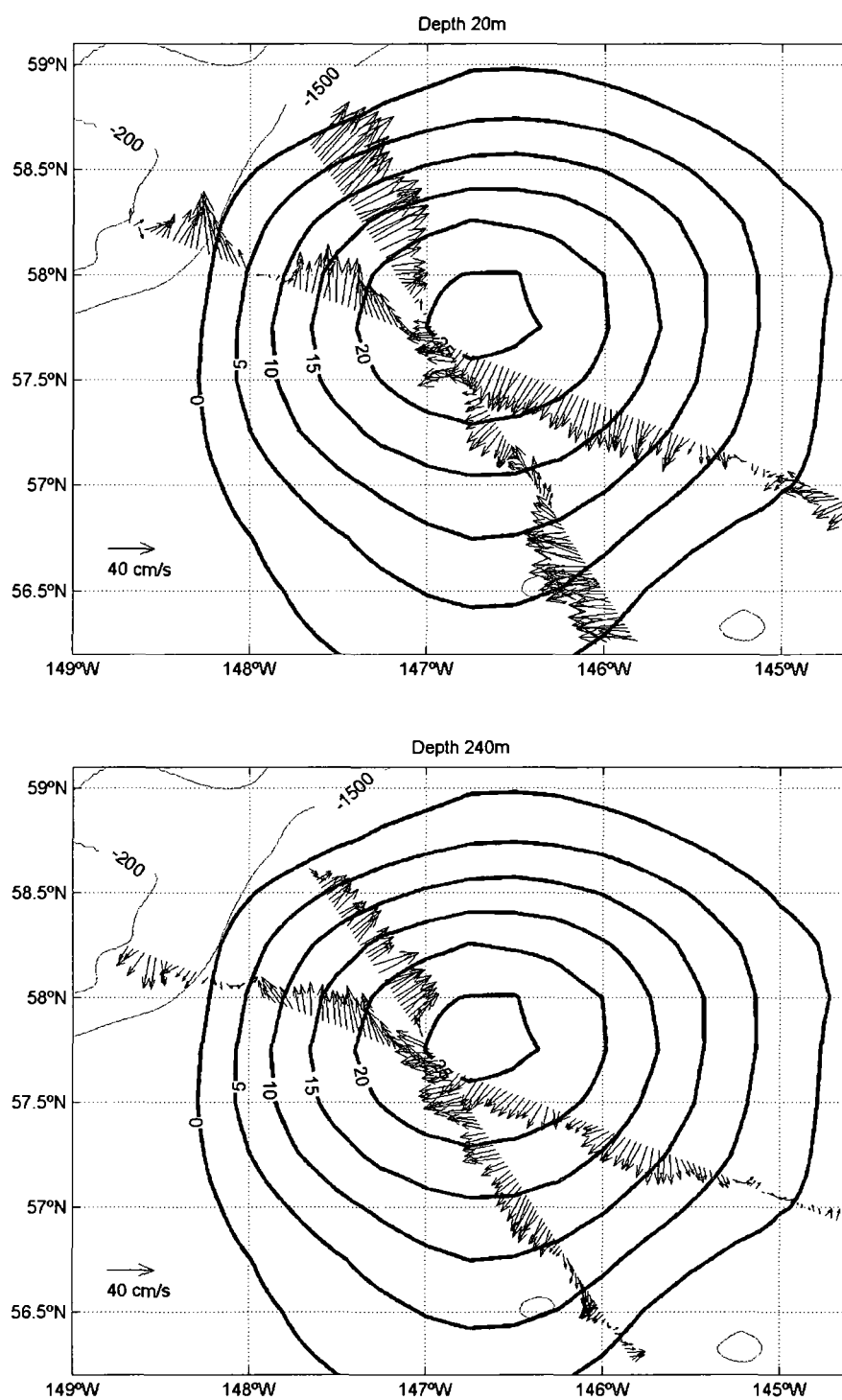


Figure 1.12: August eddy velocities. Contours of SSHA and ADCP vectors at a) 20 m and b) 240 m from August overlaid on the 200 m and 1500 m isobaths. The 40 cm s^{-1} scale arrow is in the lower left of each figure.

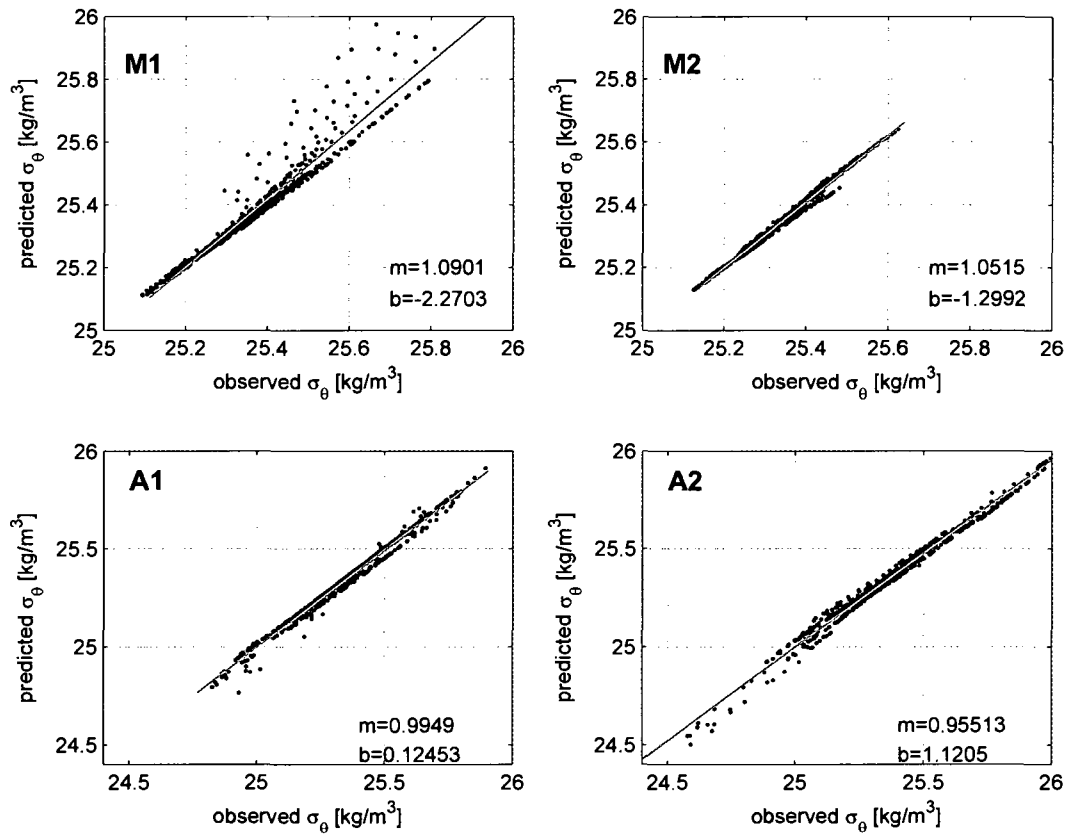


Figure 1.13: Linear regressions of sigma-theta. Linear regressions of observed σ_θ versus predicted σ_θ based on the gradient wind balance for each SeaSoar transects: M1 (upper left), M2 (upper right), A1 (lower left) and A2 (lower right). The circled points in the M1 regression are for points that are between the edge of E03 and the continental slope as marked by the circle in Figure 1.11.

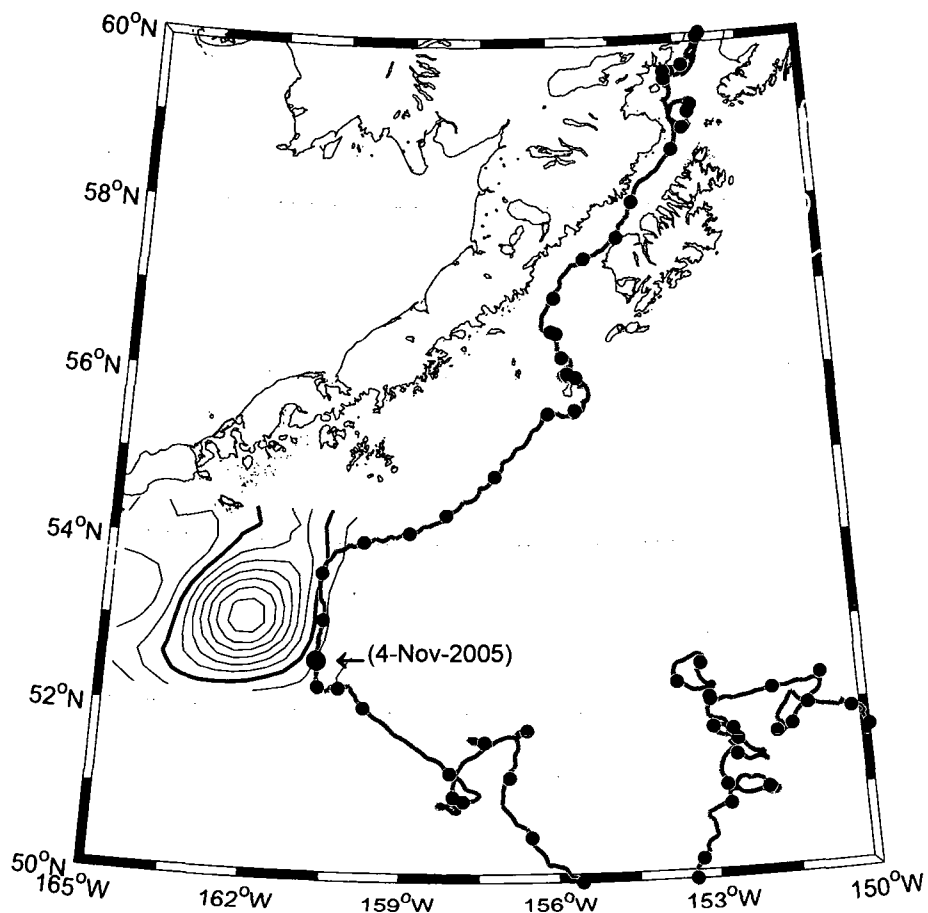


Figure 1.14: Drifter trajectory and eddy. The trajectory of a satellite tracked drifter drogued at 9 m depth that was released in Cook Inlet on August 22, 2005. Black dots mark locations at noon every second day. The drifter was located on the southeast edge of the eddy on November 4, 2005 as indicated by the arrow. SSHA contours are at 5 cm intervals with the bold contour indicating the 5 cm SSHA.

Chapter 2 On the nature of winter cooling and the recent temperature shift on the northern Gulf of Alaska shelf¹

Abstract

In spring 2006/07 northern Gulf of Alaska (GOA) shelf waters were $\sim 1.5^{\circ}\text{C}$ below average throughout the ~ 250 m deep shelf and the salinity-dependent winter stratification was anomalously weak due to above (below) average surface (bottom) salinities. Spring 2007/08 temperatures were also $\sim 1.5^{\circ}\text{C}$ below average, but the anomalies were confined to the upper 100 m due to moderate salt-stratification. Shelf temperatures in these two years were amongst the lowest observed since the early 1970s, thus interrupting a ~ 30 -year warming trend. We examined winter cooling processes using historical CTD and mooring data from hydrographic station GAK1. The 2006/07 cooling was associated with anomalously strong atmospheric heat loss in November 2006 and March 2007 and below average fall runoff. This weakened winter stratification and allowed the late cooling to penetrate throughout the water column. In 2007/08, early winter cooling was weak, fall runoff large, and stratification moderate at 100 m so that spring temperature anomalies were trapped to the upper 100 m. Analysis of the 40-year GAK1 CTD record indicates that winter averaged air-sea heat

¹ Janout, M.A., T.J. Weingartner, T.C. Royer, and S.L. Danielson, On the nature of winter cooling and the recent temperature shift on the northern Gulf of Alaska shelf, accepted for publication at the *Journal of Geophysical Research*

flux and salinity stratification anomalies explain 81% of the variation in deep (100-250 m) GOA temperatures. Although the timing and magnitude of winter runoff influences the shelf temperature distribution, temperature anomalies are a consequence of three-dimensional circulation and mixing processes. These involve the complex, but poorly understood, interplay amongst the air-sea heat flux, ocean heat flux convergences, the stabilizing influence of runoff, and the destabilizing effects of cooling, vertical mixing, and the wind driven cross-shelf buoyancy flux.

2.1 Introduction

The northern Gulf of Alaska (GOA) shelf is wide (~150 km) and deep (150-260 m) and supports a productive ecosystem and important commercial fisheries. Atmospheric conditions are governed by the strength and position of the Aleutian Low, which results in predominantly cyclonic (downwelling-favorable) winds around the GOA [Wilson and Overland, 1986] and heavy coastal precipitation. The coastal circulation is governed by the wind- and freshwater-driven Alaska Coastal Current (ACC) [Schumacher and Reed, 1980; Royer, 1981; Johnson et al., 1988; Schumacher et al., 1989; Stabeno et al., 1995; Stabeno et al., 2004; Weingartner et al., 2005]. The ACC, which has remarkable seasonal and interannual variability, transports heat and freshwater along the coast from the British Columbian shelf to the northern GOA and into the Bering Sea [Royer, 1981; Weingartner et al., 2005]. Density variations in this sub-polar ocean are primarily salinity-dependent [Royer, 1982], especially from fall through spring, so that stratification and the onset of the spring bloom are strongly

influenced by the large coastal runoff. Coastal discharge increases in spring from snowmelt and is at maximum in fall, when precipitation and runoff are greatest [Royer, 1982]. Nutrients are supplied to the deeper GOA shelf during summer when downwelling relaxes, and are vertically mixed in winter whereupon they are available for the spring bloom [Childers et al., 2005].

In spring 2007, oceanographic monitoring over the entire water column of the northern GOA shelf revealed the lowest temperatures observed in ~35 years and anomalously weak stratification. The cool signal persisted through fall 2007, and developed anew in mid/late winter 2008, although at that time the largest negative temperature anomalies were confined to the upper 50 m. This recent cooling interrupts long-term trends of increasing stratification, warming ($\sim 0.8^{\circ}\text{C}$ in 30 years) and freshening (~ 0.1 salinity decrease over 30 years) [Royer, 2005; Royer and Grosch, 2006] of the GOA's upper layer (0-100 m). Moreover, recent temperatures resemble those of the early 1970s, prior to the 1976/77 regime shift [Hare and Mantua, 2000]. Herein we describe the evolution of shelf temperatures in the winters of 2006/07 and 2007/08 and undertake a broader review of the processes that control winter cooling on the northern GOA shelf.

The paper is organized as follows. After presenting the data and the methods in section 2.2, we describe the recent cooling on the northern GOA shelf (section 2.3.1), examine the onset of the cooling and the evolution of thermohaline properties in 2006/07 in comparison to other recent years (sections 2.3.2 and 2.3.3), and then place

these findings in a broader climatological context (sections 2.3.4-6). Section 2.4 summarizes the paper.

2.2 Data and methods

We use hydrographic (temperature and salinity) data from along the Seward Line, but primarily from station GAK1 (~59.8°N, 149.5°W), which is the innermost station on this line (Figure 2.1). This 263-m deep station (<http://www.ims.uaf.edu/gak1/>) has been occupied on a quasi-monthly basis since 1970. The record consists of ~460 profiles, although there are fewer observations from the early 1970s and 1980s (Figure 2.2). The Seward Line was occupied repeatedly from 1997–2004 as part of the NOAA-NSF funded NEP-GLOBEC program (1997–2004, Weingartner et al., 2002), and since 2005 with support from the North Pacific Research Board for biannual (May and September) cruises. Prior to the mid-1980s, the accuracies in temperature and salinity are $\pm 0.02^{\circ}\text{C}$ and 0.05 and since then the accuracies are better than or equal to 0.01°C and 0.01. Prior to 1975, the salinity data originated from bottle data collected at discrete depths. We use the GAK1 CTD data to update Royer and Grosch's [2006] temperature and salinity anomaly time series after removing the warming and freshening trend per their analysis. Since 1997, the GAK1 CTD time series has been complemented by moored temperature and salinity data. The mooring was deployed annually (except 1999 and 2003), and contains Seabird SeaCats or MicroCats at nominal depths of 30 m, 60 m, 100 m, 150 m, 200 m, and

250 m. Pre- and post-calibrations indicate that sensor drifts did not exceed $\sim 0.01^{\circ}\text{C yr}^{-1}$ for temperature and 0.03 yr^{-1} for salinity during any year-long deployment.

For the 1970-2008 period we use NCEP re-analyzed estimates of zonal and meridional winds and air temperature at $\sim 60^{\circ}\text{N}$, 149°W , the grid point nearest GAK1. In addition, we use QuikSCAT wind data at 59.375°N , 149.125°W , which is ~ 55 km seaward of GAK1. This location reduces the potential bias due to localized gap winds [Macklin et al., 1988] on estimates of the along-shelf winds. The QuikSCAT wind estimates are from twice daily swaths with daily-averaged data available at 25 km resolution. Over the northern shelf the along-shelf component of the wind is nearly zonal [Royer, 2005; Schroeder, 2007], with downwelling-favorable winds being easterly (we use the meteorological convention to indicate wind direction throughout the paper).

Monthly coastal freshwater discharge anomalies from the Alaska-British Columbia boundary to 150°W are estimated from Royer's [1982] hydrological model. These are significantly correlated with upper ocean salinities at GAK1 [Royer, 2005; Weingartner et al., 2005] and the baroclinic transport in the ACC [Weingartner et al., 2005].

2.3 Results and analysis

2.3.1 Hydrographic observations at GAK1 in spring 2007 and 2008

GAK1 measurements in May 2007 indicated anomalous vertical profiles of temperature and salinity in comparison to vertical profiles of their means and standard deviations (Figure 2.3) for May based on the 1970-2008 record (41 profiles). Although the upper 10 m of the water column had already warmed to $\sim 7^{\circ}\text{C}$ in early May 2007, temperatures below 10 m were nearly uniform at $\sim 4^{\circ}\text{C}$ and 1.3 - 1.4°C below average. Overall, May 2007 temperatures were $\sim 2\sigma$ (σ : standard deviation) lower than the mean; they were $\sim 1.5\sigma$ below average from 10-100 m and nearly $\sim 3\sigma$ below average from 200-250 m. However, in May 2008, the largest temperature anomalies were at the surface (-2σ) and $\sim 2.5^{\circ}\text{C}$ lower than average. Temperature anomalies were -2°C (-1.8σ) at 10 m and -1°C ($\sim -1\sigma$) at 100 m. At depths greater than 100 m, temperatures were $\sim 0.5^{\circ}\text{C}$ below average and thus within the average May range of variability.

In May 2007, salinity varied from 31.6 at 10 m to 32.4 at 250 m, with the salinity anomalies decreasing nearly linearly from $+0.6$ (1.5σ) at 10 m to -0.3 (-1.5σ) at 250 m. This anomalous salinity distribution resulted in a relatively small density difference ($\sim 0.4\text{ kg m}^{-3}$) between the upper (0-100 m) and lower (100-250 m) layers, which we will argue induced the anomalously low spring temperatures throughout the water column. In contrast, salinities in May 2008 were within 1σ of the average, and varied from 31.3 at 10 m to 33.0 at 250 m. In particular, salinities were 0.1-0.5 above average near the surface (0-30 m), 0.1-0.2 lower than average between 30-170 m, and

nearly 0.3 above average at 250 m. Thus the (salinity-controlled) density difference between the upper and lower layer was 0.7 kg m^{-3} and near the May average of 0.65 kg m^{-3} . The winters and springs of 2007 and 2008 constitute the longest continuous period since the early 1970s of anomalously low temperatures observed on the GOA shelf (Figure 2.4).

To place the GAK1 observations in a cross-shelf context, we examined May temperature and salinity anomalies constructed for the 1998-2008 period from individual station means along the Seward Line. Figures 2.5 and 2.6 show average upper (0-100 m) and lower (100-250 m) layer temperature and salinity anomalies between the inner shelf (GAK1) and shelfbreak (GAK9). Stations GAK10-13 are not shown since these are located on the slope, where conditions may be influenced by basin processes. May temperature anomalies are generally consistent across the shelf, and were positive ($>0.5^\circ\text{C}$) in 1998, 2000, and 2003. Large negative (0-100 m) temperature anomalies (~ -0.5 to -1°C) occurred in May 2002, 2007 and 2008 and extended across the entire shelf, although the largest anomalies ($<-1^\circ\text{C}$) occurred on the inner shelf in 2007 and 2008. Lower layer (100-250 m) temperatures were above average in 1998 and 2003 ($>+0.5^\circ\text{C}$), and below average in 2007 and 2008, with the largest negative anomalies of $<-1^\circ\text{C}$ between GAK1-5 during May 2007. The cross-shelf temperature anomaly pattern distribution in May 2008 was similar, although the anomaly magnitudes were smaller than those of 2007.

Upper layer salinity anomalies along the Seward Line (Figure 2.6) were negative in 1998, generally positive from 1999 to 2002, and negative again from 2003

to 2006. Upper layer salinities in 2007 and 2008 were near average on the middle and outer shelf (GAK4-9), but above average in 2007 and below average in 2008 on the inner shelf (GAK1-4). The lower layer salinity anomalies follow the upper layer trend, except in 2007, when lower layer salinities were fresher than average across the shelf. In May 2007, salinity differences between the upper (0-100 m) and lower (100-250 m) layers were the smallest (<0.2) observed between GAK2-6 (again indicating anomalously weak stratification) and coincided with the largest negative temperature anomalies in the lower layer. The outer shelf salt stratification (GAK7-9) in 2007 was also the weakest observed amongst all these years.

2.3.2 The onset of the cooling in November 2006

In this section we use the nine years (1998-2008) of moored GAK1 temperature and salinity to show the annual cycles of 30-100 m averaged temperatures (Figure 2.7) and the stratification (Figure 2.8; based on the vertical density difference between 30 and 100 m) and to highlight November 2006 as the beginning of the recent cooling. The monthly mean temperature graph is nearly sinusoidal with a maximum in September and October ($\sim 9.5^{\circ}\text{C}$) and a minimum of $\sim 4.5^{\circ}\text{C}$ in March (Figure 2.7) when the stratification is also weakest (Figure 2.8).

In 2006, the mean 30-100 m temperatures were near average in July, but $\sim 1^{\circ}\text{C}$ above average from August through mid-October. November temperatures then declined by more than 3°C from $\sim 9.5^{\circ}\text{C}$ at the beginning of the month to 6°C by the end of the month, with this decrease being nearly twice the mean November cooling

rate. Moreover, this precipitous temperature decline signaled the transition from a relatively warm early fall to the coolest winter/spring in the GAK1 mooring record. Temperatures continued to decrease rapidly through December 2006, before falling more slowly to a minimum of $\sim 3^{\circ}\text{C}$ by late March 2007. Nevertheless the January–March temperature decrease of 2.5°C outpaced the mean temperature decrease of $\sim 1.5^{\circ}\text{C}$. Temperatures then slowly increased to $\sim 4^{\circ}\text{C}$ in early May, but the mean 30–100 m temperatures remained below average from May through September 2007. Temperatures did return to average by October and remained so through late January 2008. Upper layer waters then cooled more rapidly than average with abnormally low temperatures ($<4^{\circ}\text{C}$) reached in March 2008, when the mooring was recovered. Note that the most rapid temperature decrease (Figure 2.7) and erosion in stratification (Figure 2.8) occurred in November 2006, so a more detailed investigation into atmospheric and oceanographic conditions at this time is warranted.

Figure 2.9 shows the moored GAK1 temperature and salinity record from November 2006 along with nearby QuikSCAT winds and NCEP air temperatures. Oceanographic conditions in November evolved in response to two strong cooling events associated with westerly and northerly winds, as well as adjustments deep in the water column associated with up- and downwelling winds. The first strong cooling event began around November 7, when strongly westerly ($>10\text{ m s}^{-1}$) winds, with air temperatures of between -1°C to -5°C , blew for several days. The shelf response included upwelling reflected by a sudden decrease (increase) in near-bottom temperature (salinity) and surface cooling. A subsequent shift to strong (15 m s^{-1})

easterly winds and an increase in air temperatures to 5°C returned bottom thermohaline properties to those of early November and surface cooling rates diminished. Beginning on November 12, two strong northerly and northeasterly wind events of (10-15 m s⁻¹) advected cold (~-10 - 0°C) air over the shelf that accelerated surface cooling. These (downwelling-favorable) winds caused a depression in the isohalines below 200 m of ~25 m and decreased salinities to <33.2 at 250 m. Winds then veered northerly and the 33.2 isohaline rebounded to between 160 and 200 m depth where it remained until December. These northerlies involved the highest wind speeds observed in the mooring record and they also coincided with the second lowest November monthly mean air temperatures archived in the (1948-2008) NCEP record.

The increase in deep salinities was also accompanied by a decrease in deep water temperatures to <6°C between 200 and 250 m depth. The source of this cool, salty water is most likely the mid- and outer shelf, ~100 km seaward of GAK1 (based on data from fall and winter cruises collected during the Northeast Pacific GLOBEC program, <http://www.ims.uaf.edu/GLOBEC/results>). Since the mean GAK1 November/December salinity at 200 m is 32.7 ± 0.3 , a November salinity of 33.2 at depths <200 m is rare; indeed it has been observed only twice amongst the 24 November/December GAK1 CTD profiles in the archive. These anomalously high salinities persisted through March 2007 so that deep freshening, which normally occurs in late winter, occurred much later than normal as shown in the next section.

We next show that freshwater runoff was also anomalously low in November 2006, so that the combination of reduced runoff and the deep salinity influx weakened

the stratification early in fall. The diminished stratification and the strong cooling may have pre-conditioned the water column in late fall for the deep cooling that developed subsequently.

2.3.3 The evolution of the 2006/07 cooling compared to other years

We now compare the 2006/07 cooling with the anomalously cold winters of 2001/02 and 2007/08 and the relatively warm winter of 2000/01. The other years in the mooring record were similar to 2000/01 and not discussed. Our comparison is based on the July to June temperature and salinity time series for these four years (Figures 2.10a-d). Companion plots of monthly anomalies of freshwater runoff, NCEP air-sea heat fluxes (where negative anomalies imply increased heat loss to the atmosphere), and the meridional and zonal QuikSCAT wind anomalies are shown in Figure 2.11. The monthly anomalies, based on the 2000-2008 period, are normalized by their maximum absolute value.

In the months following November 2006, the cold surface signal deepened (Figure 2.10a), due to wind-mixing and cooling and anomalously low runoff that persisted through winter 2007. Hence by mid-January, temperatures in the upper 60 m decreased to $<4^{\circ}\text{C}$ (Figure 2.10a); with these temperatures attained a month or more earlier than the other cold winters of 2001/02 and 2007/08 (Figures 2.10c and b, respectively). The low winter runoff also led to the very weak stratification of March 2007, which together with 1971, 1996, and 1999, rank amongst the weakest stratifications observed in March in the GAK1 record. The weak stratification and the

large air-sea heat losses associated with strong northerly winds in March 2007 (Figure 2.11) resulted in water of $<4^{\circ}\text{C}$ at 200 m and lowered temperatures between 30 and 100 m to $<3^{\circ}\text{C}$ for ~one week near month's end.

March 2007 ended with the development of anomalously strong downwelling winds that persisted through May (Figure 2.11). These winds likely contributed to the persistence of anomalously cold water at depth through the summer and fall of 2007 (Figure 2.10b) due to enhanced deep mixing and possibly delayed the subsurface, onshore flow of more saline and warmer outer shelf water that occurs each spring [Royer, 1975; Xiong and Royer, 1984; Weingartner et al., 2005]. That delay could have contributed to the fresh bottom salinity anomaly observed in May 2007 (Figure 2.3). The subsurface negative temperature anomalies formed in spring 2007 waned by late December 2007, when bottom temperatures reached $\sim 6^{\circ}\text{C}$ (Figure 2.10b). While the timing of the arrival of 6°C water near the bottom (250 m) and its duration can vary from year-to-year, it usually occurs in late fall due to increased coastal downwelling and is responsible for the late fall/early winter deep (>150 m) temperature maximum on the northern GOA shelf [Xiong and Royer, 1984; Royer, 2005; Weingartner et al., 2005] as evident in the four years shown (Figure 2.10a-d).

In contrast to 2006/07, the anomalously low winter and spring temperatures of 2007/08 (Figure 2.10b) and 2001/02 (Figure 2.10c) were confined to the upper (0-100 m) layer. Furthermore, November 2007 had anomalously small air-sea heat fluxes and large freshwater runoff ($>50\%$ above the November average; Figure 2.11). Thereafter discharge anomalies were slightly negative but the stratification did not appreciably

decrease until February. Anomalously strong air-sea heat fluxes only developed in late January and February 2008 (Figure 2.11), so that cooling to temperature $<4^{\circ}\text{C}$ was confined to between the surface and 100 m (Figure 2.10b) because of the stratification induced by large freshwater discharge rates in fall 2007. The high fall discharge coincided with anomalously southerly winds, which enhance precipitation and runoff in the northern GOA [Weingartner et al., 2005].

Contrary to the large coastal runoff rates in fall 2007, below average runoff from July 2001 to January 2002 (Figure 2.11) resulted in elevated surface salinities and reduced upper layer stratification (Figure 2.10c). Oceanic winter heat loss was anomalously strong in October and December 2001 (Figure 2.11) and cooled the upper 100 m to $<5^{\circ}\text{C}$ by late January 2002 (Figure 2.10c). Runoff remained below average from January through April (except March), but air-sea heat flux anomalies were both positive and negative from November through April, so that in spite of the reduced stratification, water temperatures of $<4^{\circ}\text{C}$ were confined to the upper $\sim 60\text{-}80$ m (Figure 2.10c).

The fall and winter of 2000/01 provides a contrasting example from the cold years. Then $\sim 6^{\circ}\text{C}$ water persisted from December through April at 250 m (Figure 2.10d), and large freshwater runoff rates and anomalously southerly winds prevailed throughout the winter (Figure 2.11) so that relatively high salinities persisted at the bottom and low salinities near the surface. In aggregate, these conditions enhanced stratification and impeded vertical mixing. In addition, heat fluxes were anomalously positive during the winter of 2000/01.

In summary, the mooring record, although of limited duration, suggests that both winter cooling and reduced runoff play synergistic roles in promoting deep (> 100 m) cooling. Runoff structures the shelf stratification, while the air-sea heat flux extracts heat from the ocean. Consequently, we hypothesize that anomalously low temperatures at depth develop in winters of anomalously large air-sea heat fluxes and low fall/winter runoff. We next test this hypothesis by examining atmospheric forcing and thermal anomalies over the entire GAK1 hydrographic record from ~1970 to present.

2.3.4 Atmospheric forcing parameters and their interannual variability at GAK1

Our analysis is based on winter (November-March) anomalies (computed for the period from 1970 to present, i.e. over the length of the GAK1 record) of atmospheric parameters (Figure 2.12). We use salinity measurements from the monthly profiles to approximate upper layer stratification as the vertical salinity difference between 20 m and 100 m. We consider spring temperature anomalies in the upper (0-100 m) and lower (100-250 m) layers. To assess the integrated oceanic response to wintertime forcing, we averaged March-May temperature profiles and compare these means with winter-averaged anomalies of air temperatures, freshwater runoff, meridional and zonal winds, and latent and sensible heat fluxes. This approach increases the yearly data density, since sampling coverage was relatively sparse prior to the late 1980s (Figure 2.2).

Large negative ($>-1^{\circ}\text{C}$) temperature anomalies in the surface layer (0–100 m) occurred in the early 1970s and 2007-2008, while weaker negative anomalies ($\sim-0.5^{\circ}\text{C}$) occurred in 1982, 1991, 1995, 1996, 1999, and 2002. Each of these years had anomalously low air temperatures and all years (except 1975) had anomalously low winter runoff. Overall, 2006/07 had the largest anomalies in meridional winds, air temperatures and coastal runoff, with similar anomalies occurring in 1971/72 and 1972/73, when the lowest water temperatures were observed. By contrast, 1977, 1984, 1998, and 2003 were anomalously warm (0-100 m temperature anomalies exceeded $+1^{\circ}\text{C}$) and coincided with positive anomalies in air temperature, runoff, stratification and positive heat loss anomalies.

During cold winters, precipitation on land accumulates as snow so anomalously low runoff and air temperatures tend to be correlated. Indeed, this is factored into Royer's [1982] model of coastal freshwater discharge. However, upper ocean salinity and vertical salinity gradients between 20 and 100 m at GAK1 both reflect the freshwater discharge [Royer, 1982; Weingartner et al., 2005], and therefore provide independent measures of Royer's model. With the exception of 1975, years with anomalously low, deep (100-250 m) temperatures coincide with below average winter runoff and weak salinity gradients between 20 and 100 m (Figure 2.12). In fact, stepwise regression ($n=35$) shows that $\sim 81\%$ of the variance in lower layer (100-250 m) temperature anomalies are explained by salinity stratification and air temperatures (all regressions were significant at the 99% confidence level). Variations in air temperatures and in the vertical salinity gradient alone explain 75% and 67% of the

deep water temperature variance, respectively. Meridional winds explain 57%, and heat fluxes and runoff explain 60% and 42% of the variance, respectively; although both heat fluxes and runoff depend (in part) on air temperature.

We next investigated the surface atmospheric pressure distribution over the North Pacific during anomalously cold and warm winter months during the ~40 years of the GAK1 time series. We identified months with anomalously ($> |1\sigma|$, where σ ranges from 1.4-2.3°C) low (33 months) and high (32 months) GAK1 NCEP air temperatures between November and March from 1970-2008 (Figure 2.12, panel i) and then constructed average sea level pressure (SLP) patterns based on this sorting (Figure 2.13). The warm pattern is characterized by an extensive Aleutian Low (AL) over the central Aleutians, which results in southerly winds and large heat and moisture transport to the northern GOA. In contrast, the cold pattern consists of two weak low pressure cells, one over the western Aleutians and the other centered in the northern GOA and a high pressure ridge over the mainland. This pattern implies northeasterly winds that advect cold air over the western GOA shelf (Figure 2.11), and also favors seaward ageostrophic winds that are channeled through gaps in the coastal mountains and bays along the south coast of Alaska [Macklin et al., 1988]. Consequently, the (November-March) meridional wind component near GAK1 is significantly correlated with NCEP GAK1 air temperatures ($r=0.74$, $p<0.01$) and with coastal runoff ($r=0.53$, $p<0.01$).

In warm winters, the SLP gradient between GAK1 and the central Aleutians is large, while it is small in cold years. We found that the maximum correlation between

GAK1 air temperatures and the SLP difference was between NCEP grid points at 60°N, 150°W (nearest to GAK1) and 54°N, 176°W for the January-March period ($r=0.84$, $p<0.05$). Hence a significant fraction of the winter air temperature variability is explained by this SLP gradient, which is a function of the location of the AL.

This finding agrees with Rodionov et al. [2007], who investigated atmospheric conditions in the Bering Sea in relation to the AL, and found only weak or no correlations (depending on the method) between Bering Sea air temperatures and the North Pacific Index [Trenberth and Hurrell, 1994], a measure of AL strength. Similarly, we found no correlations between GAK1 winter air temperatures and the NPI, which underlines the importance of the location of the AL rather than its strength on the northern GOA climate.

2.3.5 On the timing of cooling events

From October to March, northern GOA waters lose heat to the atmosphere on average, while coastal freshwater discharge is at its annual minimum in February and March [Royer, 1982]. We suggest that cooling events and discharge anomalies during fall and late winter (i.e., October/November and March/April) may have a comparatively greater effect on cooling the water column than mid-winter events. For example, coastal freshwater discharge is a maximum in fall (mean November runoff is $\sim 40 \times 10^3 \text{ m}^3 \text{ s}^{-1}$) so that a 30% reduction in fall runoff (as occurred in November 2006) affects the shelf freshwater reservoir more than a similar reduction from January through March (when runoff is $\sim 10\text{-}15 \times 10^3 \text{ m}^3 \text{ s}^{-1}$). Since the flushing time scale for

the northern shelf is ~8 months [Weingartner et al., 2005] the memory of fall runoff anomalies is retained through winter. Moreover, runoff is positively correlated with the along-shelf transport; hence a negative runoff anomaly in fall will also reduce the along-shelf transport of heat [Weingartner et al., 2005].

Similarly, large negative air-sea heat flux anomalies during the transition from cooling to warming in late March may extend the cooling season and, more importantly, may allow wind-mixing and cooling to extend much deeper into the water column since stratification is at its annual minimum in late winter (Figure 2.8).

Consequently, we hypothesize that anomalously low temperatures at depths >100 m are a consequence of below average fall runoff and above average late winter cooling. The early 1970s, and 1990, 1994, and 2006 each had anomalously low late winter/spring temperatures (Figure 2.12) and in each of these years late fall or early winter runoff was below average. Coastal runoff and heat flux anomalies in November 2006 and March 2007 were among the largest negative anomalies recorded, and these coincide with some of the most anomalous hydrographic conditions in the GAKI record. However, 2006/07 is the only such winter in which highly resolved time series allowed us to observe the evolution of deep cooling. Hence, while our hypothesis seems plausible, definitive proof awaits further investigation.

2.3.6 The effect of downwelling

Recently, Shcherbina and Gawarkiewicz [2008, hereafter SG08] examined the relative importance of wind-driven buoyancy flux (WDBF) due to onshore surface

Ekman transport versus the buoyancy flux due to atmospheric cooling in the narrow (~10 km), shallow (~50 m) Outer Cape Cod Coastal Current (OCCC). They found that the winter buoyancy loss in the OCCC due to onshore advection of saline surface waters under downwelling winds exceeded the buoyancy loss due to air-sea heat exchange so that WDBF enhanced deep mixing in the OCCC. We made similar estimates of these fluxes for the ACC from October-March monthly NCEP net heat fluxes, along-shore wind stresses, and the surface density gradient between GAK1 and GAK4 estimated from Seward Line transects. On the northern GOA shelf, density increases offshore (to the south) and the surface density gradients weaken from $\sim 6 \times 10^{-5} \text{ kg m}^{-4}$ in October to $\sim 2 \times 10^{-5} \text{ kg m}^{-4}$ in March. For a mean winter along-shore wind velocity of -4 m s^{-1} [Weingartner, 2007], the WDBF ($= -[\tau^x / f\rho_0] g\rho_0^{-1} \partial\rho / \partial y$, where ρ is the density, ρ_0 a reference density, y the cross-shore coordinate, τ^x the along-shore wind stress, f the Coriolis parameter, and g gravity) varies from $\sim 2 \times 10^{-7} \text{ m}^2 \text{ s}^{-3}$ in December to $\sim 6 \times 10^{-8} \text{ m}^2 \text{ s}^{-3}$ in March (i.e. shoreward buoyancy flux in December is about three times greater than in March). Buoyancy losses due to atmospheric cooling are smaller and vary seasonally from $\sim 2 \times 10^{-8}$ to $5 \times 10^{-8} \text{ m}^2 \text{ s}^{-3}$. Our estimates of the WDBF and the atmosphere-ocean buoyancy flux for the ACC are similar in magnitude to those of the OCCC per SG08.

One might expect that the destabilizing influence associated with shoreward buoyancy flux would enhance deep mixing of winter-cooled surface waters in the ACC and GOA shelf. This does not appear to be the case however, since winter

downwelling anomalies are anti-correlated ($r = -0.3$, $p < 0.1$) with the vertical salinity gradient and water temperatures ($r = \sim -0.57$, $p < 0.01$ for both the 0-100 m and 100-250 m portions of the water column). The reasons for this are likely several. First, the mean sea level pressure maps for warm and cold winters (Figure 2.13) suggest that winters with strong downwelling are associated with above average air temperatures and greater than average runoff. Indeed, winter downwelling winds are anti-correlated with winter air temperatures ($r = -0.64$, $p < 0.01$), net air-sea heat fluxes ($r = -0.72$, $p < 0.01$) and runoff ($r = -0.39$, $p < 0.1$). Second, downwelling-favorable winds not only drive a small onshore heat flux (which we estimate to be $\sim 25 \text{ W m}^{-2}$ on average), but also enhance the along-shore advection of oceanic heat and freshwater over the northern GOA shelf. Finally, Williams et al. [2007] and SG08 show that the cross-shelf transport is sensitive to the structure and strength of the haline fronts that bound the offshore edge of the ACC and OCCC. The strength of the ACC front in winter is at least partially dependent upon the winter discharge [Weingartner et al., 2005]. In aggregate, our results suggest that the winter evolution of temperatures on the GOA shelf is a consequence of three-dimensional circulation and mixing processes involving a complex interplay amongst the air-sea heat flux, ocean heat flux convergences, the stabilizing influence of runoff, and the destabilizing effects of cooling, vertical mixing, and the WDBF. A profitable area for future research would be to examine these influences using simple process models.

2.4 Summary and Conclusion

Long-term temperature and salinity observations at hydrographic station GAK1 on the northern Gulf of Alaska (GOA) shelf revealed anomalously low water temperatures in the winters and springs of 2007 and 2008. Indeed, in spring 2007, temperatures throughout the water column were the lowest observed in ~35 years (Figure 2.4) and the vertical stratification was also unusually weak. Conditions in spring 2008 also included some of the coldest waters in the record, but the temperature anomalies then were confined to the upper 100 m of the water column because of salt stratification below this depth. Our results suggest that winter coastal runoff, by modulating upper ocean salinities and winter stratification, exerts an important influence on the temperature distribution in the northern GOA. Our analysis of NCEP atmospheric variables, coastal freshwater discharge, and QuikSCAT winds also suggests that the timing of winter cooling events, i.e. events at the beginning (October/November) and end of the cooling season (March/April) are important in shaping the hydrographic conditions for the following spring and summer.

For example, in November 2006 net air-sea heat fluxes, coastal runoff and northerly winds were amongst the most anomalous on record. These conditions cooled the water column and weakened the stratification. Deep shelf processes may also have contributed to the inflow of colder, saltier water following a sudden relaxation of strong downwelling favorable winds. Cooling continued from December through February although the air-sea heat fluxes were close to their climatological mean, but

the stratification remained below average due to below average winter runoff. Consequently, enhanced cooling and deep mixing of the GOA shelf occurred in March 2007 as a result of unusually severe cold air outbreaks. Interestingly, before vigorous cooling began in November 2006, the stratification and thermal anomalies in September and October 2006 were above average, suggesting that summer and early fall upper ocean anomalies can be obliterated rapidly on the northern GOA shelf in late fall and winter.

About two-thirds of the along-shore baroclinic geostrophic transport on the GOA shelf is within the ACC [Weingartner et al., 2005], which advects freshwater and heat along the GOA coast. In 2006/07, the along-shore heat and freshwater advection was likely reduced. While the wind-driven (barotropic) component of the ACC was likely average due to near-average along-shore winds from November-March (Figure 2.12), the near-shore baroclinic flow (estimated from Seward Line transects) in May 2007 was the lowest among 11 May (1998-2008) transects. This implies that the along-shore heat contribution was diminished and likely contributed to the cooling in 2006/07.

A comparison of the 2006/07 cooling season with the relatively cold winters of 2001/02 and 2007/08 suggests that pre-conditioning of the shelf stratification in late fall through cooling and reduced runoff along with late winter cooling events may be necessary ingredients for the production of deep temperature anomalies in spring. Deep (>100 m) temperature anomalies formed in winter may persist for 6-9 months and thereby be longer-lived than upper layer anomalies, since the deep anomalies are

subjected to dynamics governed by the along- and cross-shore winds, whereas thermodynamic processes govern the variability in the upper layer. This is supported by the observations from summer through early winter 2007, which showed that the subsurface thermal anomalies established in spring 2007 persisted into the following winter despite the absence of substantial cooling until January/February 2008 (Figure 2.11 and 2.12).

Retrospective analyses of the GAK1 time series and the recent cooling events underscore the importance of coastal runoff and upper ocean salinity on deep (>100 m) shelf temperature in the northern GOA. The upper layer (0-100 m) salinity and the lower layer (100-250 m) temperature anomalies are significantly correlated throughout the GAK1 time series (1970-present; $r=-0.33$, $p<0.01$, $n=315$), particularly during anomalously cold ($>2\sigma$) springs (March and April; $r=-0.64$, $p<0.05$, $n=12$). Our finding is consistent with Royer's [2005] report of maximum correlations ($r=0.34-0.39$) between freshwater runoff and GAK1 temperatures at depths greater than 100 m.

Anomalously low deep temperatures in spring coincide with above average upper layer salinity and with a weaker than average salinity stratification. For example, the November-March average Brunt-Väisälä frequency is $\sim 75\%$ larger during anomalously warm winters than during average winters. The relative influence of vertical temperature and salinity gradients on density stratification is determined

from $R = \frac{\partial \sigma_t}{\partial T} \frac{\partial T}{\partial z} / \frac{\partial \sigma_t}{\partial S} \frac{\partial S}{\partial z}$, with $R=1$ if temperature and salinity make equal

contributions to the stratification. Temperature (salinity) gradients dominate the

stratification for $R > 1$ (< 1). In late winter/spring $R \sim 0.25$ on average [see also Sarkar et al., 2005], so that within the ACC, salinity stratification is four times more important than temperature stratification. For winters and springs with anomalously ($< -2\sigma$) low 100-250 m temperatures (e.g., 2006/07) R averages ~ 0.66 , which is due primarily to the weakening of the vertical salinity gradient. These weak vertical salinity gradients are associated with anomalously high upper ocean salinities and low winter coastal freshwater discharge rates.

Our analysis underscores the importance of freshwater on stratification with ramifications for winter vertical mixing and temperature distribution. While much of the variability in winter heat content is associated with air-sea heat fluxes, the vertical temperature distribution on the GOA shelf is a consequence of three-dimensional circulation and mixing processes involving a complex interplay among air-sea heat fluxes, ocean heat flux convergences, the stabilizing influence of runoff, and the destabilizing effects of cooling, vertical mixing, and the wind-driven buoyancy flux due to along-shore winds. The aggregate effect of these processes is poorly understood. Moreover, the correct implementation of line or distributed runoff sources in numerical circulation models of the Gulf of Alaska remains problematic [Dobbins et al., 2009]. Until this hurdle is overcome, model predictions of the vertical distribution of springtime temperatures and stratification will remain difficult.

We have argued that the winter/spring temperature distribution in the coastal GOA depends upon fall and winter coastal freshwater discharge. The discharge depends on air temperatures, however, which affect both the moisture content (and

hence precipitation rates) of the atmosphere via the Clausius-Clapeyron relationship and the partitioning of the precipitation between the liquid (rain) and solid (snow) phases. This affects winter stratification because rain results in relatively rapid runoff whereas the snow is stored in the surrounding mountains until it melts in the following spring and summer [Royer, 1982]. At present, average winter sea level air temperatures hover near the freezing point [Brower et al., 1988], so that slight changes in air temperature can have important consequences on the thermal properties of this shelf. IPCC [2007] climate predictions for the GOA region point to warmer and wetter winters, which would result in stronger winter stratification. Our analysis suggests that this will lead to a reduction in the interannual variability of deep winter shelf temperatures, but perhaps to an increase in variability of upper ocean temperatures since winter mixing will be confined to a shallower depth. Conceivably these changes could include years in which shallow surface layers are quite cold.

The implications of deep cooling and mixing on biological production may be substantial. Weak stratification during spring may result in enhanced surface nutrient concentrations due to deep mixing, but may delay the spring bloom. A delay in the bloom and cooler temperatures may affect zooplankton growth due to changes in the phasing of primary production and in zooplankton metabolic rates. It appears that both primary and secondary production was delayed along the Seward Line in May 2007 and 2008 [Hopcroft, pers. comm.]. Whether or not 2007-2008 indicate interannual variability or a transition into a cooler period remains to be seen. However, preliminary analyses suggest that the spring of 2009 was also unusually cold

[unpublished data]. We note, however, that the 1976/77 regime shift to warmer ocean temperatures was accompanied by a transition in commercially important fish from crab and shrimp to pelagic fish populations [Anderson and Piatt, 1999; Hare and Mantua, 2000], and therefore had considerable ecological and economical impact for the region.

2.5 Acknowledgments

MAJ acknowledges the support of a University of Alaska Fairbanks (UAF) Center for Global Change Student Award funded by the International Arctic Research Center (IARC) through cooperative agreement ARC 0327664 with the National Science Foundation (NSF) and a graduate student award from the North Pacific Research Board (NPRB).

We thank the Exxon Valdez Oil Spill Trustees Council (EVOSTC project #070340) for continued support of the GAK1 mooring and monthly CTD data. Hydrographic sampling along the Seward Line from 1998-2004 was carried out as part of NEP-GLOBEC, and since 2005 under support of the NPRB (project #520, 603, 708, and 804). EVOSTC also supported TJW and SLD.

NCEP reanalysis data were provided by the NOAA-CIRES Climate Diagnostics Center, Boulder, CO, USA, from their Web site at <http://www.cdc.noaa.gov>. QuikSCAT data are produced by Remote Sensing Systems and sponsored by the NASA Ocean Vector Winds Science Team. Data are available at www.remss.com.

We thank Steve Okkonen for many helpful discussions and Andrey Shcherbina and Glen Gawarkiewicz stimulated the discussion in section 2.3.6. Isaac Schroeder provided advice on the QuikSCAT data. Dave Leech serviced the moorings and collected the monthly CTD casts at GAK1. Russ Hopcroft led CTD data collection efforts along the Seward Line since 2005. We greatly appreciate the comments of the editor and two anonymous reviewers which improved the manuscript.

2.6 References

Anderson, P.J. and J.F. Piatt (1999), Community reorganization in the Gulf of Alaska following ocean climate regime shift, *Mar. Ecol. Prog. Ser.*, 189, 117-123.

Brower, Jr., W.A., R.G. Baldwin, Jr., C.N. Williams, J.L. Wise, and L.D. Leslie (1988), *Climate atlas of the outer continental shelf waters and coastal regions of Alaska*, volume 1, Gulf of Alaska. Asheville, NC: National Climatic Data Center.

Childers, A.R., T.E. Whitledge, and D.A. Stockwell (2005), Seasonal and interannual variability in the distribution of nutrients and chlorophyll-a across the Gulf of Alaska shelf: 1998–2000, *Deep-Sea Res. II*, 52, 193–216.

Dobbins, E.L., A.J. Hermann, P.J. Stabeno, N.A. Bond, and R.C. Steed (2009), Modeled transport of freshwater from a line-source in the coastal Gulf of Alaska, *Deep-Sea Res. II*, doi: 10.1016/dsr2.2009.02.004.

Hare, S.R. and N.J. Mantua (2000), Empirical evidence for North Pacific regime shifts in 1977 and 1989, *Progr. Oceanogr.*, 47(2–4), 103–146.

IPCC (2007), *Climate Change 2007: Impacts, Adaptation and Vulnerability*. Contribution of Working Group II to the Fourth Assessment Report of the Intergovernmental Panel on Climate Change, edited by M.L. Parry, O.F. Canziani, J.P. Palutikof, P.J. van der Linden, and C.E. Hanson, pp. 7-22, Cambridge University Press, Cambridge, UK.

Johnson, W.R., T.C. Royer, and J.L. Luick (1988), On the seasonal variability of the Alaska Coastal Current, *J. Geophys. Res.*, 93(C10), 12423-12437.

Macklin, S.A., G.M. Lackmann, and J. Gray (1988), Offshore-directed winds in the vicinity of Prince William Sound, Alaska, *Mon. Wea. Rev.*, 116, 1289-1301.

Rodionov, S.N., N.A. Bond, and J.E. Overland (2007), The Aleutian Low, storm tracks, and winter climate variability in the Bering Sea, *Deep-Sea Res. II*, 54, 2560-2577.

Royer, T.C. (1975), Seasonal variations of waters in the northern Gulf of Alaska, *Deep-Sea Res.*, 22, 403-416.

Royer, T.C. (1981), Baroclinic transport in the Gulf of Alaska, Part II: Freshwater driven coastal current, *J. Mar. Res.*, 39, 251-266.

Royer, T.C. (1982), Coastal freshwater discharge in the Northeast Pacific, *J. Geophys. Res.*, *87(C3)*, 2017-2021.

Royer, T.C. (2005), Hydrographic responses at a coastal site in the northern Gulf of Alaska to seasonal and interannual forcing, *Deep-Sea Res. II*, *52* (1-2), 267-288.

Royer T.C., and C.E. Grosch (2006), Ocean warming and freshening in the northern Gulf of Alaska, *Geophys. Res. Lett.*, *33*, L16605, doi:10.1029/2006GL026767.

Sarkar, N, T.C. Royer, and C.E. Grosch (2005), Hydrographic and mixed layer depth variability on the shelf in the northern Gulf of Alaska, 1974-1998, *Cont. Shelf. Res.*, *25*, 2147 – 2162.

Schumacher, J.D., and R.K. Reed (1980), Coastal flow in the northwest Gulf of Alaska: the Kenai Current, *J. Geophys. Res.*, *85(C11)*, 6680-6688.

Schumacher, J.D., P.J. Stabeno, and A.T. Roach (1989), Volume transport in the Alaska Coastal Current, *Cont. Shelf. Res.*, *9*, 1071-1083.

Schroeder, I. (2007), Annual and interannual variability in the wind field and the hydrography along the Seward Line in the northern Gulf of Alaska, PhD dissertation, 80 pp., Old Dominion University, Norfolk, VA.

Shcherbina, A.Y., and G.G. Gawarkiewicz (2008), A coastal current in winter: 2. Wind forcing and cooling of a coastal current east of Cape Cod, *J. Geophys. Res.*, *113*, C10014, doi: 10.1029/2008JC004750.

Stabeno, P.J., R.K. Reed and J.D. Schumacher (1995), The Alaska Coastal Current: continuity of transport and forcing, *J. Geophys. Res.*, *100(C2)*, 2477-2485.

Stabeno, P.J., N.A. Bond, A.J. Hermann, N.B. Kachel, C.W. Mordy, and J.E. Overland (2004), Meteorology and oceanography of the northern Gulf of Alaska, *Cont. Shelf Res.*, *24*, 859-897.

Trenberth, K.E. and J.W. Hurrell (1994), Decadal atmosphere-ocean variations in the Pacific, *Clim. Dyn.*, *9*, 303-319.

Weingartner, T.J. (2007), The physical environment of the Gulf of Alaska, in *Long-Term Ecological Change in the Northern Gulf of Alaska*, edited by R. Spies, pp. 12-44, Elsevier, Oxford, UK.

Weingartner, T.J., K. Coyle, B. Finney, R. Hopcroft, T. Whitley, R. Brodeur, M. Dagg, E. Farley, D. Haidvogel, L. Haldorson, A. Hermann, S. Hinckley, J. Napp, P. Stabeno, T. Kline, C. Lee, E. Lessard, T. Royer, and S. Strom (2002), The Northeast Pacific GLOBEC Program: Coastal Gulf of Alaska, *Oceanography*, *15*, 48-63.

Weingartner, T.J., S.L. Danielson, and T.C. Royer (2005), Freshwater variability and predictability in the Alaska Coastal Current, *Deep-Sea Res. II*, *52*, 169-191.

Wilson, J.G. and J.E. Overland (1986), Meteorology, in *The Gulf of Alaska, Physical Environment and Biological Resources*, edited by D.W. Hood and S.T. Zimmerman, pp. 31–53, Alaska Office, Ocean Assessments Division, National Oceanic and Atmospheric Administration, US Department of Commerce.

Williams, W.J., T.J. Weingartner, A.J. Herrmann (2007), Idealized three-dimensional modeling of seasonal variation in the Alaska Coastal Current, *J. Geophys. Res.*, 112, C07001, doi:10.1029/2005JC003285.

Xiong, Q. and T.C. Royer (1984), Coastal temperature and salinity in the northern Gulf of Alaska, 1970-1983, *J. Geophys. Res.*, 89(C5), 8061-8066.

2.7 Figures

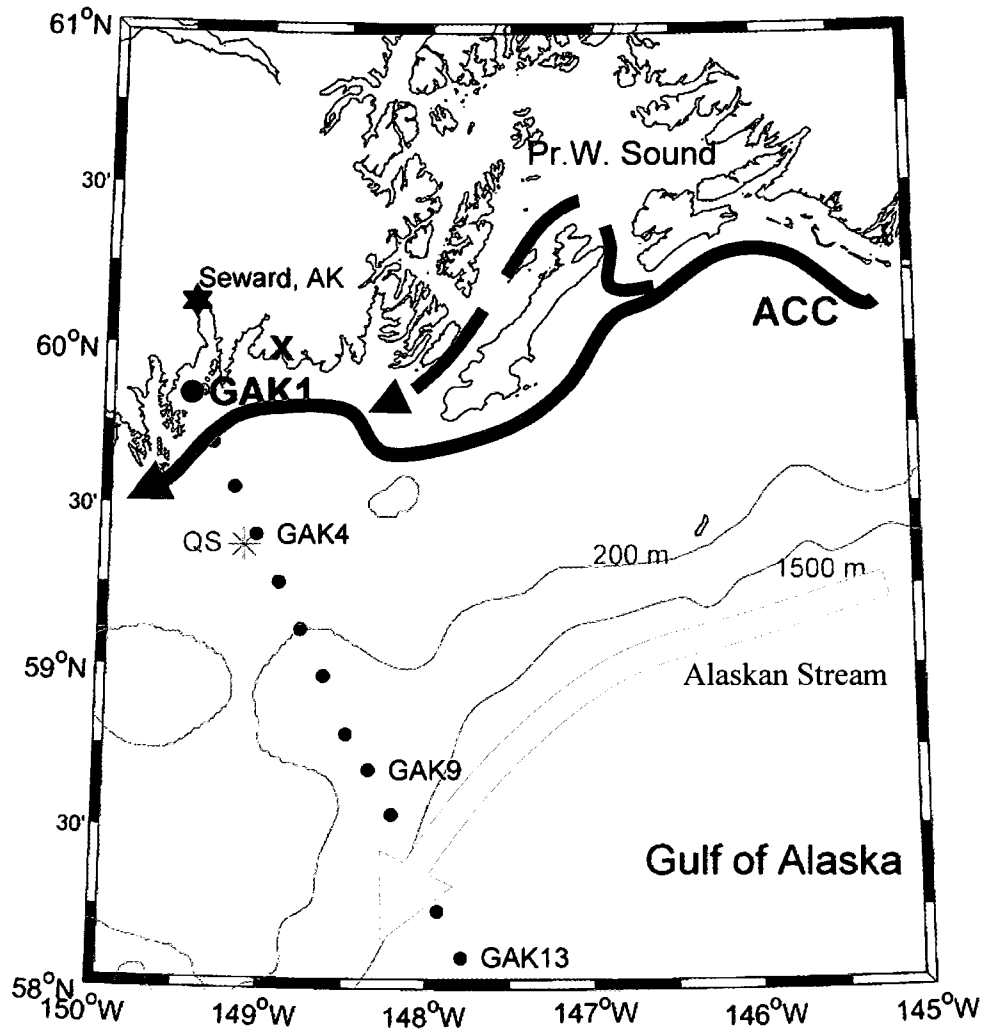


Figure 2.1: Map of the northern Gulf of Alaska. Map of the northern Gulf of Alaska, including GAK1 (large dot) and the Seward Line (dots). Bathymetric data from the GEBCO database shows the 200 m and 1500 m isobars. Grey lines indicate the course of the Alaska Coastal Current and the Alaskan Stream. Locations of QuikSCAT and NCEP grid points are marked by (*) and (x).

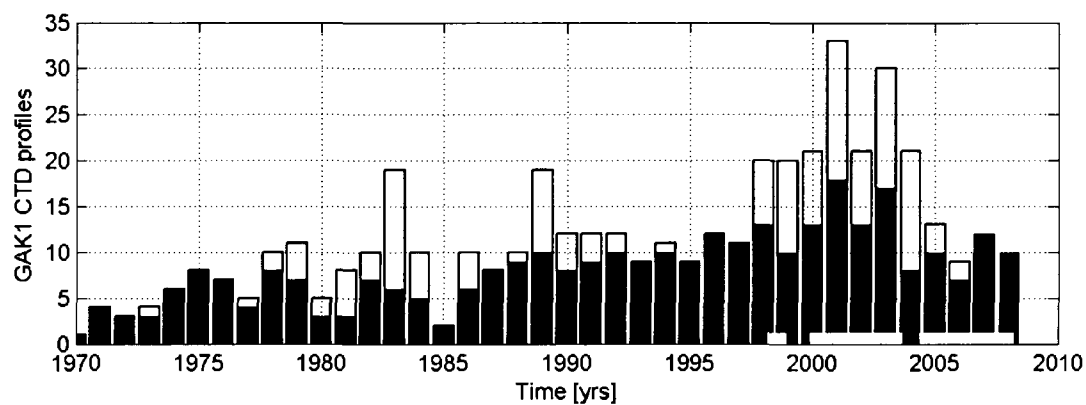


Figure 2.2: Annual number of GAK1 CTD profiles. Annual number of recorded GAK1 CTD profiles (white) and the number of profiles used in this study (black). Grey horizontal bars indicate time of mooring coverage.

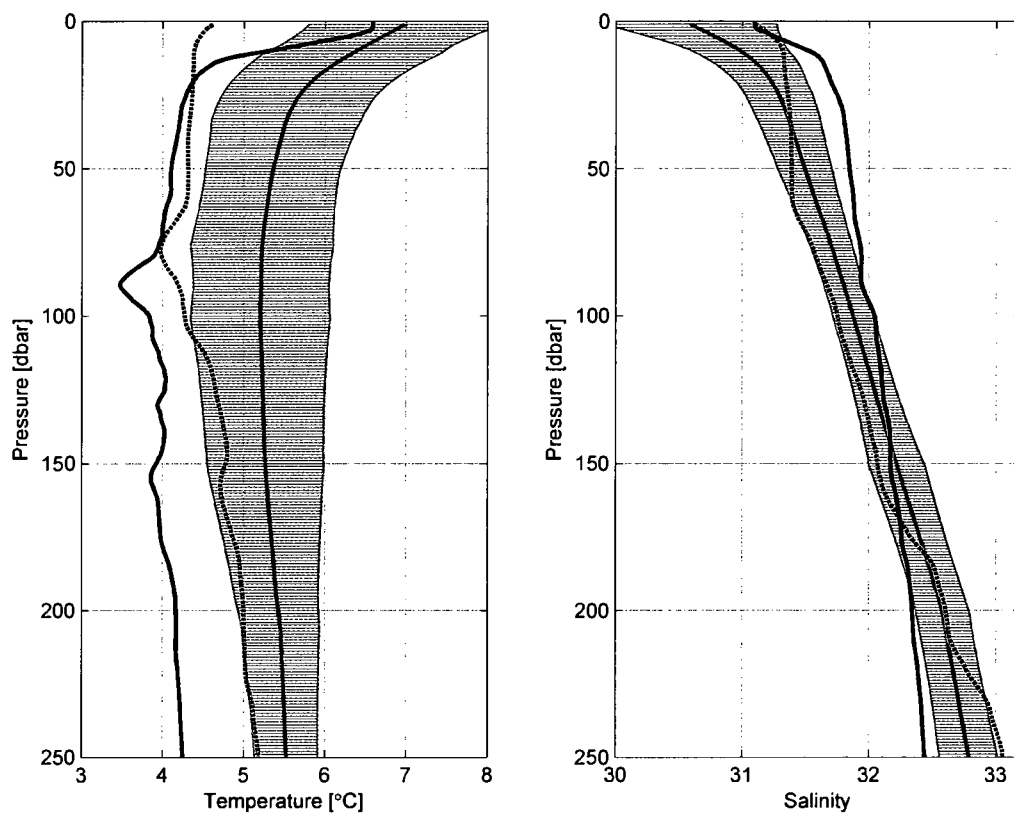


Figure 2.3: May 2007 and 2008 temperature and salinity profiles. The mean May temperature [°C] (left) and salinity (right) profiles (grey line) \pm one standard deviation (grey shading) based on 41 May CTD profiles from 1970-2008. The solid black profiles are for 8 May 2007 and dashed profiles are for 4 May 2008.

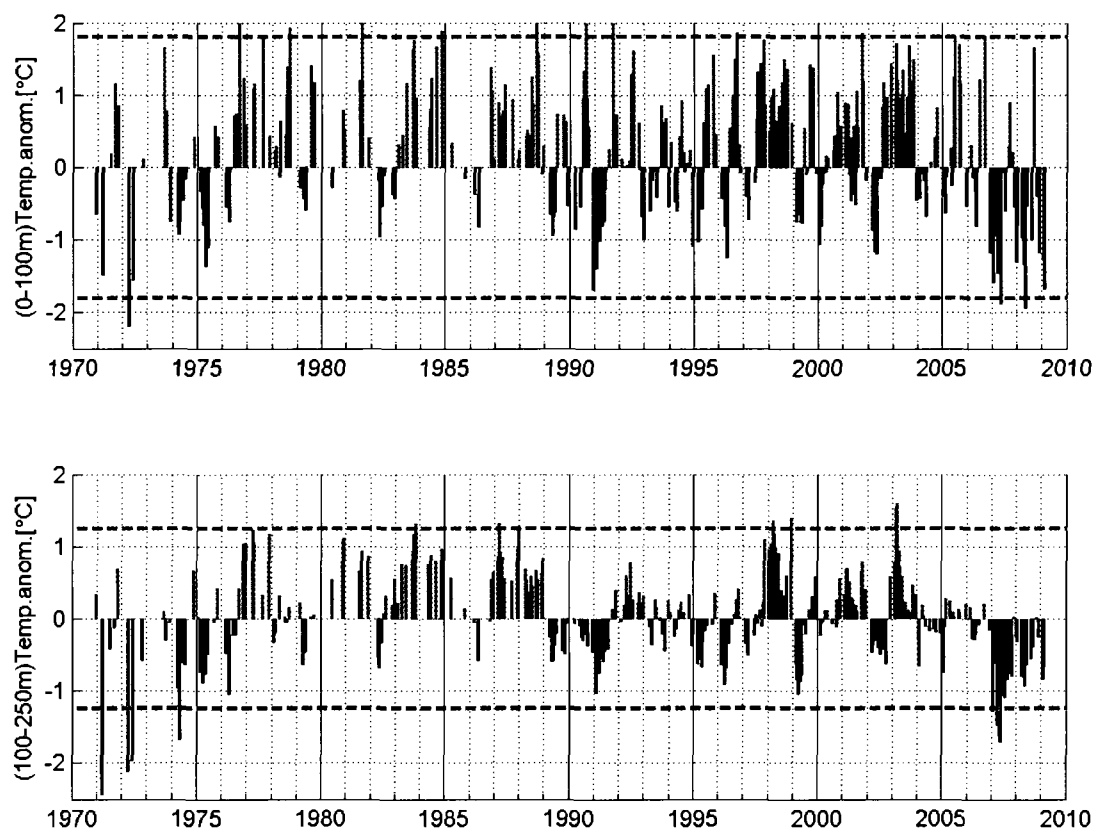


Figure 2.4: GAK1 temperature anomalies time series. Detrended upper (0-100 m, top) and lower (100-250 m, bottom) layer GAK1 monthly temperature anomalies [°C] computed from CTD profiles acquired ~1970 to January 2009. The dotted lines indicate ± 2 standard deviations. Updated from Royer and Grosch [2006].

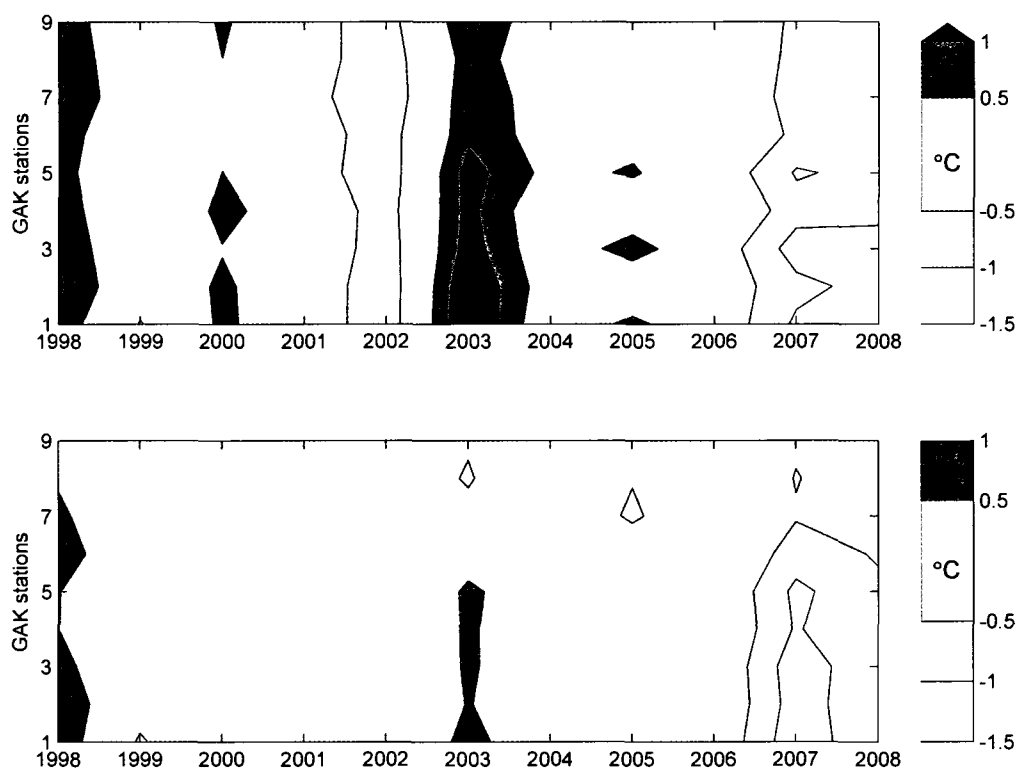


Figure 2.5: Seward Line 1998-2008 temperature anomalies. Upper (0-100 m, top) and lower (100-250 m, bottom) layer Seward Line May temperature anomalies [$^{\circ}\text{C}$] between the coast (GAK1) and the shelfbreak (GAK9). Anomalies are computed for the period 1998-2008.

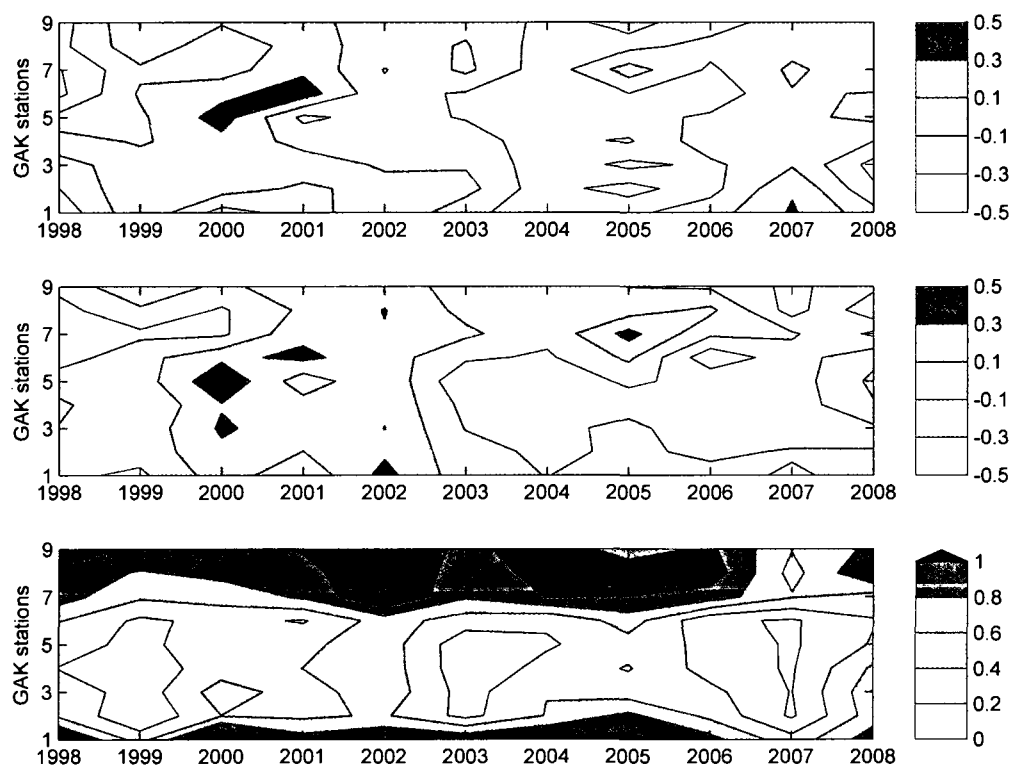


Figure 2.6: Seward Line 1998-2008 salinity anomalies. Upper (0-100 m, top), lower (100-250 m, middle) layer Seward Line May salinity anomalies between the coast (GAK1) and the shelfbreak (GAK9), and the salinity difference between upper and lower layers (bottom panel).

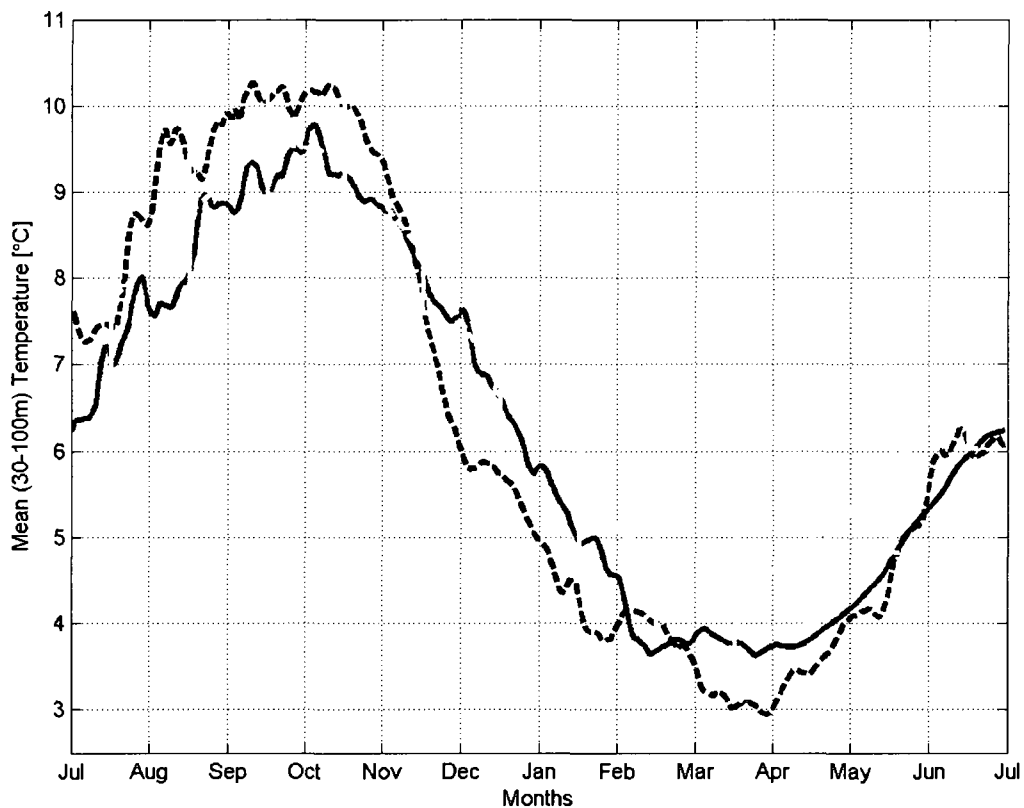


Figure 2.7: Seasonal cycle of GAK1 temperatures. Seasonal cycle of mean 30-100 m GAK1 temperatures [°C] averaged from moored temperature recordings at 30 m, 60 m, and 100 m. Temperatures from 2006/07 (black dashed) and 2007/08 (solid) are compared with monthly means from the mooring records from 1998-2008 (dashed with circles). Vertical bars on monthly means indicate one standard deviation. Monthly means are plotted in the middle of the month, x-ticks indicate the first day of each month.

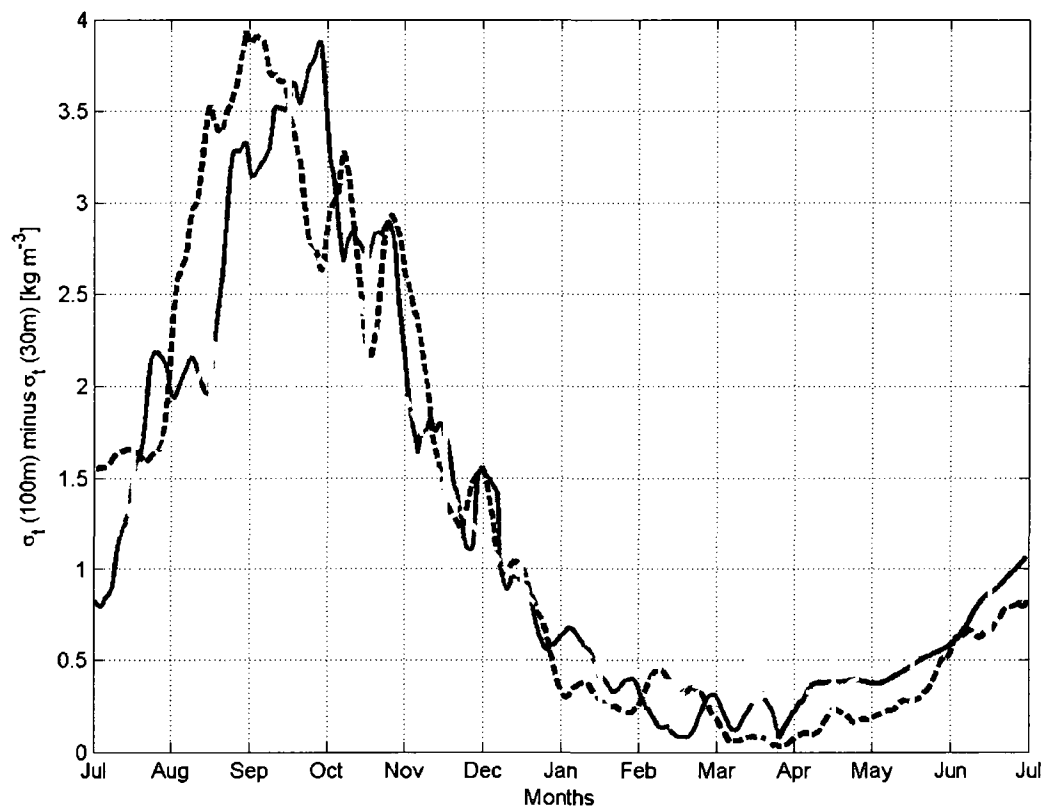


Figure 2.8: Seasonal cycle of GAK1 density stratification. Seasonal cycle of the σ_t -difference [kg m^{-3}] between 100 m and 30 m as a measure of stratification computed from moored temperature and salinity recordings at 100 m and 30 m. σ_t -differences from 2006/07 (black dashed) and 2007/08 (solid) are compared with monthly means from the mooring records from 1998-2008 (grey dashed with circles). Vertical bars on monthly means indicate one standard deviation. Monthly means are plotted in the middle of the month, x-ticks indicate the first day of each month.

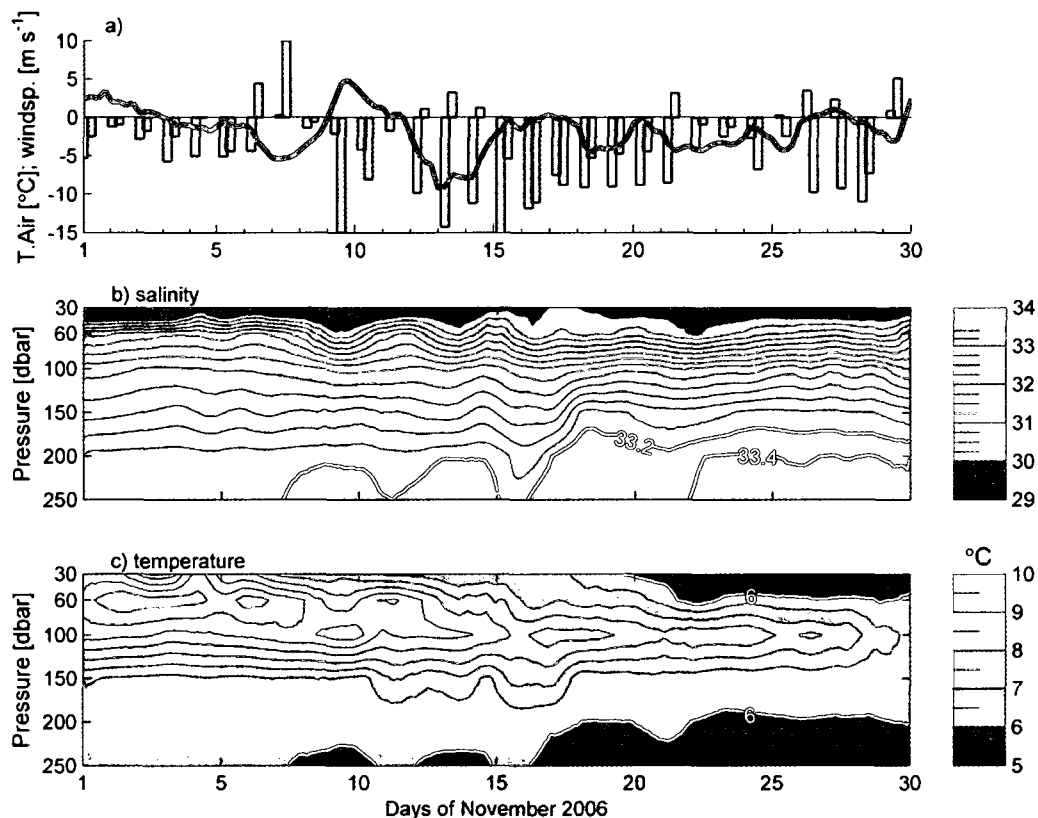


Figure 2.9: Temperature, salinity and winds in November 2006. Atmospheric and hydrographic observations from November 2006. a) NCEP 4 times daily air temperatures [°C, blue line] at (60°N, ~149°W), meridional (red bars) and zonal (green) QuikSCAT wind components [m s⁻¹] (positive indicates southerly and westerly); GAK1 moored b) salinity; c) temperature [°C], at 30 m, 60 m, 100 m, 150 m, 200 m, 250 m. Temperature and salinity are smoothed using a 1-day moving average.

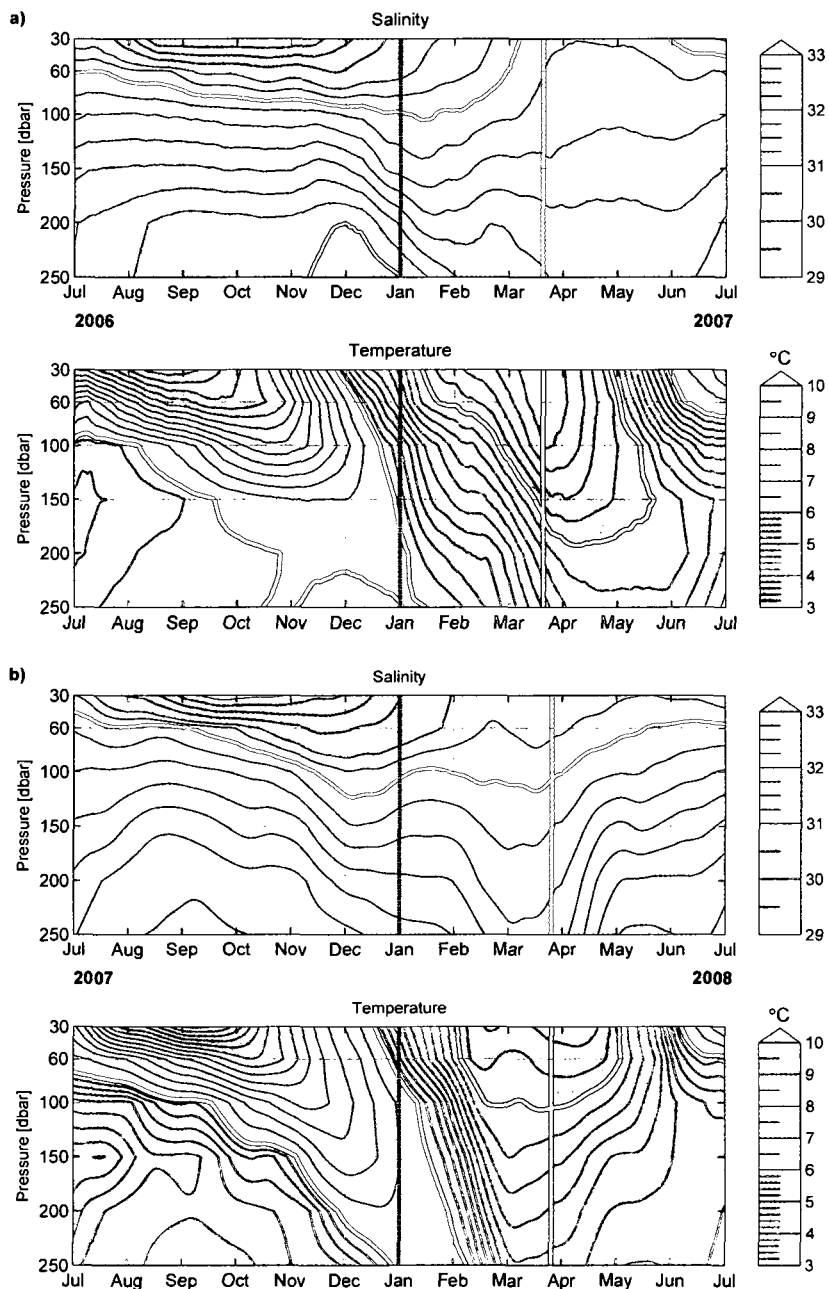


Figure 2.10: High resolution GAK1 temperature and salinity records. Salinity and temperature [°C] from the GAK1 mooring recorded at 30 m, 60 m, 100 m, 150 m, 200 m, 250 m, shown from 1 July to 30 June of a) 2006/07; b) 2007/08; c) 2001/02; d) 2000/01. Black dashed lines mark 1 January as a reference, and white vertical lines mark the data gap between mooring recovery and deployment. 4°C- and 6°C-isotherms, and 31.5 and 33.25 isohalines are highlighted by white contours. Note that isohaline increments vary between 0.25 and 0.5, and isotherms between 0.2 and 0.5 °C as indicated in color legends. Data is smoothed using a 7-day moving average.

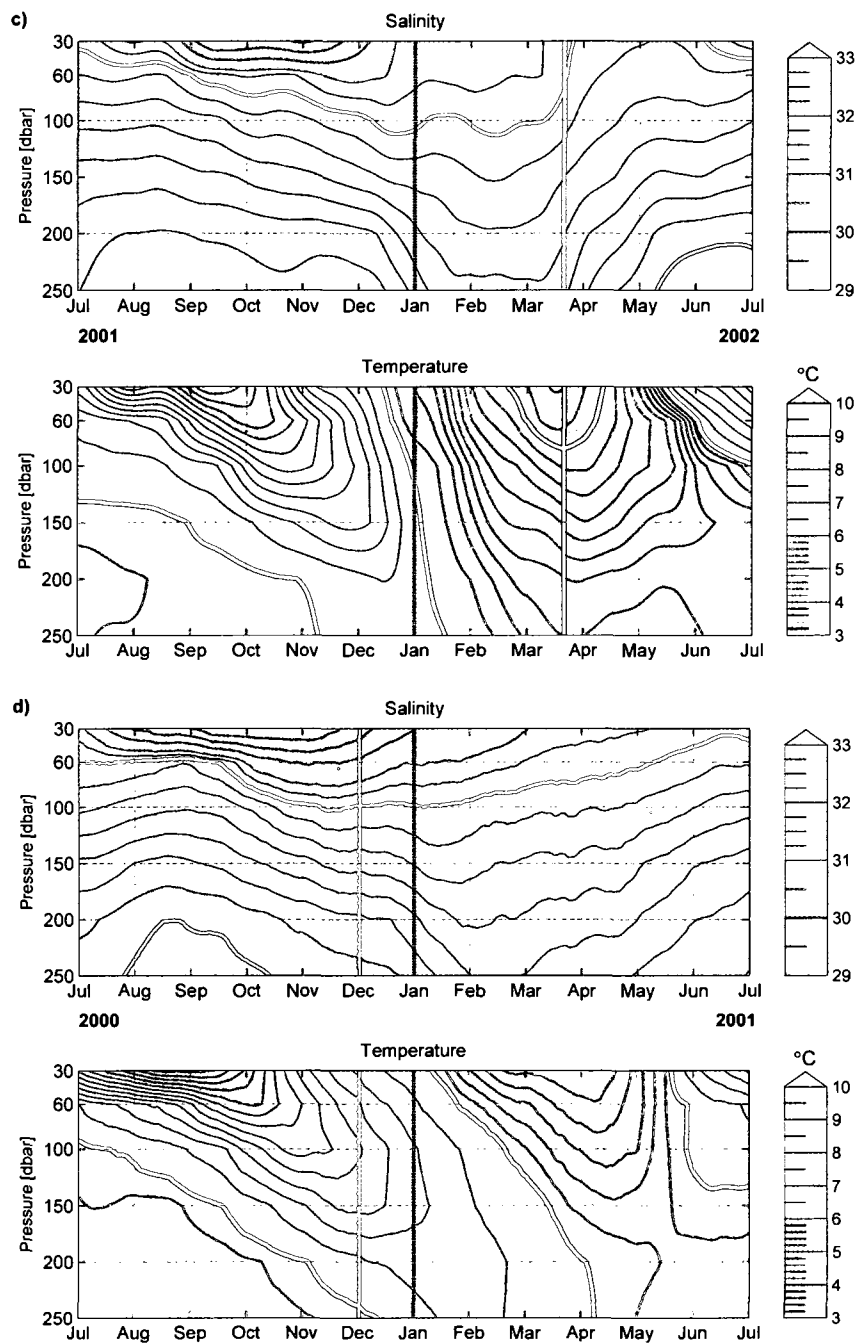


Figure 2.10 continued

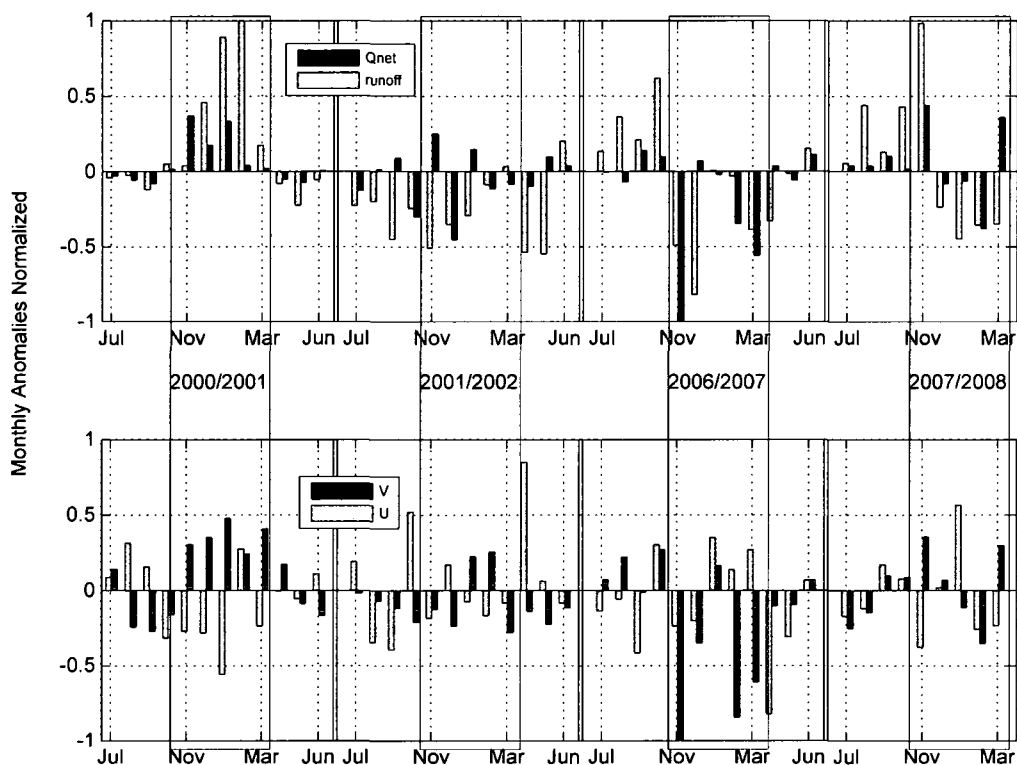


Figure 2.11: Wind, runoff and heat flux anomalies. Monthly normalized anomalies (2000-2008): (upper panel) NCEP net heat flux [W m^{-2}] (black bars); freshwater runoff [$\text{km}^3 \text{s}^{-1}$] (grey bars); (lower panel) meridional (black) and zonal (grey) QuikSCAT components [m s^{-1}] where negative anomalies indicate winds from the north and from the east. Grey shades highlight the cooling season from November to March. Months shown correspond to the mooring time series in Figure 2.10a-d.

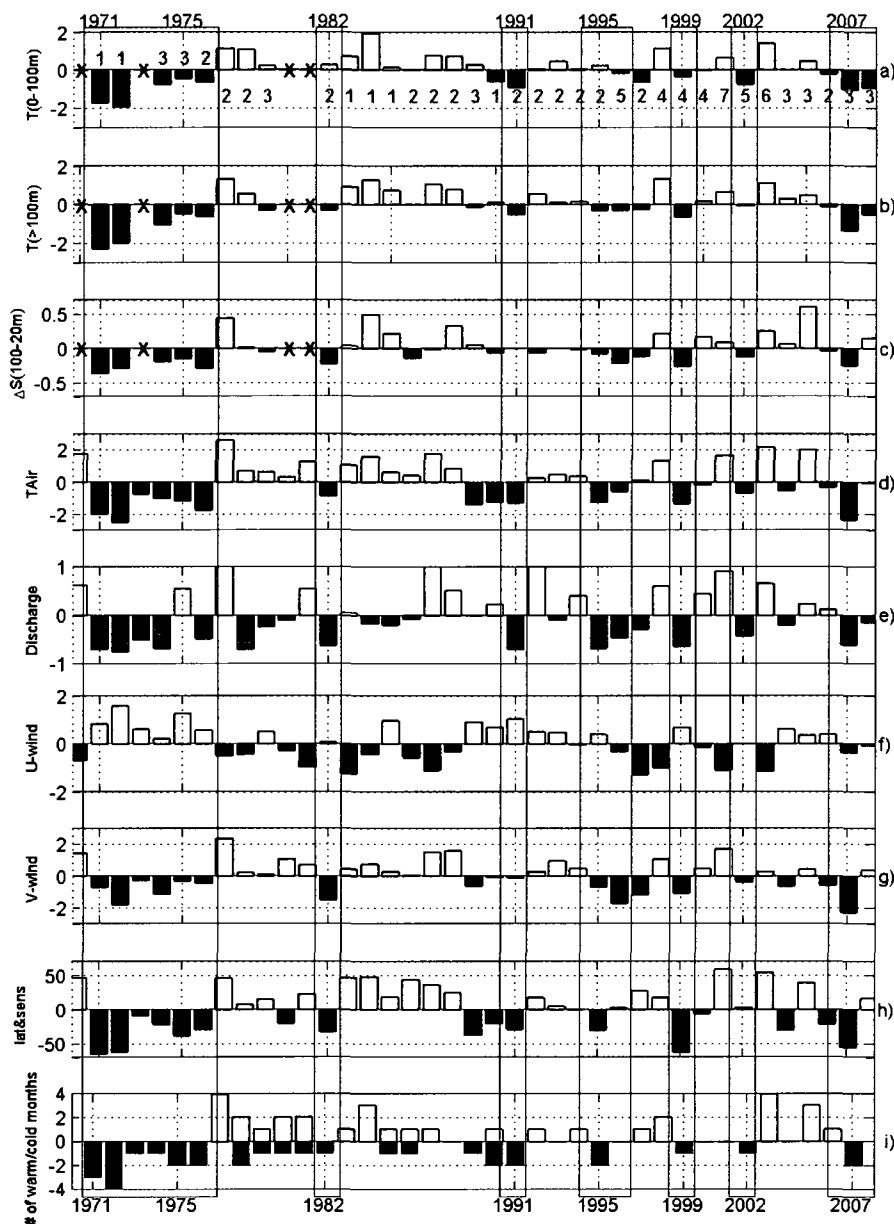


Figure 2.12: Winter anomalies of atmospheric variables 1970-2008. a) Upper layer (0-100 m) and b) lower layer (100-250 m) temperature anomalies [°C], and c) the salinity difference between 100 m and 20 m, all averaged from February-May CTD profiles, compared with winter (Nov-March) anomalies from 1970-present of: d) NCEP air temperatures [°C]; e) Freshwater runoff [$\text{km}^3 \text{s}^{-1}$]; f) zonal and g) meridional wind speed [m s^{-1}]; h) latent and sensible heat flux [W m^{-2}]; and i) the number of months with anomalously high/low air temperatures between November and March; Grey numbers in a) indicate the number of CTD casts used for averaging. Grey boxes highlight years with anomalously low ($<1\sigma$) deep (100-250 m) temperatures. Filled bars indicate negative anomalies. Note that there were no data in 1970, 1973, 1980, and 1981 for panels a-c).

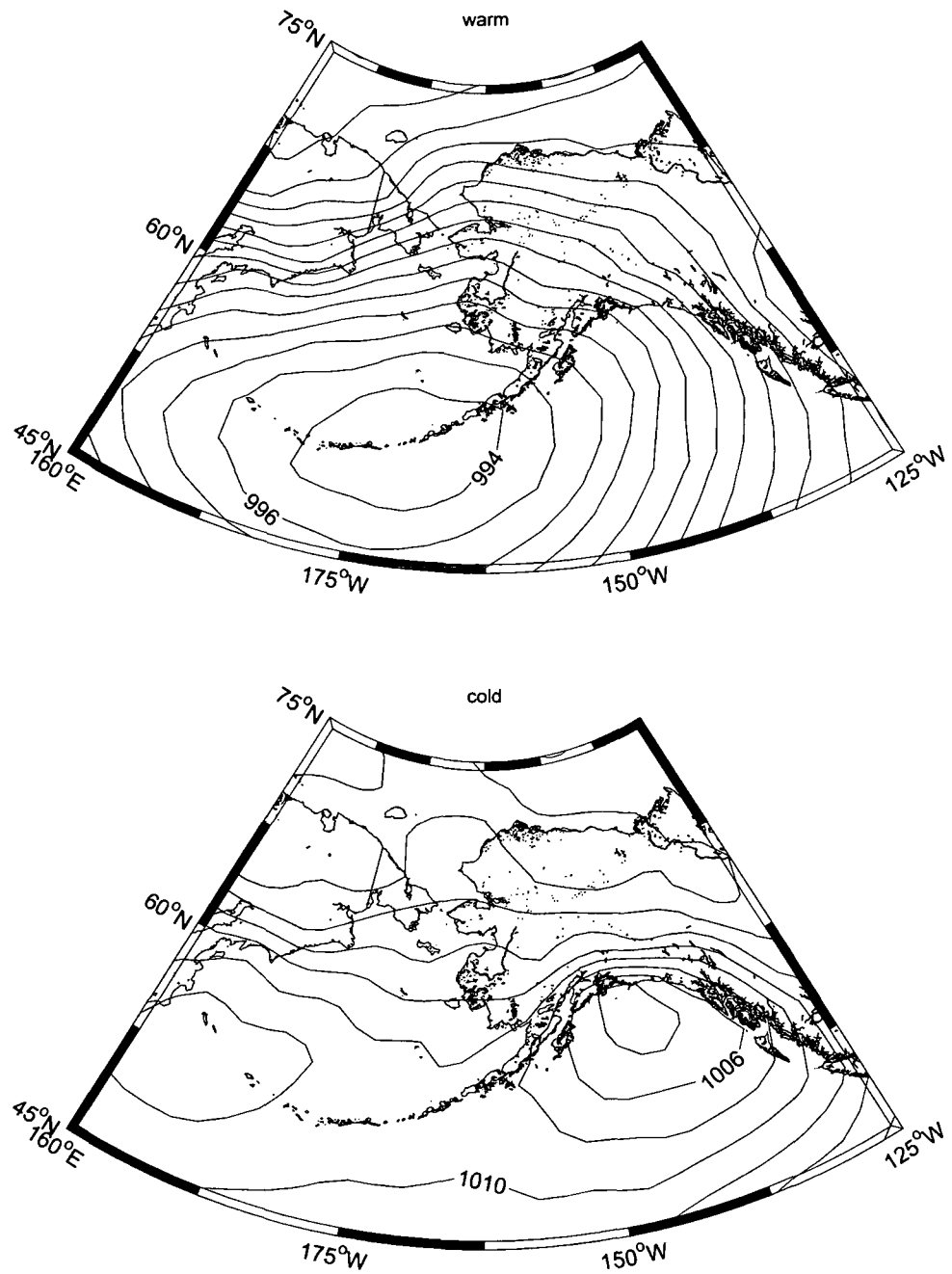


Figure 2.13: Sea level pressure patterns. Averaged SLP [mbar] distribution during months of anomalously $>|1\sigma|$ high (top) and low (bottom) November-March air temperatures at GAK1. Contours are in 2 mbar increments.

Chapter 3 Air-sea and oceanic heat flux contributions to the heat budget of the northern Gulf of Alaska shelf¹

Abstract

We constructed annual cycles of NCEP air-sea fluxes and temporal oceanic heat content change from Seward Line hydrographic surveys to quantify the different contributions to the oceanic near-shore heat budget on the northern Gulf of Alaska shelf. The deficit between air-sea fluxes and the temporal change in oceanic heat content throughout the cooling season (October-April) varies from $\sim 25\text{-}90\text{ Wm}^{-2}$ and is balanced by ocean heat flux convergence. Cross-shore heat flux convergence is insignificant on annual average, and the near-shore heat budget is likely entirely balanced by the Alaska Coastal Current (ACC), which re-supplies $\sim 10\text{-}35\%$ of the heat removed by air-sea fluxes during the cooling season.

Further, we estimated spatial heat flux gradients and conclude that air-sea fluxes increase from east to west and from off- to on-shore. The cross-shore gradients are governed by wind speed gradients, likely due to ageostrophic near-shore wind events during the cooling season, while the along-shore heat flux gradients are governed by the occurrence of low pressure systems in the northern GOA that result in cold northerly winds over the northwestern GOA.

¹ Janout, M.A., and T.J. Weingartner, Air-sea and oceanic heat flux contributions to the heat budget on the northern Gulf of Alaska shelf, for submission to the *Journal of Geophysical Research*.

These results underline the ACC's role as the dominant oceanic heat source to the northern GOA, and further imply an increased cooling rate of the ACC west of the Seward Line. Furthermore, our analysis showed that near-shore regions and particularly waters in the ACC are subjected to stronger winter cooling than the mid- and outer shelves.

3.1 Introduction

The northern Gulf of Alaska (GOA) shelf is highly productive and supports some of the world's largest fisheries. From fall through spring, the Aleutian Low is the dominant atmospheric pressure system in the North Pacific and responsible for the predominantly downwelling-favorable winds and the large precipitation rates in the northern GOA [Wilson and Overland, 1986; Stabeno et al., 2004]. Winds and freshwater input along the coast are the driving mechanisms for the Alaska Coastal Current (ACC) [Royer, 1981; Johnson et al., 1988; Schumacher et al., 1989; Weingartner et al., 2005], the dominant shelf circulation feature that advects organisms and water masses around the GOA and ultimately into the Bering Sea through passes in the Aleutian Islands.

Ecosystem responses in the GOA were observed following shifts in ocean climate in 1977 and 1989 [Anderson and Piatt, 1999; Hare and Mantua, 2000]. In the winter of 2006/07, the northern GOA's three decade-long warming trend [Royer and Grosch, 2006] was interrupted by the strongest ocean cooling since the early 1970s [Janout et al., in press]. The cooling coincided with delayed spring blooms and

delayed zooplankton development in 2007 and 2008 [Hopcroft, pers. comm.]. Salmon catches, which have been used as one indicator of the state of the Northeast Pacific (NEP) ecosystem, appear to be correlated with the Pacific Decadal Oscillation [PDO, Mantua et al., 1997], a measure of sea surface temperature variability in the NEP. The northern GOA shelf, however, has complex three-dimensional circulation and the heat budget here is strongly impacted by stratification due to freshwater runoff and its redistribution by along- and cross-shelf advection and mixing processes. For example, the recent 2007 cooling coincided with some of the lowest geostrophic velocities on the northern GOA shelf and likely complemented the cooling through reduced along-shore heat transport [Janout et al., in press]. Although ocean temperatures substantially influence marine ecosystems, the processes that control temperature variability on this shelf remain largely unquantified. Weingartner et al. [2005] estimated physical processes in the ACC and their impact on the near-shore GOA freshwater budget. The aim of this paper is to complement their findings by quantifying the relative importance of cross- and along-shore heat flux convergences in comparison to air-sea heat exchanges on the coastal GOA heat budget. Furthermore, long-term weather records are sparse on the northern GOA shelf and the National Center for Environmental Prediction (NCEP) reanalysis provides only one grid point (in the cross-shelf direction) on the wide (~150 km) northern GOA shelf, which may not necessarily be an adequate representation of shelf-wide conditions. We therefore investigate atmospheric records for along- and cross-shore gradients on the northern GOA shelf.

The paper is organized as follows. After describing the data in section 3.2, we present a climatology of hydrographic parameters and air-sea fluxes in sections 3.3.1 and 3.3.2, estimate cross- and along-shore heat transport in sections 3.3.3 and 3.3.4, and then examine gradients in air-sea fluxes in sections 3.3.5 and 3.3.6, followed by a summary and conclusion in section 3.4.

3.2 Datasets

We used oceanographic data from along the Seward Line (Figure 3.1), which was surveyed repeatedly from 1997–2004 as part of the NOAA-NSF funded NEP-GLOBEC program [Weingartner et al., 2002], and since 2005 with support from the North Pacific Research Board for biannual (May and September) cruises. We also used the data from hydrographic station GAK1 (the in-shore station of the Seward Line), which has been occupied since ~1970 and which includes ~450+ CTD profiles and eight years of moored temperature and salinity records [Janout et al., in press]. Prior to the mid-1980s, the accuracies in temperature and salinity are $\pm 0.02^{\circ}\text{C}$ and 0.05 and since then the accuracies are better than or equal to 0.01°C and 0.01. Prior to 1975, the salinity data were determined from bottle data collected at discrete depths.

Atmospheric parameters (wind speed, air and dew point temperature and sea level pressure) recorded from National Data Buoy Center (NDBC) buoys around the northern GOA shelf (Figure 3.1) were used to compute latent and sensible heat fluxes, and we also compared these with NCEP heat flux estimates at selected grid points near the Seward Line. In addition, we used QuikSCAT wind data to estimate cross-shelf

Ekman transport. The QuikSCAT wind estimates are from twice daily swaths with daily-averaged data available at 25 km resolution. Over the northern shelf, the along-shelf component of the wind is nearly zonal [Royer, 2005], so downwelling-favorable winds are easterly. We use the meteorological convention to indicate wind direction, i.e. northerly indicates winds from north to south.

We also used monthly coastal freshwater discharge anomalies from the Alaska-British Columbia boundary to 150°W from Royer's [1982] hydrological model. These discharge anomalies are significantly correlated with upper ocean salinities at GAK1 and the alongshore baroclinic transport in the ACC [Weingartner et al., 2005].

3.3 Results

3.3.1 Annual cycles of salinity and temperature along the Seward Line

We computed seasonal averages of the cross-shelf distribution of salinity (Figure 3.2) and temperature (Figure 3.3) along the Seward Line on the northern GOA shelf from ~seven annual occupations from 1997-2004 by combining March, April and May transects into one spring average, July and August transects into one summer average, while October and December resemble fall and winter averages, respectively. Standard deviations (not shown) were computed from the same transects used to compute the seasonal temperature and salinity means. From fall to spring, salinity primarily controls density variations in the northern GOA [Royer, 2005], and the

seasonal hydrographic cycle is largely governed by the variations in coastal freshwater runoff and along-shore (downwelling-favorable) winds [Figure 3.4; Weingartner et al., 2005].

The combination of strong downwelling-favorable winds and low runoff in winter leads to the highest near-shore surface salinities (31-32), the weakest stratification and steeply sloping isohalines over the inner shelf in spring (Figure 3.2). During summer, downwelling winds cease and increased freshwater runoff decreases near-shore salinities (29-31) and enhances stratification and the off-shore spreading of low-salinity surface waters. The seaward sloping of the isohalines (and isopycnals) decreases, and shoreward (along-isopycnal) transport of saline and nutrient-rich water takes place and replenishes the nutrient reservoir at depth [Childers et al., 2005]. Beginning in October, isohalines plunge downward again toward the coast and the near-shore salinity is at an annual minimum (<29) due to the fall maximum in coastal freshwater runoff (Figure 3.4). Low surface salinities (31-32) are now found throughout the shelf and beyond the shelf break. Stratification is strongest across the shelf in July/August and decreases noticeably by December. At this time strong downwelling-favorable winds steepen the near-shore isohalines and cause the formation of large horizontal salinity gradients over the inner shelf. The largest seasonal salinity variability is from July to October on the inner shelf (<40 km from shore) and within the ACC in the upper 50 m (standard dev. ± 2), while the salinity does not change considerably on the middle and outer shelves (standard dev. $<\pm 0.4$). Due to the strong freshwater influence along the coast and the comparatively greater

impact of salinity on density variations in this subarctic ocean [Royer, 1982], salinity contributes 80-100% to 0-50 m density stratification (based on the mean 0-50 m Brunt-Väisälä frequency, not shown) on the inner shelf year-round, and 60-90% on the middle and outer shelves from fall to spring. The effect of atmospheric heat transfer into and the vertical distribution of heat in the water column is therefore regulated by freshwater and salinity stratification [Janout et al., in press].

Mean temperatures are lowest in spring (5-6°C) and nearly homogenous across the shelf, although near-shore waters may cool to ~3°C during cold years [Janout et al., in press]. Thermal stratification is absent in spring, but develops in summer, when temperatures may exceed 13°C in the upper 30 m (Figure 3.3). Summer subsurface (>50 m) isotherms gently decline towards the coast. By October, surface waters cool to <11°C, and by December, temperatures are <8°C across the shelf. Temperature variability is largest near the surface (0-50 m) across the shelf during summer and fall with standard deviations (not shown) of $\pm 2^\circ\text{C}$. Thermal stratification is strongest during summer across the shelf but its contribution to 0-50 m density stratification is greatest (70-80%) on the middle and outer shelf away from the coastal influence of freshwater on the inner shelf. Cross-shelf temperature gradients are relatively weak throughout the year, with maximum temperature differences between inner and outer shelves of $\sim 1^\circ\text{C}$ in October in the upper 50 m and generally smaller differences (<1°C) in deeper (>100 m) waters and at other times.

3.3.2 Air-sea fluxes and oceanic heat content

The seasonal net air-sea heat flux on the inner shelf (60°N, 146°W, Figure 3.1), based on the sum of daily means of (1948-2009) NCEP latent and sensible heat fluxes and net long- and shortwave radiation, ranges from $<-250 \pm 250 \text{ Wm}^{-2}$ in mid-winter to $\sim 150 \pm 50 \text{ Wm}^{-2}$ in summer (Figure 3.5). The warming season begins on average on 17 April, while the average onset of the cooling season is 13 September. During the cooling season, the net heat flux is largely due to the latent and sensible heat fluxes, which have similar magnitudes of $\sim -100 \text{ Wm}^{-2}$. However, the standard deviation in latent heat flux is nearly twice as large ($\pm 150 \text{ Wm}^{-2}$) as that of sensible heat flux ($\pm 80 \text{ Wm}^{-2}$). Longwave radiation is nearly constant throughout the year ($60 \pm 20 \text{ Wm}^{-2}$). Shortwave radiation is nearly zero at the winter solstice and the largest contributor to the net heat flux in summer ($200 \pm 50 \text{ Wm}^{-2}$). Contrary to the disparity between net heat loss and gain on the inner shelf, the net heat fluxes off-shore (58°N, 148°W, near GAK13) nearly balance one another on annual average and range from $-150 \pm 150 \text{ Wm}^{-2}$ in winter to $+150 \pm 50 \text{ Wm}^{-2}$ in summer. However, the near-shore fluxes in the (1948-2009) NCEP record show an annual mean deficit of $\sim 60 \text{ Wm}^{-2}$, which may be larger ($\sim 80 \text{ Wm}^{-2}$) if the bias in shortwave radiation of 20 Wm^{-2} [Ladd and Bond, 2002] detected at Station Papa (50°N, 145°W) is applicable to the northern GOA as well. Nevertheless, this annual deficit requires additional heat input by oceanic (along- and cross-shore) sources, which we examine below. In order to investigate the oceanic heat budget, we estimated the average monthly oceanic heat content (Q_{oc}) from the

~seven annual Seward Line occupations between 1997-2004 for the inner (GAK1-2)

and outer shelves (GAK7-8) (Figure 3.6) with $Q_{oc} = \int_{150m}^0 \rho c_p T dz$, where ρ is the water

density and T the water temperature integrated over the depth z . We limit our analysis to the upper 150 m of the water column as the maximum common depth along the Seward Line and hence the depth typically used for referencing velocities calculated from the thermal wind relation [Johnson et al. 1988]. The specific heat of sea water c_p ranges between 3980-4050 J kg⁻¹ K⁻¹ for GOA water properties [Fofonoff and Millard, 1983]. The middle shelf heat content co-varies with the outer shelf and is therefore not shown. Q_{oc} is at a minimum in March/April and maximum in October, with lower amplitudes on the middle and outer shelves and the largest amplitude on the inner shelf. The temporal change in oceanic heat content ($\partial Q_{oc} / \partial t$) is the net result of air-sea heat exchange and ocean heat flux convergence, and has a higher seasonal amplitude on the inner shelf than on the outer shelf. Over the outer shelf $\partial Q_{oc} / \partial t$ varies from ~-100 Wm⁻² in winter to ~+120 Wm⁻² in summer. These changes are thus nearly balanced by air-sea fluxes discussed previously. In contrast, $\partial Q_{oc} / \partial t$ in near-shore waters varies from ~-180 Wm⁻² in winter to nearly 200 Wm⁻² during summer (Figure 3.6). The residual, i.e. the additional heat flux estimated in near-shore Seward Line waters not accounted for by the atmosphere, is ~90 Wm⁻² on October-December average, and subsequently decreases to ~25-45 Wm⁻² from

January-April (Figure 3.7). In the following we make rough estimates of the cross- and along-shore heat fluxes and their contribution to the near-shore heat budget.

3.3.3 Cross-shore heat transport

Cross-shelf transport mechanisms on the northern GOA shelf include topography-current interactions and eddy fluxes [Stabeno et al., 2004; Ladd et al., 2005]. We expect that both heat fluxes are small however, given the feeble cross-shelf temperature gradients. Moreover, in the aggregate they are likely to balance one another and therefore neglected. Large anticyclonic slope eddies may impact the outer shelf's heat and freshwater budgets [Janout et al., 2009], but these occur irregularly and do not appear to influence inner shelf properties, hence they are also neglected. However, the prevailing downwelling-favorable winds from fall through spring impel a persistent Ekman transport that may influence the shelf heat budget.

The net oceanic cross-shelf heat transport is the product of the cross-shelf water transport and the cross-shelf heat gradient in both the surface and bottom Ekman layers. We used monthly mean zonal QuikSCAT wind stress τ_x from 2000-2008 and the Coriolis parameter f to compute monthly Ekman transport ($M_{Ekman} = \tau_x f^{-1} \rho^{-1}$; note that M_{Ekman} is a transport per meter coastline with units: $[m^2 s^{-1}]$). Zonal wind stress is predominantly easterly, hence favorable for coastal downwelling and on-shelf Ekman transport, with the largest magnitude in late fall and early winter. The easterlies weaken during summer (Figure 3.4) and in some years become weak westerly (upwelling-favorable). Bottom-friction arising from the large-scale east-to-west along-

shelf flow generates an off-shelf transport in a bottom Ekman layer that balances the transport in the surface Ekman layer. Hence, the total Ekman heat flux convergence is:

$$HF_{Ek} = M_{Ek} \left(\frac{\partial Q_{surf}}{\partial y} - \frac{\partial Q_{bott}}{\partial y} \right).$$

Surface (0-20 m) and near-bottom (230-250 m) cross-shelf heat content gradients $\partial Q/\partial y$ were computed from heat content differences between the outer (GAK7-8) and inner (GAK1-2) shelf (Figure 3.8). These cross-shelf gradients are not depth-integrated, but instead are bottom- and surface-means (units of Q : [$J m^{-3}$] and $\partial Q/\partial y$: [$J m^{-4}$]). As inferred from Figures 3.3 and 3.6, the heat content varies seasonally, but in general surface heat content increases seaward ($\sim 20 Jm^{-4}$) during winter/spring and decreases seaward ($\sim 60 Jm^{-4}$) from late summer through fall. Bottom heat gradients are small ($< 20 Jm^{-4}$) except in July ($\sim 35 Jm^{-4}$), which may reflect the on-shore flow of cooler waters from the shelfbreak following the shelf's adjustment after the weakening of along-shore winds in spring (Figure 3.4). The net Ekman heat flux convergence is on-shore and a maximum between December and March ($\sim 20 Wm^{-2}$) and a minimum in summer of $< 5 Wm^{-2}$ (Figure 3.8). In October, the cross-shore heat gradient is positive so that the net Ekman heat flux convergence is off-shore at $\sim 35 Wm^{-2}$ and thus tends to cool the inner shelf. Although the standard deviation for Ekman heat flux convergence is small through most of the year ($< \pm 15 Wm^{-2}$), it is large in October ($\pm 45 Wm^{-2}$), which likely reflects the large variability seen in near-shore summer temperatures as mentioned in section 3.3.1. Although our computations suggest that Ekman transport may occasionally account for as much as

60 Wm^{-2} (but generally $<20 \text{ Wm}^{-2}$), it is unclear if or how efficiently on-shore Ekman transport can penetrate through the ACC front, which is strongest in fall when the on-shelf Ekman heat flux convergence is also a maximum (fall-spring). In aggregate, our computation suggests that on annual average the net Ekman heat flux convergence is insignificant ($\sim 3 \text{ Wm}^{-2}$) and thus does not contribute appreciably to the coastal GOA heat budget. Next we will examine the contribution of along-shore heat advection.

3.3.4 Along-shore heat transport

The mid- and outer shelves are characterized by comparatively weak and variable flow [Stabeno et al., 2004] and the temporal oceanic heat change there appears to be in approximate balance with the air-sea flux in all seasons (Figure 3.6). In contrast, the inner shelf has a large heat deficit, which is not satisfied by the cross-shelf heat flux convergence associated with Ekman transport as shown above. Therefore, the bulk of the deficit is likely balanced by along-shore heat advection. As shown in Figure 3.7, the deficit averages to $\sim 70 \text{ Wm}^{-2}$ in the cooling season (October-April), with a larger deficit ($\sim 90 \text{ Wm}^{-2}$) from October-December. The majority ($\sim 70\%$) of the baroclinic along-shore transport on the northern GOA shelf is carried within the ACC [Weingartner et al., 2005]. Seasonal velocities vary between $0.25\text{-}1.75 \text{ m s}^{-1}$ with an annual mean transport of $\sim 0.8 \text{ Sv}$ [Johnson et al., 1988; Stabeno et al., 1995]. Stabeno et al. [1995] estimated that the baroclinic component may amount to as much as 75% of the total ACC transport, depending on season and location, while

Williams et al. [2007] estimate the baroclinic transport at 80-90% under increased downwelling winds (i.e. from fall-spring).

We estimate that the 0-150 m averaged along-shore gradients in heat are $\sim 4 \pm 1 \text{ Jm}^{-4}$, based on sea surface temperature (SST) differences between National Data Buoy Center (NDBC) buoys 60082 and 60084, between different NCEP grid points and from CTD profiles at Cape Suckling (see Figure 3.1 for locations) and the Seward Line in December 1999. During winter, thermal stratification is weak and we assume that surface temperature gradients are similar throughout the water column. Summer surface temperatures show very feeble along-shelf gradients on the northern GOA shelf so we confine our estimates of along-shelf heat advection to the cooling season only.

To balance the October-December deficit of 90 Wm^{-2} on the inner shelf heat implies that for along-shelf heat gradients of $\sim 4 \pm 1 \text{ Jm}^{-4}$, current speeds must be $\sim 0.15 \pm 0.05 \text{ m s}^{-1}$. These along-shelf current speeds are comparable with the depth-averaged December ACC velocities of 0.2 m s^{-1} obtained from moored current meter records [Johnson et al., 1988]. Hence along-shelf heat flux convergence within the ACC is likely important in closing the heat budget on the inner shelf. However, along-shore temperature (and heat) gradients are difficult to estimate reliably due to a lack of synoptic measurements.

Assuming that the majority of the fall-spring transport is baroclinic [Stabeno et al., 1995], and also acknowledging that the ratio of baroclinic to barotropic transport is highly variable, we next estimate the along-shore baroclinic contribution to the heat

flux. The baroclinic (geostrophic) along-shore transport along the Seward Line is $u_{bc} = -f^{-1} \rho^{-1} \partial p / \partial y$, where the cross-shore pressure gradient $\partial p / \partial y$ is estimated from the Seward Line density structure. The level of no motion is the deepest common depth between two stations. As above, we categorized the Seward Line into inner and outer shelf and computed the average geostrophic velocities (1997-2004) of the respective stations from 0-150 m, the maximum common depth along the transect, and then interpolated the velocity to monthly values (Figure 3.9). While the outer shelf's westward velocities vary between $\sim 0 \text{ m s}^{-1}$ in July and $\sim 0.06 \text{ m s}^{-1}$ in December (and May), the inner shelf's (baroclinic) velocities are minimum in July (0.05 m s^{-1}) and maximum in December (0.18 m s^{-1}) and vary seasonally in accordance with the runoff (Figure 3.4). The along-shore heat transport (product of baroclinic transport and the along-shore heat gradient) is approximately balanced by the difference between air-sea fluxes and the change in oceanic heat content: $HF_{\text{air-sea}} - \partial Q_{oc} / \partial t = u_{bc} \partial Q / \partial x$. The deficit in the heat budget is largest during October-December ($\sim 90 \text{ Wm}^{-2}$; $\sim 110 \text{ Wm}^{-2}$ when considering a 20 Wm^{-2} bias in shortwave radiation described by Ladd and Bond [2002]), and subsequently decreases to 25-45 (45-65) Wm^{-2} from February to April (Figure 3.7). To first order, this is consistent with the seasonal variation in along-shore velocity, which is a maximum in fall. Geostrophic velocities of 0.12-0.18 m s^{-1} from October-December and a mean $\partial Q / \partial x$ of $4 \pm 1 \text{ Jm}^{-4}$ from 0-150 m (depth of ACC) yields an along-shore heat flux convergence of 72-108 Wm^{-2} . For February-April, baroclinic velocities are smaller (0.09 m s^{-1}) and result in along-shore heat

advection of $\sim 54 \pm 12 \text{ Wm}^{-2}$, which is again comparable to the residuals estimated in Figure 3.7. However, the addition of the barotropic velocity component would result in considerably higher values. Nevertheless, from the data available we suggest that along-shore heat flux convergence within the ACC can easily account for the heat budget deficit during the cooling season. Moreover, the advective heat flux is substantially greater than the cross-shore heat flux and may supply as much as 10% (late winter/spring) to 35% (fall) of the heat removed by air-sea fluxes during the cooling season. Nevertheless the uncertainties in our analysis are substantial given the imprecision in our estimates of along-shelf temperature gradients and the unknown contribution associated with the barotropic heat flux convergence.

3.3.5 Cross- and along-shelf air-sea heat flux variability

The previous sections highlighted considerable cross-shelf gradients in along-shore baroclinic transport (Figure 3.9), oceanic heat content (Figure 3.6), and along-shore wind stress (Figure 3.4). This spatial variability implies significant consequences on air-sea fluxes and the oceanic heat budget across the shelf. For a northern GOA-wide comparison of air-sea fluxes, we searched the NDBC database for weather buoys with simultaneous data coverage, and computed turbulent (latent and sensible) heat fluxes using the COARE3.0 algorithm [Fairall et al., 1996; Fairall et al., 2003]. Turbulent fluxes compose the largest part of the winter heat flux variability (Figure 3.5), and are therefore the largest source of variability in air-sea heat fluxes. Although the bulk of the winter cooling occurs from November through March, this

part of our analysis is constrained to the 120-day period between January and April for the years 2003, 2004, 2006, and 2008 due to limited concurrent buoy data. We then combine single buoys into regional averages and compute the cumulative sum of the fluxes in order to describe spatial heat flux variations over the northern GOA shelf (Figure 3.10). The results indicate that winter air-sea heat fluxes increase from off-shore to on-shore and from east to west around the GOA. For example, the cumulative turbulent heat fluxes in Shelikof Strait are more than twice those over the basin southeast of Kodiak Island. Heat fluxes in Prince William Sound (PWS) are ~20% less than those in Shelikof Strait, but ~15% greater than Cape Suckling and Southeast Alaska and 30% larger than at Middleton Island (PAMD) on the outer shelf, which is ~90 km south of the sound. The average air temperature of the PWS buoys is only ~0.4°C lower than at PAMD during the four years used to construct Figure 3.10, and therefore these cross-shelf heat flux gradients between the outer and inner shelf and PWS are largely due to cross-shelf wind gradients as shown next.

Zonal means of the 2000-2008 monthly QuikSCAT wind speeds between 140-150°W (roughly between Yakutat and GAK1) on the northern GOA shelf show that wind speeds ~80 km offshore of the coast are 30-35% smaller than those adjacent to the coast (Figure 3.11). Cross-shelf wind speed gradients diminish in spring and are slightly reversed in summer. Figure 3.12 shows how the ratio of the inner to outer shelf wind speeds, averaged over the November-March period, varies along-shelf between these two longitudes. Relatively high ratios are found at ~146°W in eastern PWS, between 143°W to 146°W near the Copper River delta and the Cordova-Valdez

mountains, and at the western entrance to PWS (148°W) and the mouth of Resurrection Bay (~149°W). These are areas where barrier jets and gap winds occur during the cooling season [Macklin et al., 1988; Loescher et al., 2006]. Barrier jets flow along the coast and are generated during on-shore air flow while (seaward-oriented) gap winds are channeled through gaps in the coastal topography [Loescher et al., 2006]. Both are intimately linked to the mountainous coastline [Macklin et al., 1988; Overland and Bond, 1993]. Loescher et al. [2006] found that >80% of all barrier and hybrid (combination of barrier and gap wind) jets are <80 km wide, which is supported by Macklin et al. [1988], who showed that these ageostrophic near-shore wind events adjust geotripticly within one Rossby radius of deformation (~60 km) from shore. Their findings are consistent with the large cross-shelf gradients observed in QuikSCAT wind speeds (Figure 3.11) and the large air-sea flux gradients between PWS and PAMD since the latter is ~90 km seaward of PWS and thus outside the influence of these mesoscale wind phenomena. The impact of these strong ageostrophic near-shore wind events on cooling of the ACC is therefore substantial. Moreover, the influence of the cross-shelf gradients in air-sea cooling between PWS and the shelf is potentially important in cooling ACC waters since a substantial portion of this current flows through PWS [Niebauer et al., 1994].

The Shelikof Strait buoy indicates that the ocean loses considerably more heat over the north-western GOA than elsewhere on the shelf. Air-sea fluxes there may be enhanced by strong low-level wind jets that often occur in the region due to channels in the topography [Macklin et al., 1990; Liu et al., 2006]. Furthermore, depth-averaged

temperature data from May CTD casts show that average temperatures can be 1-2°C lower in Shelikof Strait than at GAK1 [Stabeno et al., 2004], so that the along-shelf temperature gradient between GAK1 and Shelikof Strait is $\sim 3.3 \times 10^{-6} \text{ }^\circ\text{C m}^{-1}$ or nearly twice the $\sim 1.5 \times 10^{-6} \text{ }^\circ\text{C m}^{-1}$ temperature gradient to the east of GAK1. In the next section we investigate the sea level pressure (SLP) distributions over the northern GOA that give rise to these spatial variations in wintertime air-sea heat fluxes.

3.3.6 The role of northern GOA low sea level pressure events

A more detailed examination of the January-April turbulent fluxes discussed above indicated that each of the four years used to construct Figure 3.10 included a number of vigorous cooling events, where the heat loss exceeded the average winter heat loss by 50-100%, with each event lasting from 2-10 days. The aggregate heat loss during these events amounts to $\sim 40\text{-}60\%$ of the total January-April heat loss. Inspection of the SLP distributions (not shown) shows that each cooling event is generally associated with a low pressure system located in the northern GOA. The influence of GOA lows on the North Pacific's oceanic and atmospheric conditions are well-known [Overland and Hiester, 1980; Rodionov et al., 2007; Janout et al., in press] and we here show that the propagation and residence time of northern GOA lows may be a major parameter in the spatio-temporal variability of northern GOA heat fluxes.

Overland and Hiester [1980] used a correlation technique to identify pressure patterns, and describe the northern GOA low pressure pattern in comparison with the

Aleutian Low and other dominant patterns. We carry out a similar analysis and enumerate the occurrence of lows in the northern GOA during winter (November-March). Specifically, we extracted 6-hourly (1948-2009) NCEP SLP within 130-180°W and 50-62.5°N and enumerated occasions where the lowest SLP was found within the region bounded by 57.5-62.5°N, and 130-155°W, and compute the annual frequency of occurrence (F_o) of northern GOA low pressure systems according to:

$$F_o = \frac{\sum \text{days_with_low_SLP_within_box}}{\sum \text{days_of_winter}} \times 100\%.$$

The mean November-March anomalies of F_o and air temperatures (Figure 3.13) from a northern GOA NCEP grid point (60°N, 146.5°W) (Figure 3.1) are significantly anti-correlated ($r=-0.53$, $p<0.01$). For the November-March average, F_o is ~18% and consistent with Overland and Hiestler's [1980] findings that F_o was 16% for winters averaged from 1968-1977. The maximum F_o of ~27% occurred in 1975, and this value was only slightly larger than values in 1971, 1972, and 2007 (~25%), while 2003 was a minimum (~9%). The 1976/77 regime shift [Mantua et al., 1997] is evident in the F_o time series as high (low) F_o and low (high) air temperatures were more common during the period before (after) the regime shift. Moreover, the early 1970s and 2007 and 2008 are consistent with periods of anomalously low northern GOA shelf temperatures [Janout et al., in press]. The occurrence and duration of low SLP systems that propagate into the northern GOA therefore explain part ($r^2=0.28$; 28%) of the interannual variability of the northern GOA heat budget.

The position of the lows also explains the along- and cross-shore variations in the heat fluxes. NCEP air temperature anomalies and SLP from March 2007 (as an example of an anomalously cold month in the northern GOA) indicate that low pressure centered at the head of the GOA causes below normal air temperatures primarily along the western flank of the low due to northerly winds that bring cold continental air southward from Alaska's interior (Figure 3.14). In contrast the eastern GOA (between 50-55°N) shows positive air temperature anomalies due to eastward (i.e. shoreward) advection of oceanic air masses. Furthermore, lows tend to concentrate along the north-central portion of the GOA basin, because the coastal mountains impede inland propagation [Wilson and Overland, 1986]. For example, lows are centered between 140-150°W ~50% of the time and while east of 140°W they occur only 23% of the time. We next compare winter heat fluxes and their anomalies at three NCEP grid points at near-shore locations in the eastern, central (south of PWS), and north-western GOA (east of Kodiak) (Figure 3.1) from 1948-2009 and thereby distinguish between average winter (November-March) heat flux (Figure 3.15a) and the average winter heat flux during the occurrence of northern GOA lows (Figure 3.15b). In addition, we computed the winter heat flux anomalies (Figure 3.15c), and compare these with those heat flux anomalies associated with the presence of northern GOA lows (Figure 3.15d). On winter average, the northeastern GOA has relatively moderate mean winter heat flux of $-140 (\pm 35) \text{ Wm}^{-2}$, while mean heat fluxes are $-155 (\pm 40) \text{ Wm}^{-2}$ in the northcentral GOA, and $-190 (\pm 45) \text{ Wm}^{-2}$ in the northwestern GOA.

The winter heat fluxes and their anomalies (Figures 3.15a and c) are spatially coherent and show a uniform shift from negative to positive anomalies during the 1977 regime shift [Mantua et al., 1997] at each of the three locations. Interestingly, when averaging winter heat fluxes exclusively during the occurrence of northern GOA lows, the three grid points show significant differences (Figure 3.15b). Under these conditions the eastern GOA has an average heat loss of $-120 \pm 30 \text{ Wm}^{-2}$ with positive anomalies ($+20 \pm 25 \text{ Wm}^{-2}$) (Figure 3.15d), while the northcentral GOA loses more heat ($-190 \pm 55 \text{ Wm}^{-2}$), with negative anomalies of $-30 \pm 50 \text{ Wm}^{-2}$. In the northwestern GOA, however, heat fluxes are $-380 \pm 100 \text{ Wm}^{-2}$ with the largest anomalies of $\sim -190 \pm 95 \text{ Wm}^{-2}$, which suggests that northern GOA lows favor disproportional cooling in waters from Cook Inlet through Unimak Pass. Based on drifter observations, it takes from one to three months for water parcels to transit this $\sim 800 \text{ km}$ stretch of the GOA shelf [Stabeno et al., 2002; Janout et al., 2009]. Hence as the ACC flows through this region in winter it is subjected to substantially greater cooling than elsewhere on the shelf. Our results also imply that low pressure systems centered over the northern GOA impact the heat budget of the southeast Bering Sea shelf both directly through air-sea interactions over that shelf and indirectly through strong cooling of GOA shelf waters before they enter the southeast Bering Sea shelf.

3.4 Summary and conclusion

We presented climatological estimates of air-sea heat fluxes and oceanic along- and cross-shore heat advection and their relative contributions to the northern

Gulf of Alaska (GOA) oceanic heat budget computed from averaged Seward Line observations from 1997-2004. Further, we discussed the effect of near-shore ageostrophic wind jets and atmospheric pressure patterns on cross- and along-shore air-sea heat flux gradients, and their consequences on the northern GOA oceanography.

The difference between air-sea heat fluxes and the temporal change in oceanic heat content ($\partial Q/\partial t$) is $\sim 90 \text{ Wm}^{-2}$ in fall and decreases to $\sim 40 \text{ Wm}^{-2}$ in spring (Figure 3.7), and is balanced by ocean heat flux convergences. Our estimates suggest that the annual average cross-shelf heat flux convergence is small ($\sim 3 \text{ Wm}^{-2}$) despite persistent along-shore winds throughout the cooling season. This is due to weak cross-shelf temperature gradients, which reverse in winter and hence balance the Ekman heat flux convergence on fall-spring average. Although data are limited, our analysis suggests that along-shore heat flux convergence within the Alaska Coastal Current (ACC) may provide the residual heat to close the October-April northern GOA heat budget on the inner shelf. This is based on baroclinic transport (Figure 3.9) computed from the Seward Line density structure and on along-shore thermal gradients that we estimated on the order of $\sim 4 \pm 1 \text{ Jm}^{-4}$.

Turbulent fluxes computed from NDBC buoys (January-April of 2003, 2004, 2006, 2008) suggest positive along- and cross-shore gradients (increased oceanic heat loss from east to west and from off- to on-shore) in the northern GOA. The cross-shore heat flux gradients may primarily be explained by wind speed gradients (Figure 3.11) due to strong ($>20 \text{ m s}^{-1}$) ageostrophic near-shore wind events having limited

off-shore extent (<60-80 km) [Loescher et al., 2006; Macklin et al., 1988]. In contrast, wintertime along-shore heat flux gradients are influenced by northern GOA low pressure systems that on November-March average occur ~18% of the time. When low pressure systems occupy the northern GOA in winter, the western GOA is mostly under the western flank of the low and therefore under the influence of cold northerly winds (Figure 3.14). We estimated the frequency of occurrence of northern GOA lows and showed that it is significantly anti-correlated with northern GOA air temperatures ($r=-0.53$, $p<0.01$) (Figure 3.13). Consequently air-sea heat fluxes during the occurrence of northern GOA lows are significantly stronger in the northwestern GOA ($\sim 380 \pm 100 \text{ Wm}^{-2}$), compared with the north-central ($-190 \pm 55 \text{ Wm}^{-2}$) and north-eastern GOA ($-120 \pm 30 \text{ Wm}^{-2}$).

These results underline the ACC's role as the dominant oceanic heat source to the northern GOA, and further imply an increased cooling rate of the ACC west of the Seward Line. Furthermore, our analysis showed that near-shore regions and particularly waters in the ACC are subjected to stronger winter cooling than the mid- and outer shelves.

Our quantifications suggest that along-shore transport in the ACC contributes far more to the near-shore northern GOA heat budget than cross-shore Ekman transport. These estimates complement other studies, which showed that Ekman transport does not contribute to variability in the coastal freshwater budget [Weingartner et al., 2005]. We, however, note the difficulty in determining reliable along-shore thermal gradients, and in order to decrease the error margins of our

estimates a northern GOA-wide analysis of along- and cross-shore thermal gradients is needed. This may be best done by analyzing (realistic) numerical modeling results or by extensive mining of GOA-wide hydrographic data sets.

The large gradients between inner and outer shelf wind speeds (Figures 3.11 and 3.12) also confirm the need for higher-resolution atmospheric data. The large grid spacing (2.5°) of NCEP only provides one data point on the GOA shelf (in the cross-shelf direction) and Middleton Island's weather station is located on the outer shelf, and both reanalysis and observations (due to distance from shore) do not include ageostrophic winds caused by orographic effects, as mentioned in multiple papers [Ladd and Bond, 2002; Stabeno et al., 2004; Weingartner et al., 2005], and may hence be biased.

Barrier jets and gap winds were previously shown to affect the volume transport of the ACC [Schumacher et al., 1989]. In particular, off-shore directed gap winds [Macklin et al., 1988] may locally cause instabilities in the ACC. This may be an additional mechanism to transfer coastal heat and freshwater across the shelf, although a quantitative analysis may again be an application for high-resolution process models.

Finally, Ekman transport is generally understood as one mechanism to move waters across the northern GOA shelf break [Stabeno et al., 2004], although the role of Ekman transport in the ACC is far less understood. The northern GOA cross-shelf isopycnal (and isohaline) structure (Figure 3.2) indicates a comparatively weaker front above the shelf break than in the ACC. Shcherbina and Gawarkiewicz's [2008] and

Williams et al.'s [in press] modeling experiments showed that Ekman on-shore transport is inhibited at a vertical coastal current front and instead results in two separate circulation cells seaward and shoreward of the front. However, except in some years during March (<http://www.ims.uaf.edu/GLOBEC/results>), the ACC front generally does not intersect the bottom and, therefore, it is not entirely understood whether on-shore transport is mixed horizontally across the front or whether it is subducted along isopycnals, or likely a combination of both. While neither scenario would change our simplified estimates regarding the role of Ekman transport on the coastal heat budget, an understanding of these processes may add to the understanding of the evolution of stratification and winter cooling in the coastal northern GOA as described by Janout et al. [in press]. Simplified models of the sort carried out by Williams et al. [in press] and Rogers-Cotrone et al. [2008] may provide useful insights.

3.5 Acknowledgments

Hydrographic sampling along the Seward Line from 1998-2004 was carried out as part of NEP-GLOBEC, and since 2005 under support of the NPRB (project #520, 603, 708, and 804). NCEP Reanalysis data were provided by the NOAA-CIRES Climate Diagnostics Center, Boulder, CO, USA, from their Web site at <http://www.cdc.noaa.gov/>. QuikSCAT data are produced by Remote Sensing Systems and sponsored by the NASA Ocean Vector Winds Science Team. Data are available at www.remss.com. Buoy data were downloaded from the National Data Buoy Center

(NDBC) website at <http://www.ndbc.noaa.gov/> and from the Alaska Ocean Observing System at <http://www.aos.org/>.

3.6 References

Anderson, P.J. and J.F. Piatt (1999), Community reorganization in the Gulf of Alaska following ocean climate regime shift, *Mar. Ecol. Prog. Ser.*, 189, 117-123.

Childers, A.R., T.E. Whitley, and D.A. Stockwell (2005), Seasonal and interannual variability in the distribution of nutrients and chlorophyll-a across the Gulf of Alaska shelf: 1998–2000, *Deep-Sea Res. II*, 52, 193–216.

Fairall, C.W., E.F. Bradley, D.P. Rogers, J.B. Edson, and G.S. Young, (1996), Bulk parameterization of air–sea fluxes for Tropical Ocean Global Atmosphere Coupled Ocean Response Experiment, *J. Geophys. Res.*, 101, 3747–3764.

Fairall, C.W., E.F. Bradley, J.E. Hare, A.A. Grachev, and J.B. Edson (2003), Bulk parameterization of air-sea fluxes: Updates and verification for the COARE algorithm. *J. Clim.*, 16, 571-591.

Fofonoff, N.P. and R.C. Jr Millard (1983), Algorithms for computation of fundamental properties of seawater, *Unesco Tech. Pap. Mar. Sci.*, No. 44, 53 pp.

Hare, S.R. and N.J. Mantua (2000), Empirical evidence for North Pacific regime shifts in 1977 and 1989, *Progr. Oceanogr.*, 47(2–4), 103–146.

Janout, M.A., T.J. Weingartner, S.L. Okkonen, T. Whitledge, and D.L. Musgrave (2009), Some characteristics of Yakutat Eddies propagating along the continental slope of the northern Gulf of Alaska, *Deep-Sea Res. II*, 56, 2444-2459.

Janout, M.A., T.J. Weingartner, T.C. Royer, and S.L. Danielson (in press), On the nature of winter cooling and the recent temperature shift on the northern Gulf of Alaska shelf, *J. Geophys. Res.*

Johnson, W.R., T.C. Royer, and J.L. Luick (1988), On the seasonal variability of the Alaska Coastal Current, *J. Geophys. Res.*, 93(C10), 12423-12437.

Ladd, C. and N.A. Bond (2002), Evaluation of NCEP/NCAR reanalysis in the NE Pacific and the Bering Sea, *J. Geophys. Res.*, 107, NO.C10, 3158.

Ladd, C., P.J. Stabenro, and E.D. Cokelet (2005), A note on cross-shelf exchange in the northern Gulf of Alaska, *Deep-Sea Res. II*, 52, 667-679.

Liu, H., P.Q. Olsson, K.P. Volz, and H.Yi (2006), A climatology of mesoscale model simulated low-level wind jets over Cook Inlet and Shelikof Strait, Alaska, *Est. Coast. Shelf Sci.*, 70, 551-566.

Loescher, K.A., G.S. Young, B.A. Colle, and N.S. Winstead (2006), Climatology of barrier jets along the Alaskan coast. Part I: Spatial and temporal distributions, *Mon. Wea. Rev.*, 134, 437-453.

Macklin, S.A., G.M. Lackmann, and J. Gray (1988), Offshore-directed winds in the vicinity of Prince William Sound, Alaska, *Mon. Wea. Rev.*, *116*, 1289-1301.

Macklin, S.A., N.A. Bond, and J.P. Walker, (1990), Structure of a low-level jet over lower Cook Inlet, Alaska, *Mon. Wea. Rev.*, *118(12)*, 2568–2578.

Mantua, N.J., S.R. Hare, Y. Zhang, J.M. Wallace, and R.C. Francis, (1997), A Pacific interdecadal climate oscillation with impacts on salmon production, *Bull. Am. Meteorol. Soc.* *78 (6)*, 1069–1080.

Niebauer, H.J., T.C. Royer, and T.J. Weingartner (1994), Circulation of Prince William Sound, Alaska., *J. Geophys. Res.* *99*:14113-14126.

Overland, J.E. and T.R. Hiester (1980), Development of a synoptic climatology for the Northeast Gulf of Alaska, *J. Appl. Meteorol.*, *19*, 1-14.

Overland, J.E., and N.A. Bond (1993), The influence of coastal orography: the Yakutat storm, *Mon. Wea. Rev.* *121*, 1388-1397.

Rodionov, S.N., N.A. Bond, and J.E. Overland (2007), The Aleutian Low, storm tracks, and winter climate variability in the Bering Sea, *Deep-Sea Res. II*, *54*, 2560-2577.

Rogers-Cotrone, J., A.E. Yankovsky, and T.J. Weingartner (2008), The impact of spatial wind variations on freshwater transport by the Alaska Coastal Current, *J. Mar. Res.*, *66*, 899-925.

Royer, T.C. (1981), Baroclinic transport in the Gulf of Alaska, Part II: Freshwater driven coastal current, *J. Mar. Res.*, 39, 251-266.

Royer, T.C. (1982), Coastal freshwater discharge in the Northeast Pacific, *J. Geophys. Res.*, 87(C3), 2017-2021.

Royer, T.C. (2005), Hydrographic responses at a coastal site in the northern Gulf of Alaska to seasonal and interannual forcing, *Deep-Sea Res. II*, 52 (1-2), 267-288.

Royer T.C., and C.E. Grosch (2006), Ocean warming and freshening in the northern Gulf of Alaska, *Geophys. Res. Lett.*, 33, L16605, doi:10.1029/2006GL026767.

Schumacher, J.D., P.J. Stabeno, and A.T. Roach (1989), Volume transport in the Alaska Coastal Current, *Cont. Shelf Res.*, 9, 1071-1083.

Shcherbina, A.Y., and G.G. Gawarkiewicz (2008), A coastal current in winter: 2. Wind forcing and cooling of a coastal current east of Cape Cod, *J. Geophys. Res.*, 113, C10014, doi: 10.1029/2008JC004750.

Stabeno, P.J., R.K. Reed and J.D. Schumacher (1995), The Alaska Coastal Current: continuity of transport and forcing, *J. Geophys. Res.*, 100(C2), 2477-2485.

Stabeno, P.J., R.K. Reed, and J.M. Napp (2002). Transport through Unimak Pass, Alaska, *Deep-Sea Res. II*, 49, 5919-5930.

Stabeno, P.J., N.A. Bond, A.J. Hermann, N.B. Kachel, C.W. Mordy, and J.E. Overland (2004), Meteorology and oceanography of the northern Gulf of Alaska, *Cont. Shelf Res.*, 24, 859-897.

Weingartner, T.J., K. Coyle, B. Finney, R. Hopcroft, T. Whitley, R. Brodeur, M. Dagg, E. Farley, D. Haidvogel, L. Haldorson, A. Hermann, S. Hinckley, J. Napp, P. Stabeno, T. Kline, C. Lee, E. Lessard, T. Royer, and S. Strom (2002), The Northeast Pacific GLOBEC Program: Coastal Gulf of Alaska, *Oceanography*, 15, 48 – 63.

Weingartner, T.J., S.L. Danielson, and T.C. Royer (2005), Freshwater variability and predictability in the Alaska Coastal Current, *Deep-Sea Res. II*, 52, 169-191.

Williams, W.J., T.J. Weingartner, A.J. Herrmann (2007), Idealized three-dimensional modeling of seasonal variation in the Alaska Coastal Current, *J. Geophys. Res.*, 112, C07001, doi:10.1029/2005JC003285.

Williams, W.J., T.J. Weingartner, A.J. Herrmann (in press), Idealized 2-dimensional modeling of a coastal buoyancy front under downwelling-favorable wind-forcing with application to the Alaska Coastal Current, *J. Phys. Oceanogr.*

Wilson, J.G. and J.E. Overland (1986), Meteorology, in *The Gulf of Alaska, Physical Environment and Biological Resources*, edited by D.W. Hood and S.T. Zimmerman, pp. 31–53, Alaska Office, Ocean Assessments Division, National Oceanic and Atmospheric Administration, US Department of Commerce.

3.7 Figures

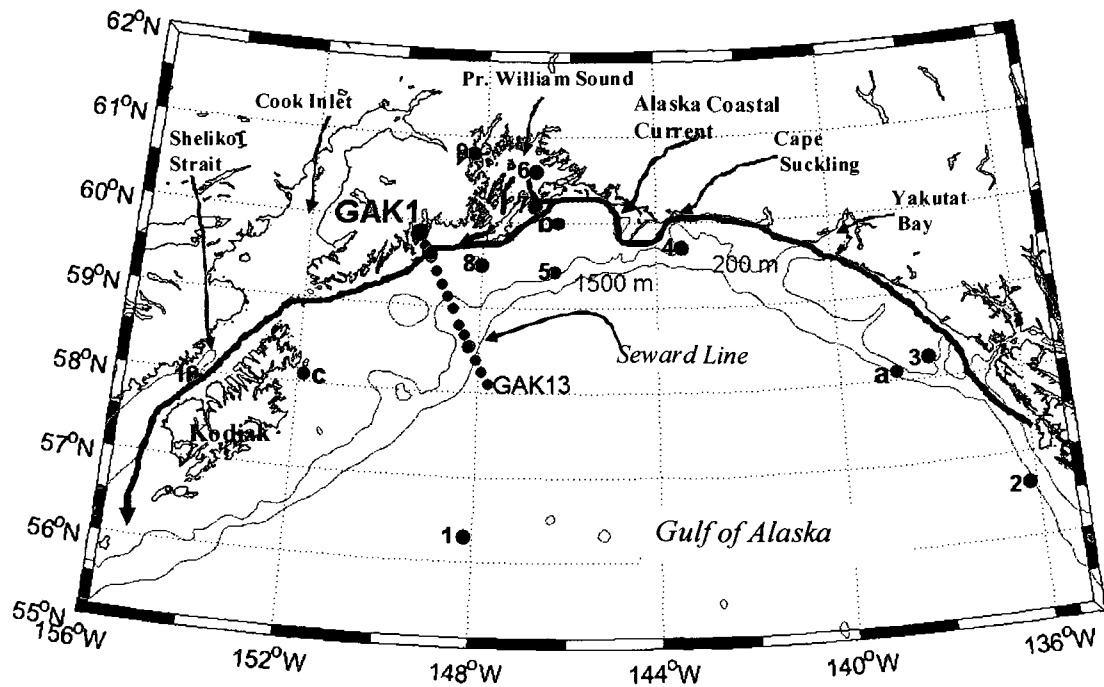


Figure 3.1: Map of the northern Gulf of Alaska. Map of the northern Gulf of Alaska, including GAK1 (large black dot) and the Seward Line (black dots). The Alaska Coastal Current pathway is sketched in blue-grey. Bathymetric data from the GEBCO database show the 200 m and 1500 m isobaths. Locations of QuikSCAT data points used in Figure 3.4 are marked by green dots. NDBC buoys (red dots) used to construct Figure 3.10: 1) 46001, 2) 46084, 3) 46083, 4) 46082, 5) PAMD, 6) 46060, 7) 46061, 8) 46076, 9) 46081, 10), 46077. NCEP grid points (blue dots) used in Figure 3.15: a) Eastern GOA, b) Northern GOA, c) Western GOA.

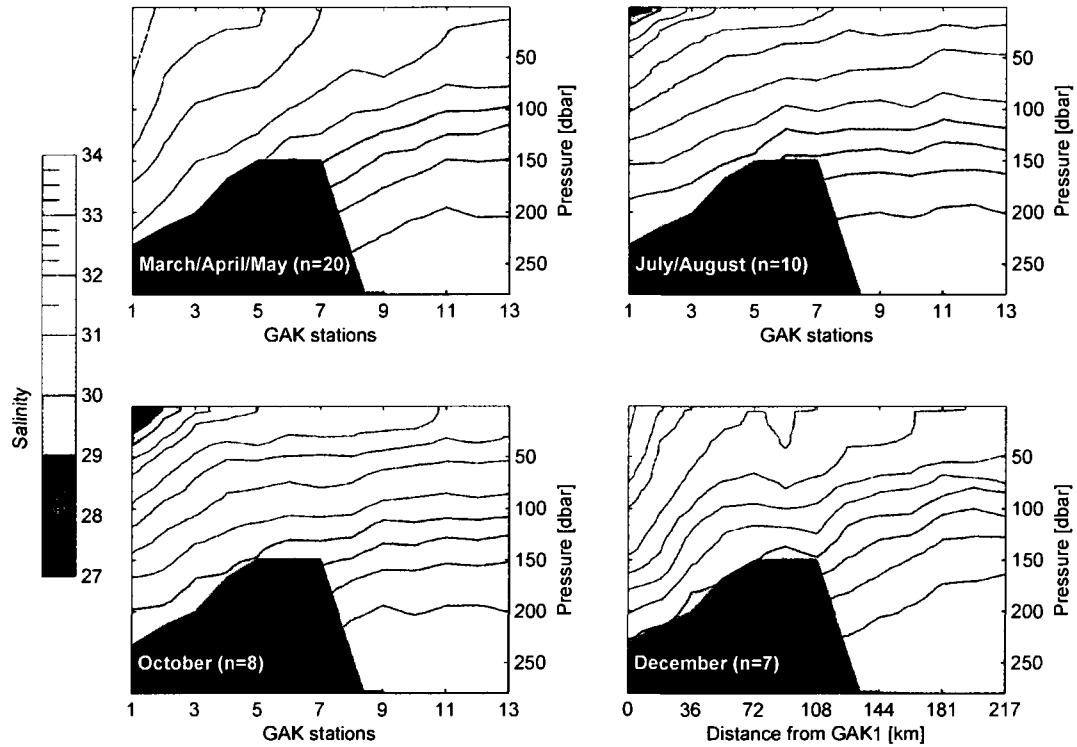


Figure 3.2: Seasonal mean Seward Line salinity. Seward Line salinity from GLOBEC cruises from 1997-2004, averaged for a) March-May, b) July-August, c) October, and d) December. Note that number of transects used for averaging are indicated with n=20, n=10 etc., also note the variable contour increments.

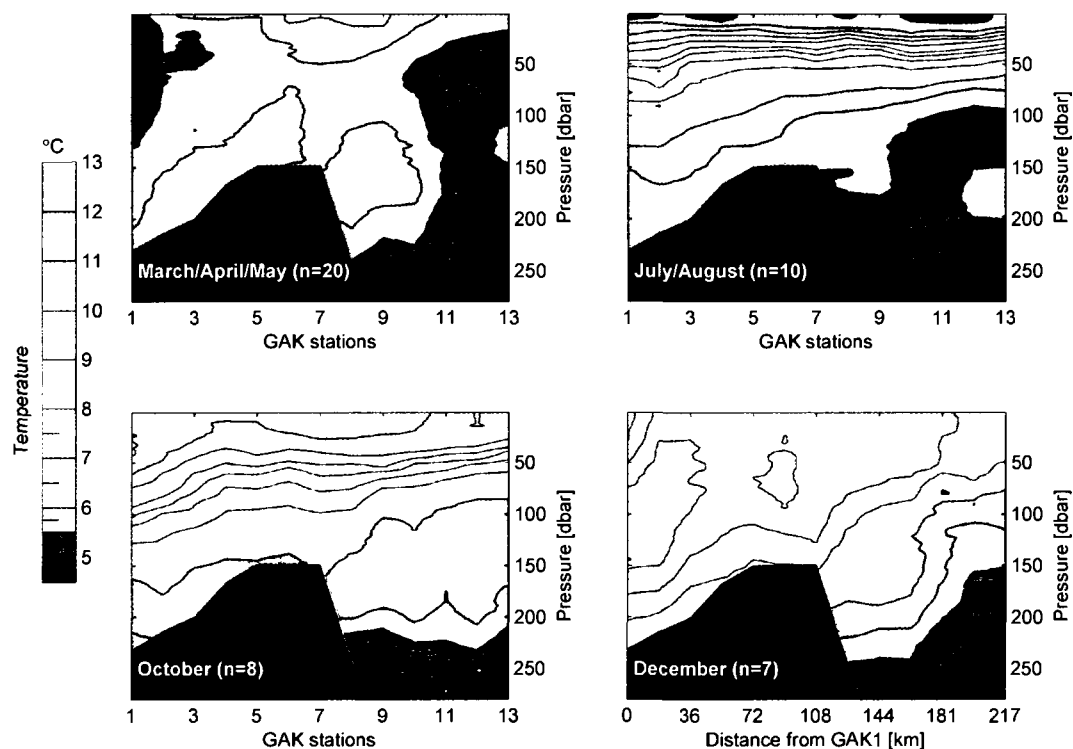


Figure 3.3: Seasonal mean Seward Line temperature. Seward Line temperature from GLOBEC cruises from 1997-2004, averaged for a) March-May, b) July-August, c) October, and d) December. Note that number of transects used for averaging are indicated with $n=20$, $n=10$ etc., also note the variable contour increments.



Figure 3.4: Climatology of wind and coastal runoff. Climatology of coastal freshwater discharge (1932-2008, black) in southcentral and southeast Alaska from Royer's (1982) hydrological model (right y-axis) and QuikSCAT along-shore wind stress [Nm^{-2}] (2000-2008, grey, left y-axis) at locations near GAK3 (solid grey) and GAK9 (dashed grey).

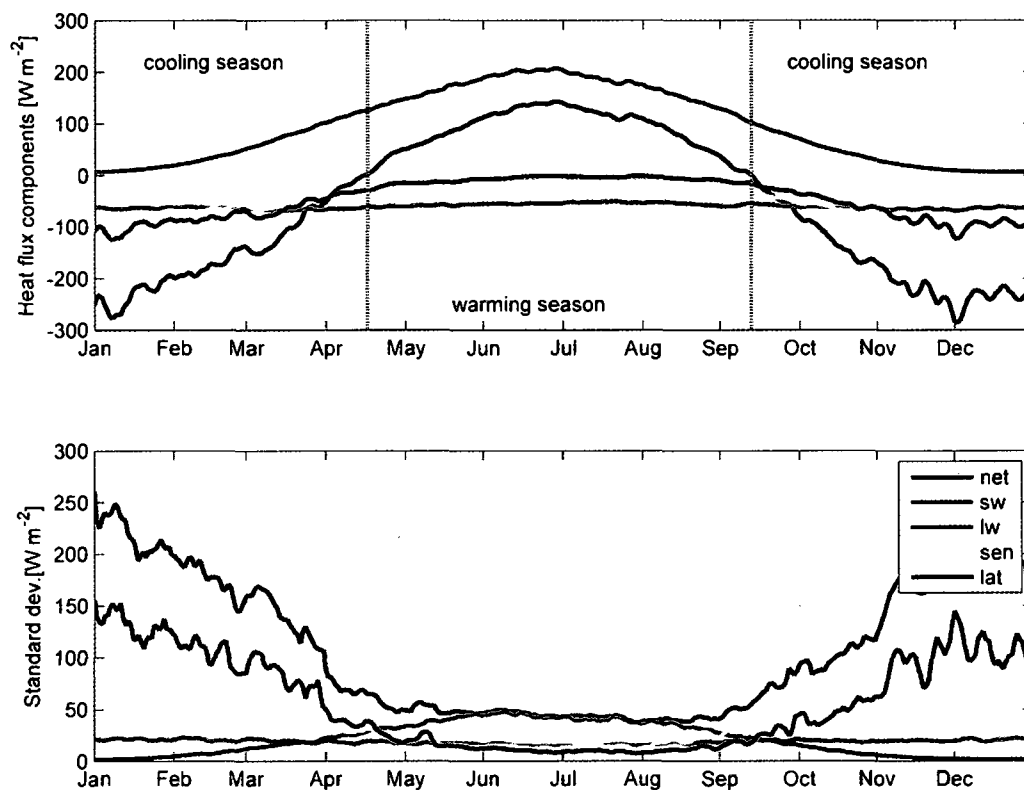


Figure 3.5: Northern Gulf of Alaska heat flux climatology. Annual cycle of heat fluxes [Wm^{-2}] at 60°N , 146°W , averaged from NCEP daily values from 1948-2009 (top) and their standard deviations (bottom). Net air-sea fluxes (black), short- (red) and longwave (magenta) radiation, sensible (yellow) and latent (blue) fluxes. Negative fluxes denote heat transfer from ocean to atmosphere. Dashed grey lines indicate the transition into heating and cooling seasons based on the zero-crossings of the net heat flux. X-ticks mark the first day of each month. Data are smoothed with a 3-day filter.

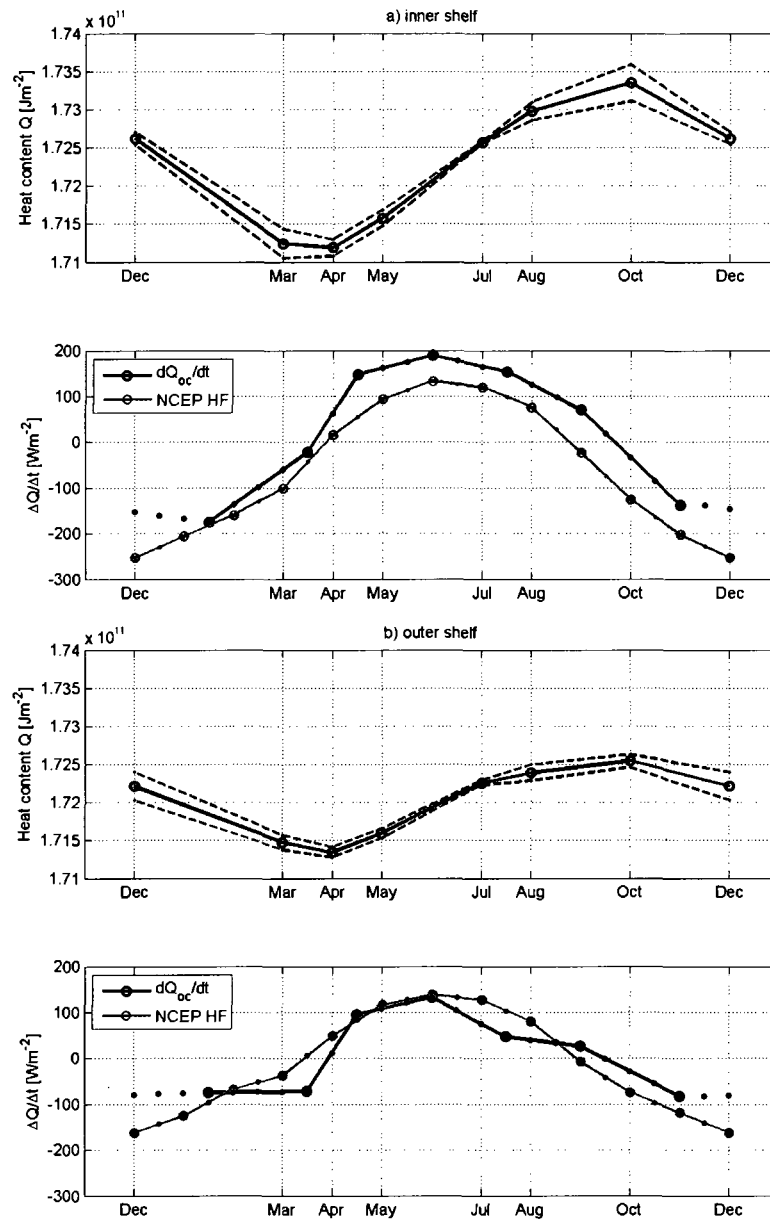


Figure 3.6: Seward Line oceanic heat content. Average seasonal depth-integrated (0-150 m) oceanic heat content [Jm^{-2}] including one standard deviation (dashed) (top) and the temporal change in oceanic heat content [Wm^{-2}] (bottom) of Seward Line stations (black, averaged from 1997-2004), compared with the nearest monthly average (1997-2004) NCEP net heat flux [Wm^{-2}] (grey). Both Q_{oc} and air-sea heat flux were interpolated from months with data coverage (large dots) to a \sim bi-weekly grid (small dots) in order to compute the residual between air-sea fluxes and $\partial Q_{oc}/\partial t$ shown in Figure 3.7. X-ticks include months with Seward Line data coverage. a) inner shelf, b) outer shelf.

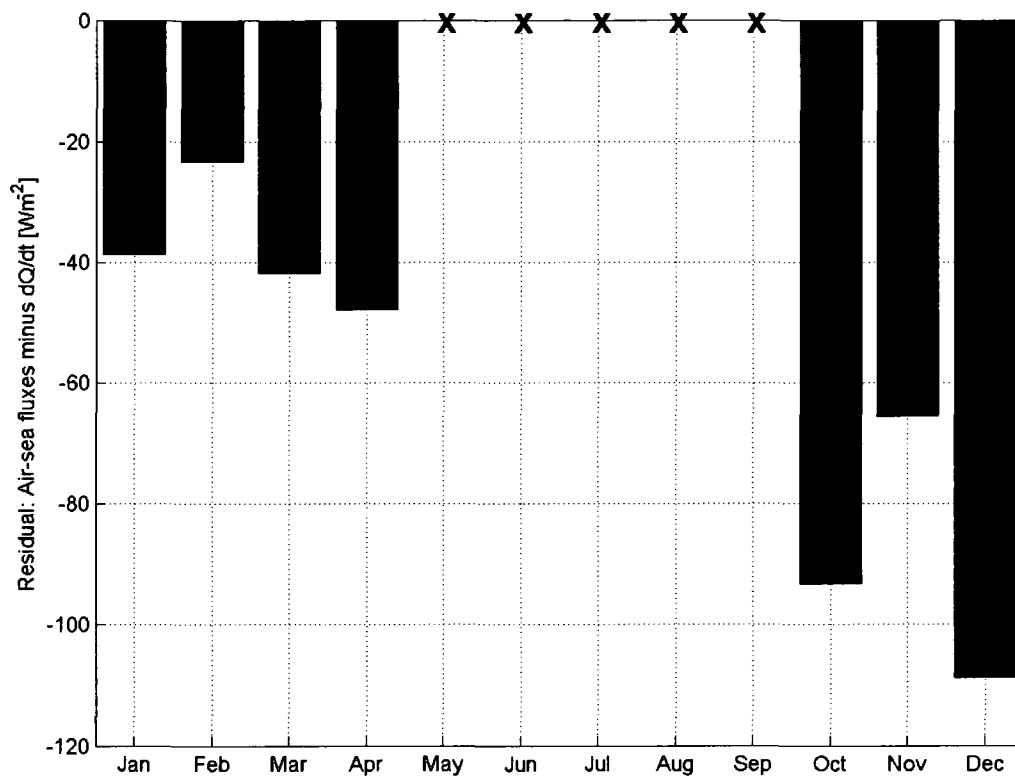


Figure 3.7: Coastal Gulf of Alaska heat deficit. Near-shore heat flux deficit between NCEP air-sea fluxes and the change in depth-integrated (0-150 m) oceanic heat content at GAK1-2 [Wm⁻²] (Figure 3.6a). Note that we only focus on the cooling season. Values suggest the amount of heat supply needed by oceanic advection in order to balance the heat budget.

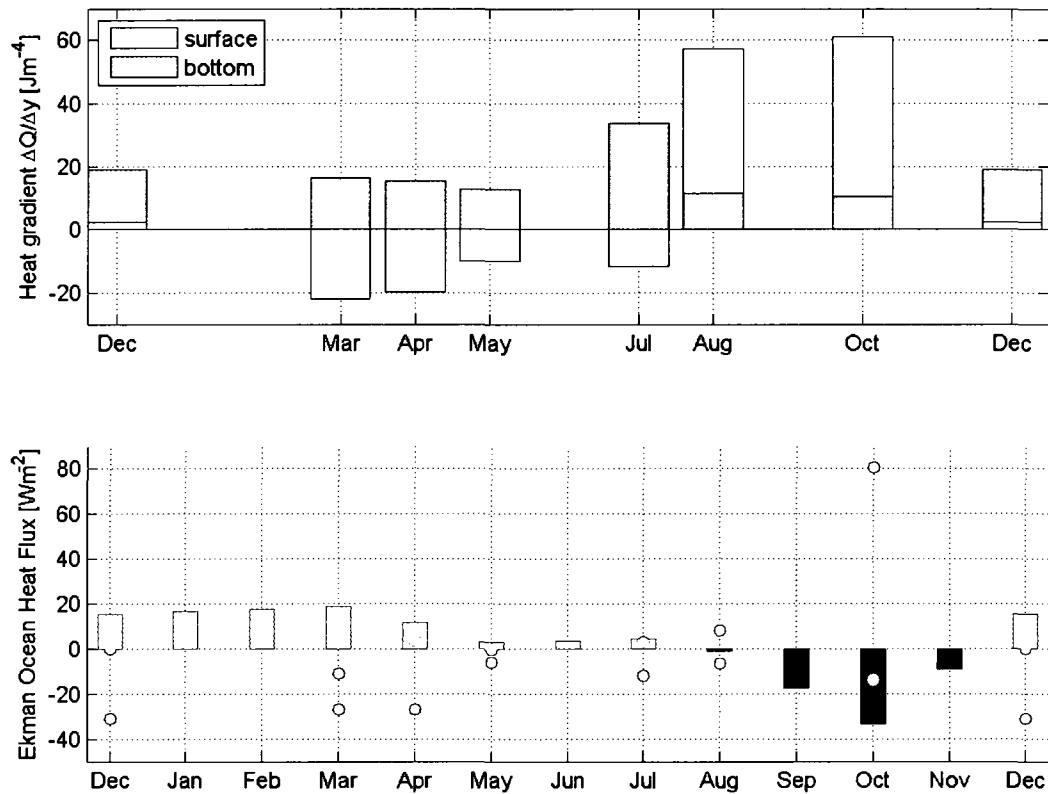


Figure 3.8: Seward Line heat gradients and Ekman heat flux convergence. Average oceanic cross-shelf heat gradient [Jm^{-4}] along the Seward Line (top) in surface (0-20 m, white) and bottom (230-250 m, grey). Negative gradients denote decreasing heat from south to north (i.e. shoreward). Lower panel shows the net oceanic heat advection [Wm^{-2}] due to Ekman transport averaged from Seward Line surveys. Missing months are interpolated between occupied months (marked by dots). Dots indicate one standard deviation. Negative (i.e. shoreward) heat flux is black, positive (i.e. seaward) heat flux is grey.

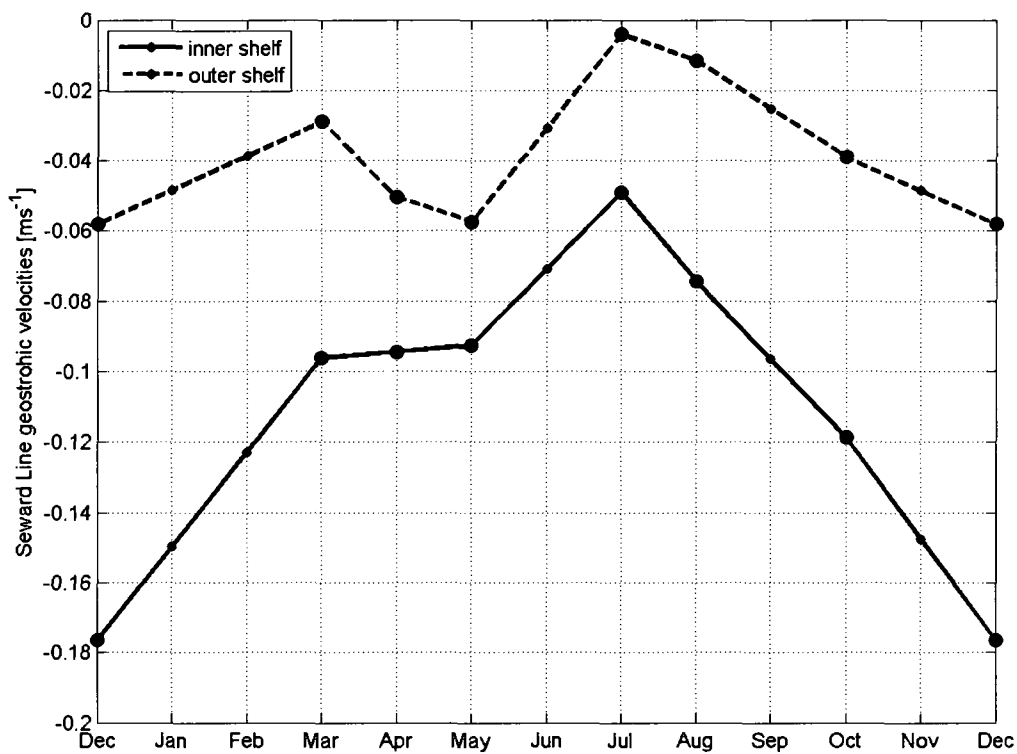


Figure 3.9: Seward Line geostrophic velocities. Mean (0-150 m) along-shore geostrophic velocities [m s^{-1}] computed from 1997-2004 Seward Line CTD data from inner (GAK1-2, solid) and outer (GAK7-8, dashed) shelf stations. Small dots indicate values interpolated from months with data coverage (large dots).

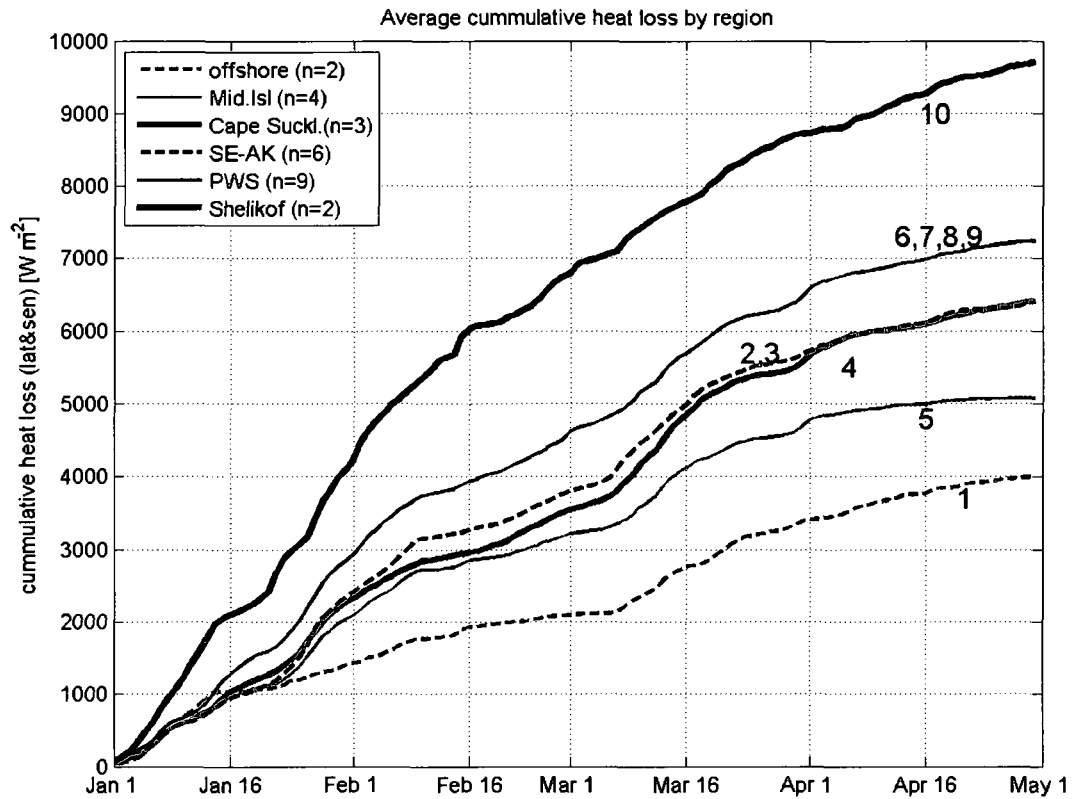


Figure 3.10: Gulf of Alaska turbulent heat fluxes. Average January-April cumulative turbulent heat loss in the GOA, computed from weather buoys from selected locations (see map Figure 3.1). Mean values were composed from available buoys among 2003, 2004, 2006, and 2008. Number of data points used for the mean is shown in legend (n=2 etc.). Numbers on the graphs correspond to the buoy number in Figure 3.1 used to construct the graphs.

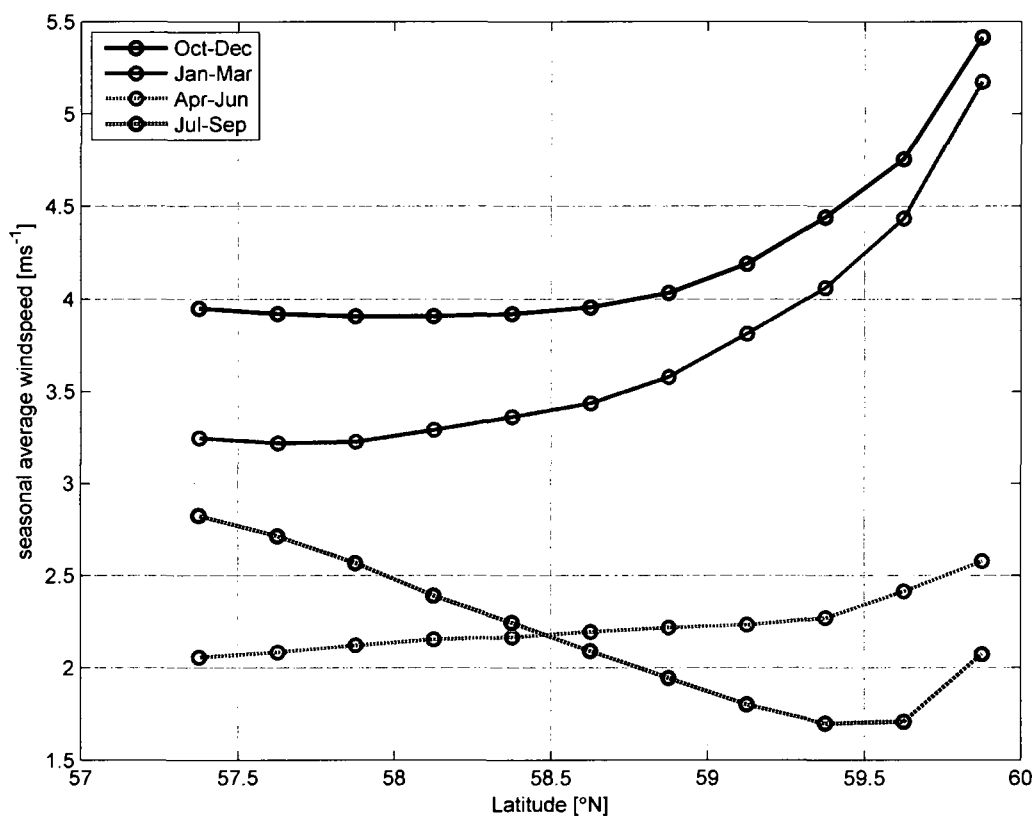


Figure 3.11: Cross-shelf wind speed gradients. Zonally averaged QuikSCAT wind speeds [m s^{-1}] between $140\text{-}150^\circ\text{W}$ for October-December (black solid), January-March (grey solid), April-June (grey dashed), and July-September (black dashed). Standard deviations (not shown) decrease seaward and are maximum in-shore in October-December ($\pm 1.1 \text{ m s}^{-1}$), except April-June, when the standard deviation is larger off-shore ($\pm 0.9 \text{ m s}^{-1}$) than near-shore ($\pm 0.6 \text{ m s}^{-1}$).

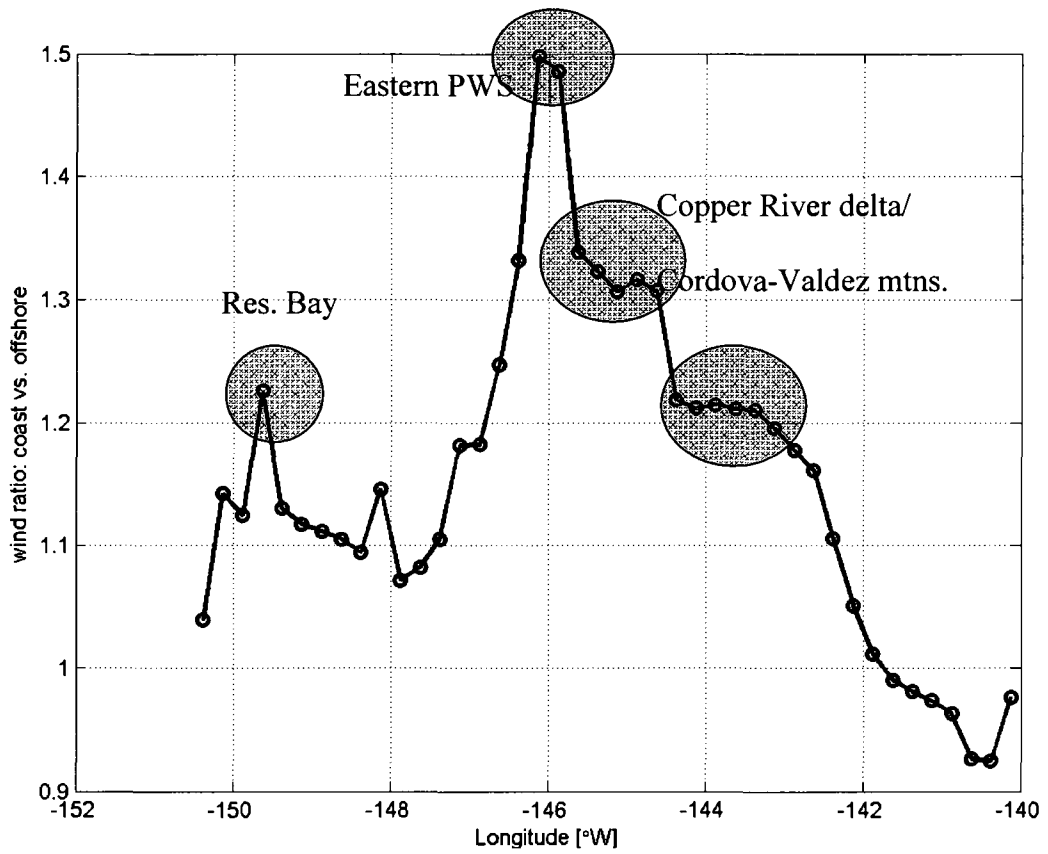


Figure 3.12: Winter coast to off-shore wind ratio. Meridional (November-March, 2000-2008) average of the QuikSCAT wind speed ratio near-shore to ~80 km (0.75° latitude) seaward of the near-shore data point. Grey shades highlight peaks in the ratio as described in the text.

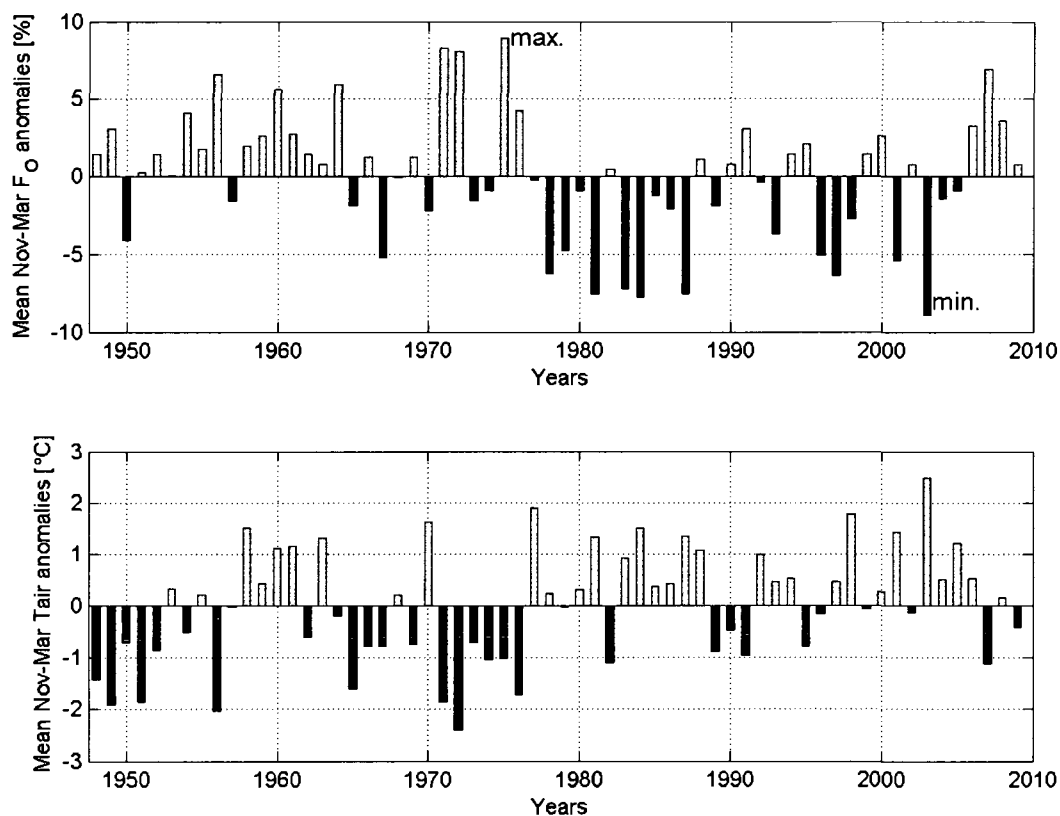


Figure 3.13: 1948-2009 frequency of Gulf of Alaska lows. Mean November-March anomalies of frequency of occurrence (F_o) of lows in the northern ($\geq 57.5^\circ\text{N}$ $\leq 62.5^\circ\text{N}$) GOA (top) and NCEP air temperatures [$^\circ\text{C}$] (bottom) from 1948-2009. Minimum (maximum) annual mean F_o occurred in 2003 (1975) with 9% (27%). These two time series are significantly anti-correlated ($r=-0.53$, $p<0.01$). Grey (black) bars indicate positive (negative) anomalies.

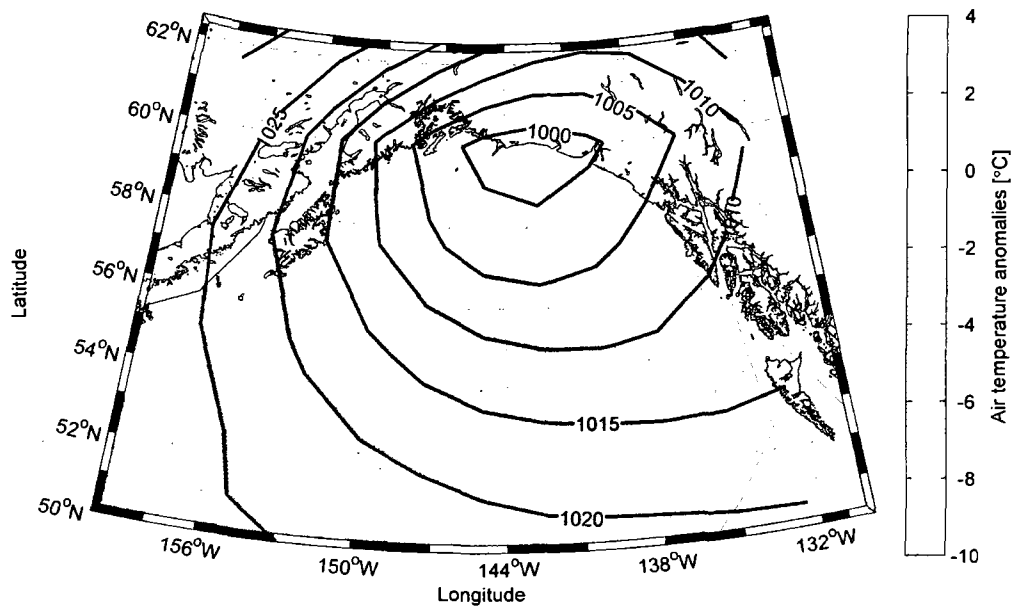


Figure 3.14: Gulf of Alaska low and air temperature anomalies. March 2007 NCEP monthly mean sea level pressure distribution (contours) and air temperature anomaly [°C] (color) about March 1948-2009. SLP contours are in 5 mbar increments.

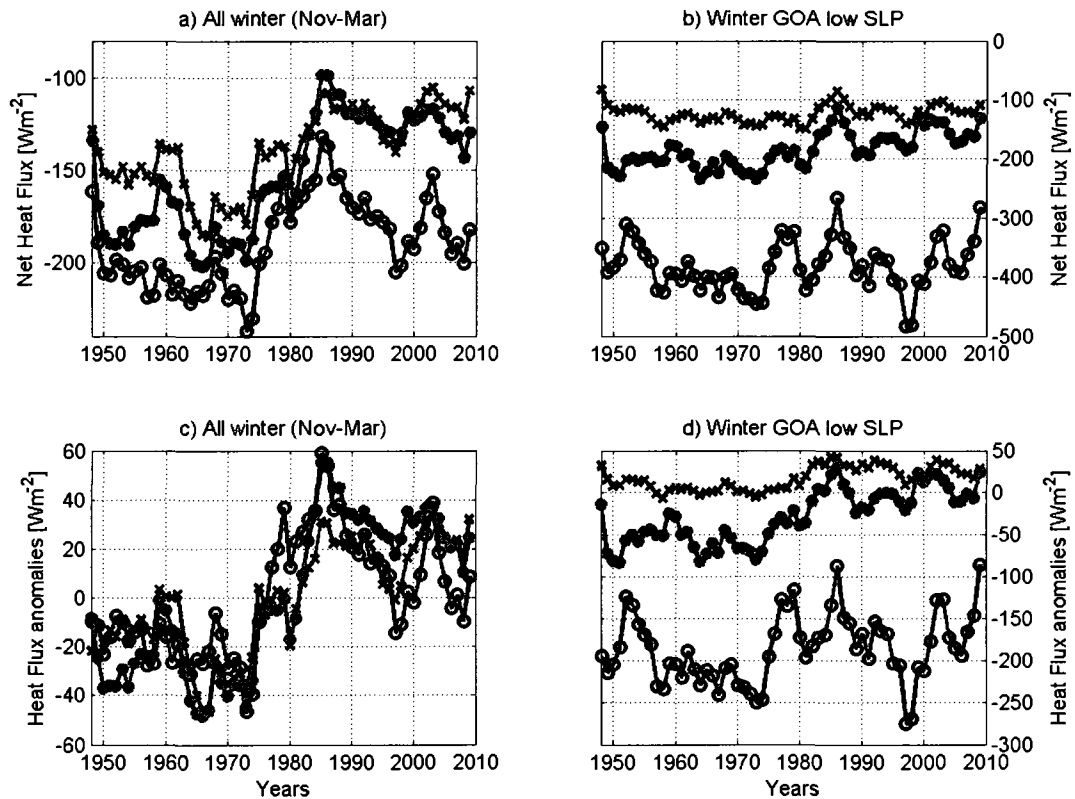


Figure 3.15: Winter heat fluxes and anomalies. Net air-sea fluxes [Wm^{-2}] a) and b) and their anomalies c) and d) from three locations around the northern GOA (red: SE-AK; black: SC-AK; blue: Western-AK. See locations in Figure 3.1). Data were averaged from 6-hourly NCEP fluxes from 1948-2009. Panels a) and c) are from net winter (November-March) air-sea fluxes. Panels b) and d) include only the data between November and March during the occurrence of a low pressure system in the northern GOA, i.e. during data points that were used for the frequency of occurrence (F_o) computations in Figure 3.13.

Summary and Conclusion

This dissertation describes investigations of processes that regulate the freshwater and heat budgets on the northern Gulf of Alaska (GOA) shelf. First, we examined characteristics of mesoscale (~200 km) anticyclonic eddies and their role on cross-shelf transport and mixing between high-nutrient, low-iron North Pacific off-shore water, and the iron-rich, nutrient-poor waters on the northern GOA shelf. Second, we analyzed temperature and salinity time series from the near-shore station GAK1, the longest hydrographic time series in the northern GOA (1970-present), to investigate processes such as freshwater runoff and air-sea fluxes that are important in controlling the temperature structure in the near-shore GOA within the Alaska Coastal Current (ACC). Finally, we quantified the different components of the northern GOA oceanic heat budget, including air-sea heat fluxes and their along- and cross-shore gradients and along- and cross-shore heat flux convergence.

Different shipboard, drifter and satellite observations showed that large eddies propagate from their formation regions off Sitka and Yakutat southwestward along the continental slope with maximum lifetimes of ~5 years. During their propagation the eddies appear to vary their size (150-250 km) and distance from the continental slope, but generally increase in size and sea level anomaly once they pass the Shelikof Sea Valley. These eddies are in gradient wind balance, except where they interact with the shelf break currents. There, the gradient wind relation fails and eddy-induced on- and off-shore transport takes place along the outer edge of the eddies. Two high resolution

eddy surveys in 2003 revealed no significant mass exchange between eddy and ambient waters, but instead the formation of low-salinity (~30 km) streamers, found seaward of the shelf break. In general and consistent with satellite-sensed surface chlorophyll-a, shipboard measured chlorophyll-a was strongly elevated inside the eddy where nitrate was utilized, while ambient waters, although high in nitrate, showed low chlorophyll-a abundance. These observations highlight the eddies as highly productive hot spots within the oligotrophic GOA basin and as important agents promoting exchange between shelf- and off-shore waters, and therefore underline the influence of eddies on the interannual temperature and salinity variability on the mid- to outer regions of the northern GOA shelf.

While the shelf is generally too wide for eddies to impact the near-shore GOA, processes controlling near-shore temperature and salinity are strongly governed by coastal freshwater runoff as shown in chapter 2. In the winter of 2006/07, ocean temperatures at the hydrographic near-shore station GAK1 revealed the lowest temperatures since the early 1970s and interrupted a three-decade-long warming trend. The water column was ~1.5°C colder than average, and salinity was higher (lower) in the upper (lower) layer, therefore strongly reducing the salinity-induced stratification. The cooling extended across much of the northern GOA shelf and was still persistent in spring 2009. We used mooring and CTD records from GAK1 and the Seward Line in combination with coastal freshwater runoff and atmospheric NCEP parameters and showed that ~81% of the variability of deep spring temperature anomalies is explained by anomalies in salinity stratification (i.e. freshwater runoff) and air-sea heat fluxes.

We also identified the dominant atmospheric pressure pattern in the northern GOA that is generally seen during strong atmospheric cooling events. This study highlighted the role of freshwater runoff and salinity stratification on the temperature distribution during spring, and suggested that temperature anomalies are the consequence of complex three-dimensional processes that include the interplay amongst air-sea heat fluxes, coastal runoff, horizontal and vertical mixing, as well as cross- and along-shore advection.

The third chapter focused on quantifying some of the processes relevant for the northern GOA heat budget as identified in chapter 2. These include the relative importance of air-sea heat fluxes and their spatial gradients, as well as the role of along- and cross-shore heat flux convergences on the northern GOA shelf. Climatological (NCEP) air-sea fluxes suggest that atmospheric winter cooling is stronger than explained by the temporal change in oceanic heat content estimated from (1997-2004) Seward line observations. The deficit between air-sea and oceanic heat budgets ranges from $\sim 90 \text{ Wm}^{-2}$ in October-December to $25\text{-}45 \text{ Wm}^{-2}$ in January-April, and our estimates suggest that along-shore heat flux convergence in the ACC can balance these deficits. The annual average net Ekman cross-shore heat flux convergence is insignificant despite persistent along-shore winds from fall-spring due to a reversal in the cross-shore heat gradient in winter. Turbulent heat fluxes computed from northern GOA weather buoys suggest positive along- and cross-shore (i.e. increased oceanic heat loss westward and shoreward) gradients. The cross-shore gradients are governed by cross-shore wind speed gradients due to strong ageostrophic

barrier and gap winds that occur along the mountainous GOA coastline. The along-shore gradients are likely due to northern GOA lows that occur during ~18% of the winter (estimated from NCEP sea level pressure) and place the western GOA under influence of cold northerly winds on the western flank of the low, and cause significantly stronger heat flux anomalies there compared with the northcentral and northeastern GOA.

The analyses carried out for this dissertation resulted in several new insights into processes that govern the physical environment of the northern GOA ecosystem, but naturally left many open questions that may be worthwhile to explore in future research. The observations presented in chapter 1 confirmed cross-shelf transport due to eddies, and suggested that the eddies' magnitudes increase south of Kodiak, which may be related to more vigorous interaction with the Alaskan Stream. However, these processes are neither understood nor quantified. The analysis of eddy-generating and -maintaining numerical model results from the northeast Pacific may be appropriate to quantify the transport of heat and salt (and nutrients) across the shelf break due to eddies. Furthermore, such budgets may be compiled as a function of longitude in order to identify and rate different GOA shelf break regions where eddies may be of higher relative importance. GOA eddies are more likely to form under strong downwelling-favorable winds, enhanced by a deep Aleutian Low, and more detailed knowledge about the impact of eddies may be extended to forecast eddy-induced oceanographic changes on the northern GOA shelf under a changing climate.

Climate change is likely to cause a shift in the seasonal runoff pattern through shifts in atmospheric conditions and processes. As concluded in chapter 2, runoff (i.e. salinity stratification) and air-sea heat fluxes explain 81% of the variability in deep GAK1 temperatures, and in order to forecast the impact of a changing climate on the GOA's ecosystem, it is crucial to understand the consequences of different runoff scenarios. Possible studies may focus on the vertical temperature distribution under various runoff volumes as well as under different phasing scenarios, i.e. runoff peaks at different times of the year, or more and less pronounced peaks. These studies would best be carried out using simplified three-dimensional process models.

Along-shore (downwelling-favorable) winds are positively correlated with coastal runoff and air temperatures, prevail from fall-spring, and govern some important processes in the GOA such as on-shelf Ekman transport, coastal downwelling or frontal dynamics within the ACC. Useful future modeling efforts may include the quantification of the role of wind-driven buoyancy flux on the near-shore water column structure as pointed out in chapter 2, or tracer studies that investigate the role of Ekman transport on the near-shore waters. Specifically, it would be useful to determine under which conditions shoreward advected water parcels penetrate through the ACC front, as this may confirm or disprove the significance of cross-shore Ekman heat flux convergence, as concluded in chapter 3.

Finally, it was shown in chapter 3 that the ACC is the dominant oceanic heat source for the near-shore heat budget and may resupply 10-35% of the heat removed by air-sea heat fluxes. The analysis relied on estimates of thermal along-shore

gradients, which are uncertain. To improve the estimates of the role of the ACC on the northern GOA heat budget, a detailed study to quantify thermal along-shore gradients may be worthwhile in order to reduce the error estimates on the along-shore heat advection term. This may be achieved by examining realistic numerical model results or by compiling and analyzing available hydrographic data in the northern GOA.